Title

Understanding Physical and Biological Processes for Pesticide Removal by Woodchip Bioreactors, with Insight Employing Microbial Enzymes and Communities

Author

Wrightwood, Olivia

Publication Date

2022

Peer reviewed|Thesis/dissertation

Understanding Physical and Biological Processes for Pesticide Removal by Woodchip Bioreactors, with Insight Employing Microbial Enzymes and Communities

By

OLIVIA MICHAEL WRIGHTWOOD
DISSERTATION

Submitted in partial satisfaction of the requirements for the degree of

DOCTOR OF PHILOSOPHY

in

Civil and Environmental Engineering

in the

OFFICE OF GRADUATE STUDIES

of the

UNIVERSITY OF CALIFORNIA

DAVIS

Approved:

Heather N. Bischel, Chair

Thomas M. Young

Frank J. Loge

Committee in Charge

2022

ABSTRACT

Contamination of surface and groundwater resources by conventional agricultural practices is becoming increasingly prevalent. In recent years, development of small footprint, low-maintenance, onsite woodchip bioreactors have helped to curb nitrate discharge from tile-drainage collection to downstream receiving waterways. Determining best practices to jumpstart microbial degradation of pesticides in similar reactors could help address pesticide pollution from agricultural areas. Chapter 1 of my dissertation provides the motivation for the following chapters, outlining the respective research objectives.

Chapter 2 of my dissertation assesses pesticide removal in woodchip bioreactor systems at three scales: field-scale, bench-scale, and micro-scale batch reactors. I constructed a bench-scale continuous-flow woodchip bioreactor and operated the reactor under field-like conditions to evaluate joint pesticide and nitrate removal. The continuous-flow reactor achieved 83.5 ± 8% diuron removal and 61.6 ± 11.9% imidacloprid removal with a 24 h hydraulic retention time (HRT). I then designed a sequencing-batch reactor configuration to evaluate the impact of an aerobic phase on denitrification and pesticide removal performance. The sequencing-batch reactor achieved 89.2 ± 8.8% nitrate removal with an HRT of 12 h, while the continuous-flow design achieved 55.6 ± 9.1% nitrate removal with a 12 h HRT. There was no significant difference between pesticide removal between sequencing-batch and continuous-flow reactor types. Kinetic batch tests revealed sorption, not microbial degradation as the main mechanisms of removal for both diuron and imidacloprid under denitrifying conditions.

Chapter 3 of my dissertation describes a combined *ex-vivo* and *in silico* screening approach I developed to understand and predict the catalytic competency of esterases for ester hydrolysis of pyrethroid pesticides and structurally related compounds. I hypothesized that esterases active toward pyrethroids would also interact with structurally similar esters. I screened fourteen

representative, wild-type microbial esterases against four pyrethroids, four alternative esters, and a suite of designed/known esterase and lipase substrates. I assayed each enzyme/substrate pair at different concentrations and analyzed assay extracts for specific esterase transformation products to confirm esterase activity. Phenyl salicylate, an ester compound with low aquatic toxicity, was found to be degradable by some of the same enzymes that were found to degrade pyrethroids. *In silico* induced fit docking of target compounds with esterases of interest highlighted amino acid residues important to substrate binding. For some enzymes, interaction fingerprint data revealed residue interaction patterns that are indicative of catalytic competency (i.e., enzymatic activity). Findings from these *in silico* experiments could be used as constraints in future molecular docking simulations.

Finally, Chapter 4 investigates the biodegradation potential of autochthonous microbial communities enriched on target pyrethroids as well as non-toxic, structurally similar substrates. I hypothesized that phenyl salicylate (identified in Chapter 3 as sharing enzyme activity with pyrethroids) stimulates enzymatic activity effective towards degradation of the two pyrethroids, bifenthrin and cypermethrin. I isolated a native microbial community from a functional woodchip bioreactor, and grew aliquots on phenyl salicylate, bifenthrin, cypermethrin, or glucose as the sole carbon substrate. I compared the growth patterns and metabolic characteristics. I found that the microbial consortia grew similarly on phenyl salicylate and glucose, while the growth curves of the bifenthrin and cypermethrin enrichments were characteristic of a more recalcitrant substrate (i.e., longer lag phase). I also employed a suspect screening approach to track the formation of commonly found metabolites of bifenthrin, cypermethrin, and phenyl salicylate. Results demonstrated that esterase activity occurred in each of these enrichments using the respective substrates. Results also provided evidence that phenyl salicylate-enriched communities may share

enzyme profiles with bifenthrin- or cypermethrin-enriched communities and suggest that phenyl salicylate may act as a low-toxicity biostimulant for pyrethroid degradation.

ACKNOWLEDGEMENTS

To my advisor Dr. Heather Bischel—I hope you know how much of an inspiring force you are. Your consistent support in research and personal endeavors epitomizes the ideal mentor. I don't think I'll ever quite be able to articulate how lucky I feel to have crossed paths with you, and that you agreed to support me on this journey. Thank you.

I would also like to thank my committee members, Dr. Thomas Young and Dr. Frank Loge. Thank you for being excellent instructors and patient, encouraging mentors. I would not have stuck around for a PhD if it weren't for professors like you. Additionally, thanks to Dr. Jeannie Darby and Dr. Harold Leverenz for helping me get my footing in Davis and in the department, and to our lab manager Jessica Hazard for keeping us grounded and for always being up for a hallway chat.

To my woodchip bioreactor folks, Ross Clark, Jessica Williamson, Pat Krone, and the Central Coast Wetland Group, thank you for always facilitating our intensive field sampling days and last-minute woodchip runs. And I'd be remised to not mention Dr. Madison Hattaway here—lab partners since 140A. Gosh, you made sampling trips and reactor times so much better, even when we got locked out of the office.

Thanks to Dr. Jennifer Teerlink for sitting on my qualifying exam committee, and to Dr. Aniela Burant for guidance and management on the woodchip bioreactor project.

The undergraduate researchers I worked with—Jacob Newman and Fatima Prada—thank you for being rockstars in the lab and putting up with weekend sampling and field trips.

To Dr. Justin Seigel, and your lab, especially Morgan Connolly, Akanksha Majumdar, and Ryan Castor, thank you for teaching me how to produce and purify enzymes and letting me be a transient in your lab. I have to say the whole Seigel lab is an awesome group of people, always selfless and helpful.

To the Young Lab, namely Chris Alaimo, Dr. Gabby Black, Luann Wong, thank you for teaching me the MS ropes. I would be at square one without you.

Thank you to Jeff Saunders for modifying the original Schrödinger python script calculating atomic distances, and to Dr. Andrew Blandino for help with processing data from the induced fit docking runs.

Dr. Wenting Li, you're one of a kind and I'm honored to have had you as my grad school bestie. In a personally tumultuous time in my life, you scraped me off the floor, was there during those late nights in the lab, and were always ready for a beer run (or most recently, an actual run) and wings. Thanks for going through the worst and best of it with me.

To the rest of Bischel Lab, Dr. Camille Wolf, Dr. Hannah Safford, Michelle Clauzel, Mel Johnson, and most recently Jordan Boeck, thank you for your never-ending support, weekend adventures, and laughs. This lab group is unique and amazing because of you.

A shoutout to some amazing roommates over the years—Liam Eckblad, Janis Patiño, and Aaron Alexander—thanks for making a house a home.

Last, I would not have been able to finish a PhD without my family. Thank you to my parents Kathi and Peter for always being supportive in my endeavors, even though I don't call home nearly as much as I should. Thanks to the best sibling, Soph, and the best-partner-of-a-sibling, Dylan—your visits out west were some of the happiest memories. And to Laura, thank you for putting up with all this, and especially for moving to California not once, but twice to be with me. I love you lots.

TABLE OF CONTENTS

ABBREVIATIONS

2-HYD	2-hydroxyphenylacetic acid
3-PBA	3-phenoxybenzoic acid
4-MPBu	4-methylumbelliferyl butyrate
4-NPA	4-nitrophenyl acetate
4-NPBe	4-nitrophenyl benzoate
4-NPBu	4-nitrophenyl butyrate
4-NPO	4-nitrophenyl octanoate
4-NPP	4-nitrophenyl palmitate
Ala (A)	alanine
Arg (R)	arginine
Asn (N)	asparagine
Asp (D)	aspartic acid
AZO	azoxystrobin
BEN	bensulfuron methyl
BIF	bifenthrin
CYP	cypermethrin
Cys (C)	cysteine
DEL	deltamethrin
EC	enzyme class
ECD	electron capture detection
EI	electron impact (ionization)
ESF	esfenvalerate
ESI (+/-)	electrospray ionization (positive/negative mode)
GC	gas chromatography
GFP	green fluorescent protein
Gln (Q)	glutamine
Glu (E)	glutamic acid
Gly (G)	glycine
His (H)	histidine
IFD	induced fit docking
IFP	interaction finger print
Ile (I)	isoleucine
IPTG	isopropyl β-d-1-thiogalactopyranoside
ISTD	internal standard
LB	luria broth
LC	liquid chromatography
Leu (L)	leucine
Lys (K)	lysine
Met (M)	methionine
MS	mass spectrometry
MSM	mineral salt medium
NCI	negative chemical ionization
OD600	optical density (600 nm)
PBS	phosphate-buffered saline
PCA	principal component analysis

PCDL	personal compound database library
PDB	proten data bank
Phe (F)	phenylalanine
Pro (P)	proline
PS	phenyl salicylate
PTFE	Polytetrafluoroethylene
QTOF	quadrupole-time-of-flight
RMSD	root-mean-square deviation
RNA	ribonucleic acid
SASA	solvent-accessible surface area
Ser (S)	serine
SMARTS	SMILES arbitrary target specification
SPE	solid phase extraction
TFP acid	3-(2-Chloro-3,3,3-trifluoroprop-1-en-1-yl)-2,2-dimethylcyclopropanecarboxylic acid
Thr (T)	threonine
Trp (W)	tryptophan
Tyr (Y)	tyrosine
Val (V)	valine

LIST OF TABLES

LIST OF FIGURES

CHAPTER 1: INTRODUCTION

Conventional agriculture is a primary source of nutrients and pesticides to surface water bodies and groundwater aquifers. Transport of nutrients and xenobiotics (e.g., pesticides, pharmaceuticals)[1] via infiltration, drainage, and runoff of water from agricultural plots can cause harm to non-targeted aquatic organisms. A range of pesticides, including herbicides, have been found by researchers in both urban and agricultural watersheds throughout California, some above aquatic toxicity thresholds.[2-5]

The development of low-cost, low-maintenance best management practices (BMPs) to reduce contaminant loading from agricultural drainage is instrumental to maintaining clean waterways. Woodchip denitrification bioreactors are one such BMP that have been implemented in the Midwestern United States[6] as well as in agricultural areas of California. Woodchip bioreactors remove nitrate (NO_3^-) from agricultural tile drains before discharging the effluent to downstream waterways.[6] Woodchip media provide both a physical surface and a carbon substrate to facilitate denitrification, reducing NO_3^- to dinitrogen gas (N_2) by facultative anaerobes.[7] Most woodchip bioreactor designs take minimal cultivable land area, making them attractive to farmers as a BMP.[6] However, the cost effectiveness of woodchip bioreactors is site-dependent.: when solely considering the cost of nitrate treatment benefits, woodchip bioreactors can have a reasonable annual cost ($ 994/year),[8,9] though still can require proportionally high capital investment depending on site and design ($5,000 to $27,000).[9] The geomorphology of a site will also determine whether additional pumps, sedimentation ponds, and pipe flushing will be required for proper bioreactor functioning.[10] Moreover, in some cases the substituted land area can be significant if the replaced cultivable land would otherwise be producing high-value crops.[10] While woodchip bioreactors are efficient nitrate treatment solutions for field-side drainage management,

defining and optimizing their treatment of other contaminants (e.g., pesticides) may encourage and incentivize more widespread adoption to improve downstream habitat health.

The goal of pesticide remediation is generally to mineralize the toxic compounds such that they become benign in the environment. Microbial transformation of pesticides and other xenobiotics has been studied primarily in the context of soil remediation,[11] but also in specific treatment trains, such as for hospital wastewater.[12-14] Discovery of wild-type microbial enzymes capable of breaking down xenobiotics has been gaining momentum, as multi-omics technologies allow for more detailed understanding of the scope of enzyme catalysis, as well as biodegradation pathways. Such enzymes can be produced and purified to be used in several environment types (e.g., *in situ* soils to well-controlled reactors) to target the remediation of corresponding contaminant classes. However, due to nonideal environmental conditions, the use of enzymes for *in situ* treatment can be short lived or limited.[15,16] Nonetheless, expanding our knowledge of native microbial enzyme specificity and mechanisms with respect to pesticide mineralization can help further other "green" remediation efforts.

Biostimulation and bioaugmentation are two "green" technologies that are used to train microbes to metabolize noxious contaminants in *ex situ* or *in situ* treatment plans. Such tools allow for the manipulation of both community composition and metabolic profiles to better target degradation of contaminants of concern.[17] The use of a BMP such as woodchip bioreactors in conjunction with microbial stimulation tailored for a specific class of contaminants could increase the efficacy of pesticide dissipation prior to water reaching surface or groundwater reservoirs.[18]

The second chapter of this dissertation focuses on the pesticide removal capacity of woodchip bioreactors as they are commonly employed in field-side settings. Here, we studied the dissipation of imidacloprid and diuron, two widely used pesticides, in reactors at three scales to

better understand the removal mechanisms of reactors operating at status quo. Here, adsorption was the primary removal mechanism of both pesticides while microbial degradation was not observed at any meaningful scale. Additionally, we hypothesized a sequencing-batch style bioreactor design would improve denitrification rate and pesticide degradation as compared against the common continuous-flow reactor design by introducing an aerobic cycle step. We demonstrated that the sequencing-batch style bioreactor achieves greater denitrification rates, though does not improve imidacloprid or diuron removal as adsorption occurs rapidly (i.e., faster than the HRT) with no appreciable microbial degradation.

The remainder of my dissertation addresses facets of microbial degradation of the pyrethroid pesticide class. Pyrethroids are widely used for control of urban and agricultural pests and tend to accumulate in the environment, especially in soils around agricultural plots.[19] Microbial esterases have been highlighted as good candidate remediation tools, as they are able to catalyze the hydrolysis of the central ester bond.[20] Chapter 3 covers an enzyme screening experiment, complemented by computational molecular docking studies to better understand the employment of microbial esterases for pyrethroid degradation. Additionally, we assessed non-pesticide esters to see if overlap in the enzymes' catalytic capabilities occurred. I hypothesized that compounds with similar structures would interact with esterases in a similar manner. Phenyl salicylate was highlighted as an ester exhibiting activity with several enzymes that were active toward screened pyrethroids. This demonstrates enzymatic promiscuity in these enzymes, suggesting that similar enzymes and their respective microbes may be used for pyrethroid remediation. While the molecular docking screening experiments were selectively successful in predicting active ligand/enzyme pairs, the assessed workflow can be used as a tool to highlight enzyme structures for future research or manipulation to further mechanistic understanding.

After learning of overlapping enzymatic activity toward pyrethroids and phenyl salicylate, I hypothesized that both substrate types could be utilized catabolically by microbial consortia. Chapter 4 is my evaluation of enzymatic degradation processes for pesticides in a complex environmental system, showing that microbial communities harvested from functional woodchip bioreactors can catabolize two pyrethroids, bifenthrin and cypermethrin, and the non-pesticide ester, phenyl salicylate. As enzymatic profiles are directly related to substrate composition,[21] it was expected that enrichments using structurally similar substrates (i.e., pyrethroids and phenyl salicylate) may stimulate similar microbial functionality. Together, these studies lay groundwork for expanding knowledge on how we may work better with native or autochthonous microbial communities to improve pesticide treatment in agricultural settings.

1.2 References

(1) Capel, P.; McCarthy, K.; Coupe, R.; Grey, K.; Amenumey, S.; Baker, N.; Johnson, R. *The Quality of Our Nation's Waters: Agriculture--A River Runs Through It--The Connections Between Agriculture and Water Quality*; Reston, VA, 2018.

(2) Ensminger, M. P.; Budd, R.; Kelley, K. C.; Goh, K. S. Pesticide Occurrence and Aquatic Benchmark Exceedances in Urban Surface Waters and Sediments in Three Urban Areas of California, USA, 2008-2011. *Environ. Monit. Assess.* **2013**, *185* (5), 3697–3710. https://doi.org/10.1007/s10661-012-2821-8.

(3) Morrissey, C. A.; Mineau, P.; Devries, J. H.; Sanchez-Bayo, F.; Liess, M.; Cavallaro, M. C.; Liber, K. Neonicotinoid Contamination of Global Surface Waters and Associated Risk to Aquatic Invertebrates: A Review. *Environment International*. **2015**, 291–303. https://doi.org/10.1016/j.envint.2014.10.024.

(4) Batikian, C. M.; Lu, A.; Watanabe, K.; Pitt, J.; Gersberg, R. M. Temporal Pattern in Levels of the Neonicotinoid Insecticide, Imidacloprid, in an Urban Stream. *Chemosphere* **2019**, *223*, 83–90. https://doi.org/10.1016/j.chemosphere.2019.01.165.

(5) Velki, M.; Di Paolo, C.; Nelles, J.; Seiler, T. B.; Hollert, H. Diuron and Diazinon Alter the Behavior of Zebrafish Embryos and Larvae in the Absence of Acute Toxicity. *Chemosphere* **2017**, *180*, 65–76. https://doi.org/10.1016/j.chemosphere.2017.04.017.

(6) Christianson, L. E.; Bhandari, A.; Helmers, M. J. A Practice-Oriented Review of Woodchip Bioreactors for Subsurface Agricultural Drainage. *Appl. Eng. Agric.* **2012**, *28* (6), 861–874.

(7) Crittenden, J.; Trussell, R. R.; Hand, D.; Howe, K.; Tchobanoglous, G. *MWH's Water Treatment: Principles and Design - John C. Crittenden, R. Rhodes Trussell, David W. Hand, Kerry Howe, George Tchobanoglous - Google Books*; 2012.

(8) DeBoe, G.; Bock, E.; Stephenson, K.; Easton, Z. Nutrient Biofilters in the Virginia Coastal Plain: Nitrogen Removal, Cost, and Potential Adoption Pathways. *J. Soil Water Conserv.* **2017**, *72* (2), 139–149. https://doi.org/https://doi.org/10.2489/jswc.72.2.139.

(9) Christianson, L. E.; Cooke, R. A.; Hay, C. H.; Helmers, M. J.; Feyereisen, G. W.; Ranaivoson, A. Z.; Mcmaine, J. T.; Mcdaniel, R.; Rosen, T. R.; Pluer, W. T.; Schipper, L. A.; Dougherty, H.; Robinson, R. J.; Layden, I. A.; Irvine-Brown, S. M.; Manca, F.; Dhaese, K.; Nelissen, V.; Von Ahnen, M.; Cooke, R. A.; Helmers, M. J.; Rosen, T. R.; Schipper, L. A.; Dougherty, H.; Robinson, R. J.; Agronomist, R.; Layden, I. A. Effectiveness of Denitrifying Bioreactors on Water Pollutant Reduction from Agricultural Areas. *Agric. Conserv. Pract. Eff. Collect. by Nat. Resour. Environ. Syst. Community ASABE* **2021**, *64* (2), 641–658. https://doi.org/10.13031/trans.14011.

(10) Plauborg, F.; Hørning Skjødt, M.; Audet, J.; Christian Hoffmann, C.; Jacobsen, B. H. Cost Effectiveness, Nitrogen and Phosphorus Removal in Field-Based Woodchip Bioreactors Treating Agricultural Drainage Water. Unpublished. **2022**. https://doi.org/10.21203/RS.3.RS-2037342/V1.

(11) Ellegaard-Jensen, L.; Knudsen, B. E.; Johansen, A.; Albers, C. N.; Aamand, J.; Rosendahl, S. Fungal-Bacterial Consortia Increase Diuron Degradation in Water-Unsaturated Systems. *Sci. Total Environ.* **2014**, *466–467*, 699–705. https://doi.org/10.1016/J.SCITOTENV.2013.07.095.

(12) Mir-Tutusaus, J. A.; Parladé, E.; Llorca, M.; Villagrasa, M.; Barceló, D.; Rodriguez-Mozaz, S.; Martinez-Alonso, M.; Gaju, N.; Caminal, G.; Sarrà, M. Pharmaceuticals Removal and Microbial Community Assessment in a Continuous Fungal Treatment of Non-Sterile Real Hospital Wastewater after a Coagulation-Flocculation Pretreatment. *Water Res.* **2017**, *116*, 65–75. https://doi.org/10.1016/J.WATRES.2017.03.005.

(13) Cruz-Morató, C.; Lucas, D.; Llorca, M.; Rodriguez-Mozaz, S.; Gorga, M.; Petrovic, M.; Barceló, D.; Vicent, T.; Sarrà, M.; Marco-Urrea, E. Hospital Wastewater Treatment by Fungal Bioreactor: Removal Efficiency for Pharmaceuticals and Endocrine Disruptor Compounds. *Sci. Total Environ.* **2014**, *493*, 365–376. https://doi.org/10.1016/j.scitotenv.2014.05.117.

(14) Naghdi, M.; Taheran, M.; Brar, S. K.; Kermanshahi-pour, A.; Verma, M.; Surampalli, R. Y. Removal of Pharmaceutical Compounds in Water and Wastewater Using Fungal Oxidoreductase Enzymes. *Environmental Pollution*. **2018**, 190–213. https://doi.org/10.1016/j.envpol.2017.11.060.

(15) Caldwell, S. R.; Raushel, F. M. Detoxification of Organophosphate Pesticides Using a Nylon Based Immobilized Phosphotriesterase from Pseudomonas Dirninuta. *Appl. Biochem. Biotechnology* **1991**, *59*.

(16) Gao, Y.; Truong, Y. B.; Cacioli, P.; Butler, P.; Kyratzis, I. L. Bioremediation of Pesticide Contaminated Water Using an Organophosphate Degrading Enzyme Immobilized on Nonwoven Polyester Textiles. *Enzyme Microb. Technol.* **2014**, *54* (1), 38–44. https://doi.org/10.1016/J.ENZMICTEC.2013.10.001.

(17) Cycoń, M.; Mrozik, A.; Piotrowska-Seget, Z. Bioaugmentation as a Strategy for the Remediation of Pesticide-Polluted Soil: A Review. *Chemosphere*. **2017**, 52–71. https://doi.org/10.1016/j.chemosphere.2016.12.129.

(18) Cahn, M. D.; Phillips, B. Best Management Practices for Mitigating Pesticides in Runoff from Vegetable Systems in California. *ACS Symposium Ser*. **2019**. https://doi.org/10.1021/bk-2019-1308.ch026.

(19) Tang, W.; Wang, D.; Wang, J.; Wu, Z.; Li, L.; Huang, M.; Xu, S.; Yan, D. Pyrethroid Pesticide Residues in the Global Environment: An Overview. *Chemosphere* **2018**, *191*, 990–1007. https://doi.org/10.1016/J.CHEMOSPHERE.2017.10.115.

(20) Bhatt, P.; Huang, Y.; Zhan, H.; Chen, S. Insight into Microbial Applications for the Biodegradation of Pyrethroid Insecticides. *Frontiers in Microbiology*. Frontiers Media S.A. August 2, 2019, p 1778. https://doi.org/10.3389/fmicb.2019.01778.

(21) Gangola, S.; Sharma, A.; Bhatt, P.; Khati, P.; Chaudhary, P. Presence of Esterase and Laccase in Bacillus Subtilis Facilitates Biodegradation and Detoxification of Cypermethrin. *Sci. Reports 2018 81* **2018**, *8* (1), 1–11. https://doi.org/10.1038/s41598-018-31082-5.

CHAPTER 2: ASSESSMENT OF WOODCHIP BIOREACTOR CHARACTERISTICS AND THEIR INFLUENCES ON JOINT NITRATE AND PESTICIDE REMOVAL

This chapter is primarily mirrors the structure of the published manuscript, Wrightwood et al. (2022)[a]:

- Section 2.1 discusses the motivation and study goals.
- Section 2.2 presents the manuscript's methods and materials.
- Sections 2.3 presents the results and related discussion of each set of experiments.
- Section 2.4 concludes.

2.1 Motivation and Study Goals

In California, agricultural runoff and drainage is a large source of nutrients and pesticides contaminating natural waterways,[1,2] posing risks to both environmental[3] and human health.[13,14] Imidacloprid, a neonicotinoid pesticide that targets the nicotinic cholinergic nervous system of insects, is commonly used in California and has been detected in both agricultural and urban watersheds above aquatic toxicity thresholds.[4,5,6] Because of its solubility in water (580 to 610 ppm in water),[7,8] imidacloprid is easily transported from point of application to neighboring waterways[6] where it can cause acute neurotoxicity to non-target species and drive significant shifts in invertebrate community composition.[3] Diuron, an herbicide of low-to-moderate solubility (42 ppm in water)[9] that targets the electron transport chain of weeds, is also widely used in California. Exceedances of toxicity thresholds for aquatic plants has triggered the state to implement total maximum daily load requirements and associated monitoring measures.[10] Though an herbicide, diuron also has been linked to developmental and behavioral changes in zebrafish at sub-acute

[a] Wrightwood, O. M.; Hattaway, M. E.; Young, T. M.; Bischel, H. N. Assessment of Woodchip Bioreactor Characteristics and Their Influences on Joint Nitrate and Pesticide Removal. *ACS Environ. Sci. Technol. Water* **2022**, *2* (1), 106–116. https://doi.org/10.1021/acsestwater.1c00277.

concentrations.[11] In 2018, the California Pesticide Use Report (PUR) showed 211,178 kg of imidacloprid, and 85,468 kg of diuron applied statewide.[12]

Woodchip bioreactors, an already-implemented BMP for treatment of agricultural drainage, have been recognized for their denitrification capacity and are beneficial in the removal of additional contaminants.[15,16,17] Attempts to optimize nitrate reduction have included modification of carbon media type,[19,20] media particle size,[21] hydraulic retention time,[22] and reactor geometry.[17] These reactors can achieve between 22% and >99% of NO_3^- removal depending on the abovementioned parameters.[15]

Of the studies examining pesticide removal from water via bioreactors, most have focused on the sorptive capacity of woodchips and other plant and plant-derived materials (e.g., straw,[23] lignocellulose, chitosan[24]) or the sorption processes of pesticides in soil/water systems.[25] Analysis of how operational characteristics of woodchip bioreactors affect the treatment of pesticides will help optimize an already accepted BMP for prevention of downstream contamination from agricultural drainage.

The aims of the present study are to 1) assess the joint removal of nitrate and selected pesticides across rectangular, continuous-flow bench-scale reactors; 2) design and assess bench-scale, sequencing-batch style reactors to increase the reliability of denitrification while improving pesticide removal; and 3) evaluate the relative importance of sorption and microbial degradation to the removal of imidacloprid and diuron from tile drainage with woodchip media.

2.2 Study materials and methods

2.2.1 Bench-scale reactor development

The bench-scale reactor development consisted of three phases: 1) monitoring field-scale reactors to obtain reference characteristics, 2) construction of continuous-flow bench-scale reactors to mimic denitrification performance of field-scale reactors, and 3) development of a sequencing-batch-style reactor to assess the influence of hydraulics and redox conditions on performance. We monitored the Multichannel Bioreactor located in the Central Coast Region of California (Castroville, CA), operational since June 2017. The bioreactor consists of 12 parallel channels (22.6m x 1.68m x 0.762m, length x width x depth; HRT ranging from about 16 to 43h) with different media that process agricultural tile drainage from approximately 4 km^2 of nearby agricultural lands all growing similar crops (e.g., artichokes, brussel sprouts, celery, strawberries). The bioreactor is managed by the Central Coast Wetlands Group (CCWG) located at the Moss Landing Marine Laboratories (California State University Monterey Bay). This field system is described in greater detail by Krone et al..[26]

We completed five sampling events at the field site to collect data on dissolved oxygen concentration (DO), oxidation reduction potential (ORP), pH, electrical conductivity (EC), and water temperature at multiple locations along the length of the three bioreactor channels that contain woodchips (Channels 1, 5 and 9). Samples along the length of the bioreactors were collected from perforated PVC monitoring wells. Where there were no monitoring wells, samples were collected by digging into the woodchip media (30cm below water level) and sampling from the cleared area. ORP, pH, EC, and temperature data were measured using a MyronL Ultrameter III (MyronL Company, Carlsbad, CA). DO was measured using a HACH Dissolved Oxygen Test Kit, Model OX-2P (modified Winkler method). We also monitored influent/effluent samples for dissolved organic carbon (DOC) and nitrate concentrations in the woodchip channels, collected in 500mL, baked amber glass jars, and kept on ice during transport. Samples collected for DOC

analysis were preserved with phosphoric acid (H_3PO_4) to pH < 2 and stored at 4°C until analysis. Samples for nutrient analysis were stored at 4°C and analyzed within 24 h of collection. We also pulsed a conservative bromide tracer (KBr, Spectrum Chemical Manufacturing Group, New Brunswick, NJ) into two of the field woodchip bioreactors (Channel 1 and Channel 5) for hydraulic characterization. Bromide tracer samples were collected with a Teledyne ISCO 6712 Portable Sampler programmed to collect 850mL every 2 or 6 hours. Tracer samples were transported in the sampler back to UC Davis, where they were diluted with 70% nitric acid (HNO_3), centrifuged, and analyzed via inductively coupled plasma-mass spectrometry (Agilent 7900 ICP-MS, Santa Clara, CA).

We constructed bench-scale, continuous-flow reactors to mimic the above-listed parameters. Denitrification efficacy was used to confirm biochemical (i.e., denitrification rate) similarity between scales. Three regression analyses were compared for their goodness of fit in modelling the measured denitrification data from the bench-scale reactors, described in Table A2. Obtained model parameters were compared to denitrification modelling of the field bioreactors completed by Krone et al.[26] for the same system, as well as to similar woodchip bioreactors.

Conservative bromide tracer modelling was used to confirm hydraulic similarities between the field and bench-scale bioreactors. Bromide tracer data from Krone et al.[26] was used to characterize the field system (i.e., the Multichannel Bioreactor), to be compared with bromide tracer data from the bench-scale bioreactors. Two analytical modelling methods were performed to obtain dispersed-flow models (DFM)[27] and compared for goodness of fit to the bromide data for respective bench- and field-scale data. Obtained Péclet numbers and hydraulic residence times were compared between field- and bench-scale reactors. Specifics of bromide tracer modelling are in Table A1.

The drainable porosity was measured prior to each experiment to calculate treatment volume, theoretical, and exact HRT. All continuous-flow bench-scale reactors were fed with a peristaltic pump (Cole-Parmer, Vernon Hills, IL) to maintain a constant theoretical HRT to match the field reactors.

Sequencing-batch reactors were developed as an alternative operational strategy. The sequencing-batch reactors were fitted with 2-way ball valves at the inlet and outlet to control the filling and draining of the reactors by gravity, creating a sequencing-batch reactor effect. The valves were controlled by a programmable logic controller (PLC; Arduino®) to allow different time combinations of alternating 'full' and 'empty' cycles, HRT, and air-exposed time (AET), respectively. Note that AET represents the hold time while the reactor is empty and does not include fill/drain times. Three sequential side-by-side experiments were carried out to assess the denitrification and pesticide removal potential of both reactor configurations (section 2.4).

2.2.2 Sourcing and characterization of woodchips

Woodchips collected from the operational field-scale denitrification bioreactors were used in bench-scale reactors to obtain similar microbial activity between field- and bench-scale reactors, as well as to avoid needing to "age" woodchips to obtain stable operating conditions.[20,28] The bioreactor woodchip media is composed of tree-removal and recycled construction wood, leaving out pressure-treated and eucalyptus wood as these contain antimicrobial characteristics.[29] To avoid wall effects in the bench-scale reactors, we sieved the woodchips to pass a 9mm square mesh (no lower size limit) to obtain more even woodchip size distribution within the bench-scale reactors. Woodchips were collected periodically, stored at 4°C unsubmerged in airtight buckets, and used within one month of collection to minimize degradation until use. The percent moisture content of

the undried woodchips was approximately 59.5 ± 6.8%, determined by drying representative samples at 105°C until constant mass was reached. Prior to use in bench-scale bioreactors, samples of woodchips from each collection were analyzed for pesticide content (section 2.2.6.1).

2.2.3 Synthetic tile drainage

A synthetic tile drainage was formulated to mimic nitrate, sulfate, and pesticide concentrations measured in tile drainage from Castroville, CA. The final salt concentrations were as follows: 3.7mmol $MgSO_4$, 1.7mmol KNO_3 (Ward's Science, Rochester NY), 7.5mmol NaCl and 5.7mmol $NaHCO_3$ (BioWORLD Molecular Tools for Life Science, Dublin OH). Imidacloprid and diuron were chosen as the pesticides of interest. These three compounds represent three different classes of pesticides, exhibiting a range of hydrophobicities, molecular size, and functional groups. The commercial formulations used are Altriset Termiticide by Syngenta Crop Protection, LLC (chlorantraniliprole; 200.1 kg/L active ingredient), Diuron 4L by Drexel (diuron; 479.3 kg/L active ingredient), and Dominion 2L by Control Solutions Inc. (imidacloprid; 239.7 kg/L active ingredient). The final electrical conductivity level was maintained at ~3,000 µS/cm. In all experiments, dilutions of commercial pesticide formulations were used for cost efficiency as well as to capture potential effects of product adjuvants.

2.2.4 Comparison of sequencing-batch and continuous-flow bioreactors

The continuous-flow and sequencing-batch style bench-scale reactor designs were first compared for their nitrate removal capacity. One of each reactor configuration was run at three different HRTs: 6 h, 12 h, and 24 h. Influent and effluent samples were collected from the reactors over 15 days, obtaining at least 4 time points per HRT. The percent removal was calculated for each time point. For this experiment, the AET of the sequencing-batch reactor was 0 h (a hold time

of 0 hours when the reactor was fully drained) for each cycle. Draining and refilling took a total of 30 minutes, during which portions of the reactor were exposed to air.

Next, a set of side-by-side experiments compared two control continuous-flow reactors (without woodchips), two continuous-flow reactors, and two sequencing-batch reactors. The continuous-flow reactors were operated at an HRT of ~24 h, while the sequencing-batch reactors were operated with a 12 h HRT/12 h AET cycle (24 h total). Nitrate removal data from the sequencing-batch reactor was comprised of an initial time point along with removal data at HRTs 6 h, 12 h, and 24 h. The data were used to determine denitrification rates and reaction order for continuous-flow and sequencing-batch bench-scale reactors. Following the comparison of the continuous-flow and sequencing-batch style bioreactors, the sequencing-batch reactor setup was then run for an additional 14 days to assess the effect of AET on denitrification. The effect of AET was evaluated by setting AET at 0 h, 2 h, 4 h, 6 h, and finally 12 h. For each AET, the bioreactor was set to cycle at least three times with a water-filled time (HRT) of 12 h. No significant change in denitrification was observed with increasing AET (Figure A15). Therefore, a 12 h AET was used in subsequent side-by-side pesticide removal experiments to assess potential benefits of the sequencing-batch operation mode for pesticide degradation at an equivalent treatment cycle time.

The reactors were fed synthetic tile drainage water containing the salt buffer along with imidacloprid (2.4–10 ng/mL), diuron (1.0–7.0 ng/mL), and chlorantraniliprole (0.2–5.0 ng/mL) from commercial formulations. Due to challenges delivering consistent dosages of the chlorantraniliprole commercial product in aqueous matrices, only analysis of imidacloprid and diuron will be discussed. The dosing challenges with chlorantraniliprole were likely due to non-homogenous dosing solutions, as the ratio of water to formulation was less than recommended for field use. The side-by-side comparison was conducted three times, once for each woodchip batch

(February 2020, August 2020, and October 2020). Experiments spanned between eight and seventeen days each and sampling was conducted every 1 to 3 days. Influent and effluent samples were collected and analyzed for nitrate, DOC, and pesticide concentrations.

2.2.5 Small-scale batch tests

We performed small-scale (40-mL tube) batch tests to assess the relative contributions of sorption and microbial degradation to pesticide removal in denitrifying woodchip bioreactors. Individual kinetic batch tests for both imidacloprid and diuron were performed to assess the removal of each contaminant under denitrifying conditions. The three treatments studied in these batch tests were: 1) treatment batch (TB), containing woodchips and synthetic tile drainage; 2) microbial control (MC), containing woodchips, synthetic tile drainage, and NaN_3 to limit microbial activity;[30] and 3) no-woodchip control (NWC), containing only synthetic tile drainage and NaN_3. These treatments were selected to distinguish between sorption and microbial removal. For each treatment, triplicate batches were sacrificed at each of six time points, which spanned between 1 hour and 8 days separated by at least 24 hours. Aqueous pesticide concentration, nitrate concentration (to ensure denitrifying conditions), and DOC were measured at each time point.

2.2.6 Chemical analyses

2.2.6.1 Pesticide analysis

Extraction and analysis of field- and bench-scale water samples for pesticide content were carried out following Moschet et al.,[31] with some modifications. Briefly, samples from the bench-scale reactors were collected in 250 mL amber glass bottles, filtered through 0.47 µm glass fiber filter, and extracted using Oasis HLB solid phase extraction (SPE) cartridges. The glass fiber filters

were subsequently extracted with two volumes of 20 mL hexane:acetone with 1:1 volumetric ratio, and analyzed in combination with the water extract.[31] Batch samples were extracted without the first filtration step due to the small (25 mL) extraction volumes. Instead, the tubes containing synthetic tile drainage water and woodchips were centrifuged (2,350 G; 10 min), then the supernatant was pipetted directly onto the SPE cartridge. All water samples were extracted within 24 h of collection.

Methods for analyzing pesticide content of woodchips prior to experimentation were adapted from related methods.[32,33] Briefly, three replicates of about 10 g of sieved woodchips were freeze dried using a HarvestRight (North Salt Lake, UT) freeze dryer, then ground using a Retsch Ball Mill MM 400 (Verder Scientific GmbH & Co. KG) at a frequency of 30 cycles/s for 6 minutes. Ground samples were sieved using a 106 μm sieve, and about 0.4 g of the sieved samples were weighed out into 15mL centrifuge tubes. Samples were extracted with 6 mL 3:1 v/v hexane:acetone, and again with 6mL of acetone. All examined pesticides were analyzed using LC-MS-QTOF, ESI+ mode (Agilent 1260 Infinity HPLC coupled to an Agilent 6530 QTOF-MS with a Zorbax Eclipse Plus C18 column; 100 mm, 2.5 mm, 1.8 μm, Agilent Technologies, Inc.). Data acquisition methodology was adapted from Moschet et al..[31] Woodchip extractions were analyzed semi-quantitatively, while all water samples were analyzed quantitatively.

2.2.6.2 Nutrients and dissolved organic carbon

Nitrate concentrations were measured with flow injection analysis (QuikChem 8500; Lachat Instruments, Loveland, CO) for all microbial active bioreactor samples. Controls containing NaN_3 were analyzed with HACH TNT835 due to azide interaction with nitrite following the cadmium reduction step in the flow injection analysis.[34] Samples collected for DOC

analysis were acid preserved using H_3PO_4 (pH<2) and stored at 4°C until analysis.[35] DOC samples were subsequently filtered to 0.45 µm and analyzed with a M5310 C Laboratory TOC Analyzer (Suez WTS Analytical Instruments, Inc., Trevose, PA).

2.2.7 Statistical methods

2.2.7.1 Analysis of bench-scale bioreactor experiments

The pesticide removal across both the continuous-flow and sequencing-batch bench-scale bioreactor designs were compared using a Student's two-tailed, homoscedastic T-Test. This was performed on the percent removal values (Eq. 1) across all sampled time points of the side-by-side experiments. Imidacloprid percent removal values were calculated using only the August 2020 and October 2020 results, omitting the February 2020 experimental data due to irregularities (section 3.2.2).

$$\%\ Removed_t^{r,i} = \frac{[influent]_t - [effluent]_{t+HRT}^{r,i}}{[influent]_t} \times 100\% \qquad \text{Equation 1}$$

In Equation 1, $[influent]$ is the average influent concentration of diuron or imidacloprid (ng/L), $[effluent]$ is the effluent concentration of diuron or imidacloprid of a single bioreactor, t is a given time point, and r, i is duplicate, i, of a given reactor type, r (continuous-flow or sequencing-batch). The average concentration of duplicate influent samples was used since the influent for all reactors came from the same feed water carboy.

The DOC data collected from the sequencing-batch style reactors was compared between AET treatments. The effects of the AET treatments on the effluent DOC concentrations of the four tested AETs of 0 h (n=3), 2h (n=14), 6 h (n=7), and 12 h (n=6), was compared using a one-way ANOVA. Following the significant ANOVA result (p = 1.7E-10), a post-hoc Tukey's Test was used to assess differences between the AET treatment groups.

2.2.7.2 Analysis of small-scale batch tests

The performance of the treatment batch (TB) and the microbial control (MC) small-scale batch reactors were compared for both the imidacloprid and diuron kinetic batch tests. The kinetic time series data was first fit to pseudo-first and pseudo-second order functions, as commonly performed with sorption data.[36-39] For both TB and MC, the pseudo-second order model fit the data best (Table A4) as determined by mean squared error (MSE) and root mean squared error (RSE). The comparison between TB and MC sets was conducted by the addition of an interaction term into the pseudo-second order model to see whether there was a significant difference between modelling the TB and MC separately, or together as one treatment. Complete data (i.e., both TB and MC data) for each pesticide were fit to a pseudo-second order model with an interaction term (Eq. 2).

$$\frac{C_t}{C_0} = 1 - \frac{(k_2+bG)C_0 t}{1+ (k_2+bG)C_0 t} \qquad \text{Equation 2}$$

In Equation 2, C_t is the aqueous pesticide concentration at time t (ng/L), C_0 is the aqueous pesticide concentration at the initial time point (ng/L), k_2 is the second order rate constant (h^{-1}), G is a binary treatment group code (TB = 1 and MC = 0), and b is the model interaction coefficient. If the fitted interaction coefficient (b) is statistically different from 0, we conclude that the two treatment groups (TB and MC) are best modelled separately, and as such, are two statistically different functions. If b is not statistically different from 0, we conclude that the two treatment groups are best modelled together and are therefore statistically similar.

2.3 Results and discussion

2.3.1 Field reactor monitoring and bench-scale reactor construction

2.3.1.1 Field-scale monitoring

Monitoring of the Multichannel Bioreactor produced several expected biochemical patterns. First, denitrification was achieved across all the woodchip channels as exhibited by nitrate removal. Removal varied between channels as well as between sampling events, from a low of 17% to a high of >99% (Figure A2). Highly variable denitrification rates have been reported for a variety of field-scale woodchip bioreactors.[15] Nitrate removal between channels and sampling dates in this study was likely influenced by ambient temperature changes[18], channelization caused by sedimentation and storm events, potential leakage between bioreactor channels (observed in April 2019), and changing influent conditions. Influent nitrate concentration varied between ~10 mg NO_3 – N/L to ~ 60 mg NO_3 – N/L. Variability in influent nitrate was expected due to periodic fertilizer application and increased transport of fertilizer during rain events[40,41] across the relatively large agricultural watershed that feeds the bioreactors.

Measurements along the length of the reactors yielded expected patterns for dissolved oxygen and redox potential (ORP). As shown in Figure A2.B, the inlet of the woodchip channels typically exhibited a medium to high redox potential (25 to 200 mV), along with a dissolved oxygen concentration of about 6 to 8 mg/L. Along the length of the woodchip bioreactors, both ORP and DO dropped, eventually reaching conditions under which microbiological denitrification typically occurs (ORP below about 50 mV and DO around 0 mg/L).[42] This pattern has been reported in other woodchip bioreactors[43,44] and is consistent with microbial metabolism energetics.[18] Measurements taken of sulfate, pH, electrical conductivity, and temperature yielded little variability both spatially and seasonally, and are provided in Figure A10. Dissolved organic carbon (DOC) ranged from 7.5 to 21.5 mg-C/L.

Widespread application of imidacloprid and diuron in the study region was evident from field sampling results (Figure A2.C). Imidacloprid and diuron were detected in all grab samples

taken from the influent and effluent of the three field-scale woodchip bioreactors during six sampling events. Yet systematic evaluation of the pesticide removal potential of the field-scale bioreactors proved challenging. Influent and effluent concentrations of imidacloprid and diuron were highly variable, ranging from 30.2 to 898 ng/L of imidacloprid (February 2019 woodchip channel effluent, and August 2018 woodchip channel effluent, respectively), and 6.52 to 372 ng/L of diuron (May 2019 influent, and June 2018 influent, respectively). Unlike observations of nitrate removal, removal of either imidacloprid or diuron across the woodchip bioreactors was inconsistent at best (Figure A2.C). Because of their frequent detection in the field, imidacloprid and diuron were chosen as focal compounds for bench-scale experiments. Despite known sorptive capacity of woodchips,[23,24,45] the variable concentrations of pesticides observed in the field highlights the need to understand sorptive and biodegradative removal in woodchip bioreactors, and how routes of removal (sorption, aerobic, and anaerobic degradation) can be combined in a treatment cycle.

2.3.1.2 Hydraulic and biochemical comparison between field- and bench-scale continuous-flow reactors

The bulk hydraulic conditions of the bench-scale continuous-flow reactors successfully mirrored those of the field reactors. Bromide tracer results indicated similar dispersion behaviors between woodchip Channel 5 of the sampled field bioreactor and the bench-scale continuous-flow reactor, while woodchip Channel 1 of the field bioreactor exhibited earlier breakthrough (Figure A13).[26] The following comparison considers Channel 5, as this channel was more closely mirrored by bench-scale hydraulics: the average residence times for both the field and bench-scale reactors were approximately 43 hours, well above the theoretical HRT of 24 hours. The dispersion

coefficients (1/Pe) for Channel 5 and the bench-scale reactor were less similar (0.045 and 0.156[b], respectively), indicating greater levels of dispersion at the bench-scale. As maintaining a similar HRT between the field and bench-scale reactors was the primary aim and dispersion levels observed in the present study at both field- and bench-scales are not uncommon,[17,28] differences in dispersion characteristics between the two scales were not further assessed.

The dissolved oxygen and ORP measurements were also similar between the bench-scale and field reactors. The DO consistently measured <1 mg/L at the bioreactor outlets and the ORP measured well below -50 mV. Despite similar operating conditions, the bench-scale continuous-flow reactors exhibited consistently high levels of denitrification as compared to field bioreactors (upwards of 70% removal) when fed an influent of ~20 mg NO_3 – N/L (Figure A14).

2.3.2 Side by side comparisons between bench-scale reactor designs

A sequencing-batch configuration may offer several treatment benefits over a continuous-flow reactor configuration. First, the batch-style hydraulics inherently eliminates the formation of preferential flow paths and short-circuiting. Under these conditions, treatment performance can be more accurately predicted because the theoretical HRT approximately equals the actual HRT. Second, integrating an aerobic phase into woodchip bioreactor operation may stimulate denitrification by allowing a short-term increase in DOC. Incorporation of drying-rewetting (DRW) cycles in the operation of a woodchip bioreactor increased nitrate removal by 71% to 81% immediately after rewetting as compared to the continuously submerged continuous-flow design.[46] This improvement may be linked to the generation of bioavailable DOC by aerobic lignocellulose degradation.[47,48] We hypothesized that incorporation of an aerobic phase into the reactor operation

[b] 95% confidence intervals for Channel 5 Pe [18.89, 25.38], and for bench-scale Pe [4.50, 8.35].

would also provide improved pesticide treatment performance, as aerobic transformation of both imidacloprid[49,50] and diuron[51,52] by microbes have been previously observed.

2.3.2.1 Nitrate reduction

We compared the denitrification performance of the continuous-flow and sequencing-batch style reactors in a series of side-by-side experiments with different hydraulic residence times. The AET of the sequencing-batch style reactor was held constant at 0 h for the duration of this comparison. The sequencing-batch style reactor consistently reduced nitrate at greater levels for each examined HRT than the continuous-flow reactor (Figure A14.a).

Using nitrate removal data from the sequencing-batch reactor, we constructed three different denitrification models using the differential method, integral method, and a nonlinear regression fitting to the commonly employed Michaelis-Menten equation[53,54] (details in Figure A12). Obtained rate parameters of each method are in Table A2. Rate constants (k) obtained from the differential (0.187 h^{-1}, 90% CI: [0.005, 7.52]) and integral (0.223 h^{-1}, 90% CI: [0.174, 0.272]) methods are comparable to rates obtained by Ghane et al.[44], who found first-order reaction rate constants (k) between 0.21 and 0.27 h^{-1} for dosed influent nitrate concentrations of 14.9 and 25.5 mg-N/L. Ghane et al.[44] also obtained K_m and V_{max} values of 7.2 mg-N/L and 7.1 mg-N/L·h, respectively. Of the three models we considered (Table A3), the Michaelis-Menten model fit has the lowest mean squared error (MSE) and root mean squared error (RSE). This result is theoretically consistent, as the model is derived from an enzymatic reaction network; the V_{max} parameter is a function of enzyme density, $V_{max} = k_{cat}[E]_T$, where $[E]_T$ is total enzyme concentration, and k_{cat} is the catalytic rate constant.[18] Zero-[26,55] and first order[56] models using nitrate reduction data have also been used to describe denitrification in similar bioreactors, and

characterize high (> K_m) and low (< K_m) influent substrate concentrations in Michaelis-Menten kinetics, respectively.[18] Krone et al.[26] found a zero-order denitrification model best fit the nitrate data from the field bioreactor managed by the Central Coast Wetlands Group (CCWG), within the observed range of influent nitrate concentration (7.5 to 60.8 mg/L). The relatively slower denitrification rate of Krone et al.'s [26] field-scale model (k = 0.91 mg-N/L·h; adjusted to 22°C using Arrhenius constant, θ, 1.12) as opposed to the V_{max} of 2.19 mg-N/L·h of the present bench-scale model (Figure A12) may be due to several differences between the two systems: 1) influent composition of the field bioreactor system was variable which may have indirectly slowed denitrifying activity, while the bench-scale reactors were run around steady state; 2) the microbial community composition in the bench-scale reactors may have shifted from its native state while in the lab environment, therefore shifting kinetic characteristics; 3) the bench-scale model was constructed with far fewer data points than Krone et al.'s [26] field-scale model, thus may not be as representative as Krone et al.'s more thorough model. Nonetheless, as the Michaelis-Menten K_m value of 4.8 mg/L of the present study is below most of the field influent nitrate concentrations, Krone et al.'s[26] conclusion that zero-order kinetics (non-substrate-limited) best explained their data is consistent with our findings.

Differences in carbon substrate (electron donor) characteristics can also create disparities in denitrification observations. Because denitrification kinetics are influenced by the concentration of labile carbon substrate as the electron donor, variations in both carbon concentration and carbon source can explain the range of fitted model parameters found in previous literature.[18,57] Moreover, differences in carbon substrate may also influence which empirical rate law (i.e., zero-order, first-order, or Michaelis-Menten) best fits a specific set of data. Influent concentrations of DOC to the field-scale system (7.46 to 21.5 mg-C/L from grab samples; Figure A10) may help to explain why

the field-scale model constructed by Krone et al.[26] was not substrate limited, thus best followed zero-order kinetics. No additional DOC was fed into bench-scale reactors to complement DOC production from the woodchip media. For the purposes of the present study, carbon substrate dependencies were not examined in depth because our denitrification observations were to confirm the occurrence of denitrification in the bench-scale reactors and were generally on par with similar experimental denitrification studies.[44,55,56]

To examine the potential for a longer aerobic phase to ultimately increase denitrification rates in sequencing-batch bioreactors, we assessed the impact of AET on denitrification while keeping the HRT constant at 12 h. We found that denitrification was not impacted by an increase in AET and thus the introduction of appreciable DO in the reactors for several hours after refilling neither achieved greater nitrate removal, nor compromised denitrification (Figure A15). The consistency in denitrification observed with increasing AET was accompanied by a steady increase in effluent DOC (Figure A3). Robertson[58] demonstrated that greater levels of DOC leached from newer woodchips increased denitrification rates as compared to woodchips that had been used for several years. Greater denitrification rates may also be achieved in sequencing-batch style woodchip bioreactors with longer "unsaturated" times.[47] However, because nitrate was almost entirely removed ($\geq$ 85 %) across all examined AET values in the present study, the explicit relationship between DOC and denitrification rate cannot be described. The attribution of greater denitrification rates to greater available DOC levels is reasonable in a laboratory context where the feed water to the reactors is low in DOC, making it a limiting reactant for facultative anaerobes. In contrast, the influent DOC concentration in the field bioreactors ranged between 7.46 mg-C/L and 21.5 mg-C/L and likely did not limit denitrification, therefore a relationship between denitrification and DOC would not be apparent from the field data (Figure A10).

2.3.2.2 Pesticide Treatment Potential

Three side-by-side joint pesticide and nitrate spiking experiments were carried out to evaluate the potential removal of imidacloprid and diuron alongside nitrate under the two reactor operating conditions. Continuous-flow reactors were operated with an HRT of 24 h, and the sequencing-batch reactors were operated with an HRT of 12 h and an AET of 12 h. The use of alternating full and dry cycles of the batch reactors was intended to assess the effect of cycling redox conditions on denitrification rates, as well as to assess potential for aerobic pesticide degradation. The introduction of AET to the treatment cycle created about 4 hours after refilling during which time the dissolved oxygen concentration remained well above 1 mg/L (Figure A7). Previous studies have observed aerobic biodegradation of diuron within the first 24 hours,[52] however removal rates for both imidacloprid and diuron are more often measured after several weeks.[25,49,50]

Each experiment was replicated three times using different batches of woodchips collected from the same field reactor (collected in February, August, and October 2020). The three experiments exhibited an average percent removal of diuron of 83.5 ± 8.0% across the continuous-flow reactors, and 82.0 ± 9.1% across the sequencing-batch reactors. During the August and October side-by-side experiments, removal of imidacloprid averaged 61.6 ± 11.9% across the continuous-flow reactors, and 56.2 ± 12.6% across the sequencing-batch reactors. The effluent levels of both diuron and imidacloprid were not significantly different between the two reactor types ($p = 0.66$ and $p = 0.32$, respectively; Student's two-tailed, homoscedastic T-Test). This result is consistent with the conclusions of the kinetic batch tests (section 2.3.2.3). Throughout all trials, denitrification levels between the two reactor types remained comparable. Therefore, the

sequencing-batch reactor design achieved comparable levels of treatment of imidacloprid, diuron, and nitrate as the continuous-flow design, with half the hydraulic residence time (Figure A4).

While the removal of diuron was consistent across the side-by-side experimental replicates, the removal of imidacloprid was low across both the reactor types for the February 2020 woodchip collection. In February, removal of imidacloprid averaged 24.6 ± 10.1% in continuous-flow reactors and 10.5 ± 13.5% in sequencing-batch style reactors, while removal averaged 61.6 ± 11.9% and 56.2 ± 12.6% in the August and October experiments. Imidacloprid removal in related kinetic batch tests averaged 56.9 ± 8.1% (treatment batch, TB) after 48 hours. Because different batches of woodchips were used for the kinetic batch tests and each side-by-side experiment, we expect that the discrepancy in imidacloprid removal in February 2020 was due to higher concentrations of imidacloprid sorbed on the woodchips, creating a greater background concentration than during subsequent experiments. Pesticide extractions of each collected batch of woodchips confirmed that the woodchips collected for the February bench-scale reactor experiment contained about a 7.5-fold greater concentration of imidacloprid than the following two woodchip batches (Figure A16). Because the drainage canal that feeds the multichannel field bioreactor collects from 4km^2 of cultivated land growing similar crops (e.g., artichokes, strawberries), we expected fluctuations in influent concentration throughout the growing year (e.g., Figure A2), which may further influence the sorbed concentration to the bioreactor woodchip media.

Introducing an air exposed time (AET) to the treatment cycle did not appear to promote microbial degradation of the examined pesticides. While microbial degradation of pesticides has often been observed under aerobic conditions, the treatment cycle times of this study were likely too short to realize any significant degradation.[59] Treatment would also be limited to adsorbed

pesticides on the woodchips during the aerobic phase. Sabourmoghaddam et al.[60] observed between 25.4% and 45.5% imidacloprid degradation by microbial soil isolates over 25 days. Liu et al.[25] observed 22.5% degradation of imidacloprid by a soil consortium over 25 days. Microbial degradation of pesticides under reducing conditions has also been explored, with promising results. Mulligan et al.[61] observed about a 3-fold decrease in clothianidin half-life under flooded, anaerobic rice field conditions. Similar to the results under aerobic conditions, past studies found that degradation under anaerobic conditions typically occurs over much longer timescales (several days to months) irrespective of the throughput rate of woodchip bioreactors.[62,63] Integrating longer sequencing (HRT/AET) timescales into woodchip bioreactor treatment cycles may improve microbial degradation of pesticides.

2.3.2.3 Evaluating removal mechanisms in kinetic batch studies

Imidacloprid and diuron kinetic studies indicated that sorption was the main mechanism of removal for both compounds, and that sorption occurred independently of denitrification (Figure A5). We observed imidacloprid sorption between 440.4 and 532.0 ng/g-woodchip (dwt) and diuron sorption of between 468.6 and 553.8 ng/g-woodchip (dwt) within 24 hours, after which no appreciable increase in sorption occurred (Figure A4). Imidacloprid adsorption coefficients (K_d) were 40.5 ± 4.34 L/kg and 47.8 ± 11.5 L/kg for the microbial control (MC) and treatment batch (TB) samples, respectively. Diuron adsorption coefficients were 78.2 ± 21.3 L/kg and 98.0 ± 37.8 L/kg for MC and TB samples, respectively. Mandal and Singh[64] reported adsorption coefficients of between 84.81 to 106.6 L/kg for imidacloprid on eucalyptus bark. Huang et al.[45] reported an adsorption coefficient of 129.6 L/kg for diuron on shredded cedar mulch. The lower adsorption coefficients obtained by this study as compared to others may have been due to the use of aged

(used) woodchips in the present study, and/or differences in mean wood particle surface area between studies.[30]

Comparisons of the pseudo-second order diuron removal models (Table A5) of the microbial control (MC) and treatment batch (TB) datasets showed no significant difference between the treatments ($b = 0.00$, $p = 1.00$), indicating that microbial degradation of diuron did not occur within the studied timeframe. This finding is consistent with other batch tests investigating removal mechanisms of atrazine ($\log K_{ow} = 2.60$)[20,30] and bentazone (logKow = -0.46),[20] for which sorption is the strongest driver of removal across woodchip systems.

The same model comparison performed with the imidacloprid treatments yielded a small, but significant difference between the TB and MC models ($b = 4.88 \times 10^{-7}$, $p = 0.019$), suggesting that microbial activity contributed to imidacloprid removal in the treatment batch bioreactors. A microbial contribution to imidacloprid abatement is reasonable considering previous work showing anaerobic degradation of imidacloprid (half-life 27 days in anaerobic soil[7]). However, the magnitude of the observed degradation is small, again demonstrating sorption to be the primary removal mechanism under the conditions evaluated. Mortensen et al.[65] demonstrated the potential for microbial degradation in denitrification woodchip bioreactors by isolating microbes directly from field bioreactors for selective culturing. The authors grew several strains of facultative anaerobes on minimal growth media with selected pesticides as the sole carbon sources, demonstrating that microbial degradation in woodchip bioreactors can play a role in removal.[65] Studying efficient means to upregulate microbial enzymes capable of pesticide degradation in such bioreactors could lead to improved designs for the degradation of pesticides across BMPs like woodchip bioreactors.[66]

An isotherm batch test set up in the same manner as the microbial control (MC) kinetic batch tests was conducted for imidacloprid to characterize sorption behavior on woodchips collected from the multichannel bioreactor. This isotherm experiment was performed to further evaluate discrepancies found between bench-scale reactor runs. The nls() function of base R was used to perform a nonlinear regression fitting the resulting data to a Freundlich isotherm model, yielding a Freundlich constant (K_F) of 245 L/kg and exponent of non-linearity (1/n) of 0.751 (Figure A17). Leiva et al.[67] observed K_F values of 290.4 L/kg and 157.4 L/kg, and 1/n values of 0.77 and 1 for imidacloprid on peat and pine bark, respectively. Mandal and Singh[64] obtained a K_F value of 85.71 L/kg, and a 1/n value of 0.920 for imidacloprid sorption to eucalyptus bark. Sorption coefficients can vary significantly based on factors such as solution ion content,[68] and neonicotinoids such as imidacloprid have been shown to be highly influenced by adsorbent organic matter content.[69] Nonetheless, the sorption behavior of imidacloprid in the present study is consistent with these previous results.

The imidacloprid isotherm results also offered insight to the inconsistent imidacloprid removal observed during the February side-by-side experiment (section 3.2.2). Examining the imidacloprid sorption isotherm on woodchips from the earlier batch tests, the bench-scale reactor effluent concentrations and pre-adsorbed imidacloprid mass concentration from the February experiments suggest the reactors were indeed operating near isothermal equilibrium, further explaining the poor imidacloprid removal (Figure A17).

2.4 Conclusions and future considerations

Taken together, this study suggests that a sequencing-batch operation configuration for woodchip bioreactors may provide improved treatment of nitrate and opportunities for enhanced

system control. The sequencing-batch style bioreactor can reduce nitrate in less time than continuous-flow systems, allowing for greater drainage throughput without sacrificing effluent nitrate concentrations. A sequencing-batch configuration also provides opportunities for tailored controls that could improve pesticide removal. Relatively rapid sorption of pesticides to the woodchip media (<24 h for the relatively hydrophilic compound imidacloprid) is expected for unloaded woodchips. Previous studies suggest a timescale of microbial degradation of pesticides over several days.[7,59] A periodic "extended hold time" (increasing HRT and/or AET) over several weeks following a sorption phase of operation may enhance pesticide degradation. The construction of sequencing-batch, woodchip bioreactors in parallel would enable this strategy by switching influent and woodchip loading between parallel channels, much like some commercial adsorbent beds.[18] The increased level of control would allow users to adjust both HRT and AET in response to fertilizer and pesticide application schedules. Once pesticide sorption is achieved in one bioreactor, users could then take it offline to allow for microbial degradation of retained pesticides. Future work is needed to evaluate parallel operating configurations, scaling for incoming flows, and promoting *in situ* pesticide degradation.

2.5 References

(1) Capel, P.; McCarthy, K.; Coupe, R.; Grey, K.; Amenumey, S.; Baker, N.; Johnson, R. *The Quality of Our Nation's Waters: Agriculture--A River Runs Through It--The Connections Between Agriculture and Water Quality*; Reston, VA, 2018.

(2) Anderson, B.; Hunt, J.; Markiewicz, D.; Larsen, K. Toxicity in California Waters. Surface Water Ambient Monitoring Program. *Calif. State Water Resour. Control Board* **2010**.

(3) Hayasaka, D.; Korenaga, T.; Suzuki, K.; Saito, F.; Sánchez-Bayo, F.; Goka, K. Cumulative Ecological Impacts of Two Successive Annual Treatments of Imidacloprid and Fipronil on Aquatic Communities of Paddy Mesocosms. *Ecotoxicol. Environ. Saf.* **2012**, *80*, 355–362. https://doi.org/10.1016/j.ecoenv.2012.04.004.

(4) Ensminger, M. P.; Budd, R.; Kelley, K. C.; Goh, K. S. Pesticide Occurrence and Aquatic Benchmark Exceedances in Urban Surface Waters and Sediments in Three Urban Areas of California, USA, 2008-2011. *Environ. Monit. Assess.* **2013**, *185* (5), 3697–3710. https://doi.org/10.1007/s10661-012-2821-8.

(5) Morrissey, C. A.; Mineau, P.; Devries, J. H.; Sanchez-Bayo, F.; Liess, M.; Cavallaro, M. C.; Liber, K. Neonicotinoid Contamination of Global Surface Waters and Associated Risk to Aquatic Invertebrates: A Review. *Environment International*. Elsevier Ltd January 1, 2015, pp 291–303. https://doi.org/10.1016/j.envint.2014.10.024.

(6) Batikian, C. M.; Lu, A.; Watanabe, K.; Pitt, J.; Gersberg, R. M. Temporal Pattern in Levels of the Neonicotinoid Insecticide, Imidacloprid, in an Urban Stream. *Chemosphere* **2019**, *223*, 83–90. https://doi.org/10.1016/j.chemosphere.2019.01.165.

(7) Koshlukova, S. Imidacloprid Risk Characterization Document Dietary and Drinking Water Exposure. *Health Assessment Section, Medical Toxicology Branch, Department of Pesticide Regulation, California EPA* **2006**.

(8) Tomlin, C. *The Pesticide Manual: A World Compendium*, 15th ed.; MacBean, C., Ed.; CABI: Alton, Hampshire, 2009.

(9) Lee, R.; Abdel-Saheb, I.; Breithaupt, J.; Bailey, T. Environmental Risk Assessment for the Reregistration of Diuron (Case 818790). USEPA **2001**.

(10) Longley, K.; Creedon, P. Central Valley Diruon Total Maximum Daily Load and Basin Plan Amendment: Informational Document. *Central Valley Regional Water Quality Control Board, CEQA Scoping Meeting* **2012**.

(11) Velki, M.; Di Paolo, C.; Nelles, J.; Seiler, T. B.; Hollert, H. Diuron and Diazinon Alter the Behavior of Zebrafish Embryos and Larvae in the Absence of Acute Toxicity. *Chemosphere* **2017**, *180*, 65–76. https://doi.org/10.1016/j.chemosphere.2017.04.017.

(12) *Pesticide Use Reporting, Annual 2018*; California Department of Pesticide Regulation, 2020.

(13) Belden, J. B.; Gilliom, R. J.; Lydy, M. J. How Well Can We Predict the Toxicity of Pesticide Mixtures to Aquatic Life? *Integr. Environ. Assess. Manag.* **2007**, *3* (3), 364–372. https://doi.org/10.1002/ieam.5630030307.

(14) Klarich, K. L.; Pflug, N. C.; DeWald, E. M.; Hladik, M. L.; Kolpin, D. W.; Cwiertny, D. M.; LeFevre, G. H. Occurrence of Neonicotinoid Insecticides in Finished Drinking Water and Fate during Drinking Water Treatment. *Environ. Sci. Technol. Lett.* **2017**, *4* (5), 168–173. https://doi.org/10.1021/acs.estlett.7b00081.

(15) Christianson, L. E.; Bhandari, A.; Helmers, M. J. A Practice-Oriented Review of Woodchip Bioreactors for Subsurface Agricultural Drainage. *Appl. Eng. Agric.* **2012**, *28* (6), 861–874. https://doi.org/10.13031/2013.42479.

(16) Clark, R. *Oceanmist Bioreactor*; Moss Landing, CA, 2017.

(17) Christianson, L. E.; Hanly, J. A.; Hedley, M. J. Optimized Denitrification Bioreactor Treatment through Simulated Drainage Containment. *Agric. Water Manag.* **2011**, *99* (1), 85–92. https://doi.org/10.1016/j.agwat.2011.07.015.

(18) *Wastewater Engineering: Treatment and Reuse - George Tchobanoglous, Franklin Louis Burton, H. David Stensel, Metcalf & Eddy - Google Books*; Metcalf, Eddy, Eds.; 2003.

(19) Blowes, D. W.; Robertson, W. D.; Ptacek, C. J.; Merkley, C. Removal of Agricultural Nitrate from Tile-Drainage Effluent Water Using in-Line Bioreactors. *J. Contam. Hydrol.* **1994**, *15* (3), 207–221. https://doi.org/10.1016/0169-7722(94)90025-6.

(20) Krause Camilo, B.; Matzinger, A.; Litz, N.; Tedesco, L. P.; Wessolek, G. Concurrent Nitrate and Atrazine Retention in Bioreactors of Straw and Bark Mulch at Short Hydraulic Residence Times. *Ecol. Eng.* **2013**, *55* (3), 101–113. https://doi.org/10.1016/j.ecoleng.2013.02.010.

(21) van Driel, P. W.; Robertson, W. D.; Merkley, L. C. Upflow Reactors for Riparian Zone Denitrification. *J. Environ. Qual.* **2006**, *35* (2), 412–420. https://doi.org/10.2134/jeq2005.0027.

(22) Hoover, N. L. Denitrification Woodchip Bioreactor Two-Phase Column Study: Evaluation of Nitrate Removal at Various Hydraulic Retention Times and Effect of Temperature on Denitrification Rates. *Graduate Theses and Dissertations, Iowa State University* **2012**. http://lib.dr.iastate.edu/etd/12348.

(23) Aslan, Ş.; Türkman, A. Combined Biological Removal of Nitrate and Pesticides Using Wheat Straw as Substrates. *Process Biochem.* **2005**, *40* (2), 935–943. https://doi.org/10.1016/j.procbio.2004.02.020.

(24) Tran, V. S.; Ngo, H. H.; Guo, W.; Zhang, J.; Liang, S.; Ton-That, C.; Zhang, X. Typical Low Cost Biosorbents for Adsorptive Removal of Specific Organic Pollutants from Water. *Bioresource Technology*. Elsevier Ltd April 1, 2015, pp 353–363. https://doi.org/10.1016/j.biortech.2015.02.003.

(25) Liu, Z.; Dai, Y.; Huang, G.; Gu, Y.; Ni, J.; Wei, H.; Yuan, S. Soil Microbial Degradation of Neonicotinoid Insecticides Imidacloprid, Acetamiprid, Thiacloprid and Imidaclothiz and Its Effect on the Persistence of Bioefficacy against Horsebean Aphid Aphis Craccivora Koch after Soil Application. *Pest Manag. Sci.* **2011**, *67* (10), 1245–1252. https://doi.org/10.1002/ps.2174.

(26) Krone, P.; Clark, R.; Adelaars, J.; Leandro, M.; Henson, A.; Williamson, J.; Bischel, H.; Wright, O.; Watson, F. Using a Tanks-in-Series Model to Determine Nitrate Reaction Kinetics for a Pump-Assisted Open-Channel Woodchip Bioreactor Treating Tile Drain Agricultural Water. *Ecol. Eng.* **2021**. [submitted]

(27) Crittenden, J.; Trussell, R.; Hand, D.; Howe, K.; Tchobanoglous, G. *MWH's Water Treatment: Principles and Design*, 3rd ed.; John Wiley & Sons, Inc.: Hoboken, NJ, 2012.

(28) Hoover, N. L.; Bhandari, A.; Soupir, M. L.; Moorman, T. B. Woodchip Denitrification Bioreactors: Impact of Temperature and Hydraulic Retention Time on Nitrate Removal. *J. Environ. Qual.* **2016**, *45* (3), 803–812. https://doi.org/10.2134/jeq2015.03.0161.

(29) de Souza Araújo, E.; Pimenta, A. S.; Feijó, F. M. C.; Castro, R. V. O.; Fasciotti, M.; Monteiro, T. V. C.; de Lima, K. M. G. Antibacterial and Antifungal Activities of Pyroligneous Acid from Wood of *Eucalyptus Urograndis* and *Mimosa Tenuiflora*. *J. Appl. Microbiol.* **2018**, *124* (1), 85–96. https://doi.org/10.1111/jam.13626.

(30) Ilhan, Z. E.; Ong, S. K.; Moorman, T. B. Herbicide and Antibiotic Removal by Woodchip Denitrification Filters: Sorption Processes. *Water. Air. Soil Pollut.* **2012**, *223* (5), 2651–2662. https://doi.org/10.1007/s11270-011-1057-5.

(31) Moschet, C.; Lew, B. M.; Hasenbein, S.; Anumol, T.; Young, T. M. LC- and GC-QTOF-MS as Complementary Tools for a Comprehensive Micropollutant Analysis in Aquatic Systems. *Environ. Sci. Technol.* **2017**, *51* (3), 1553–1561. https://doi.org/10.1021/acs.est.6b05352.

(32) Moschet, C.; Anumol, T.; Lew, B. M.; Bennett, D. H.; Young, T. M. Household Dust as a Repository of Chemical Accumulation: New Insights from a Comprehensive High-Resolution Mass Spectrometric Study. *Environ. Sci. Technol.* **2018**, *52* (5), 2878–2887. https://doi.org/10.1021/acs.est.7b05767.

(33) Kim, K.; Shin, H.; Wong, L.; Young, T. M.; Bennett, D. H. Temporal Variability of Indoor Dust Concentrations of Semivolatile Organic Compounds. *Indoor Air* **2020**, *31* (3), 693–701. https://doi.org/10.1111/ina.12759.

(34) Goel, R. K.; Cooper, A. T.; Flora, J. R. V. Sodium Azide Interference in Chemical and Biological Testing. *J. Environ. Eng. Sci.* **2003**, *2*, 407–411. https://doi.org/10.1139/S03-043.

(35) Lipps, W.; Baxter, T. 5310 Total Organic Carbon (TOC). *Standard Methods for the Examination of Water and Wastewater*; Braun-Howland, Eds. 2018. https://doi.org/10.2105/SMWW.2882.104.

(36) Ho, Y. S.; McKay, G. Pseudo-Second Order Model for Sorption Processes. *Process Biochem.* **1999**, *34* (5), 451–465. https://doi.org/10.1016/S0032-9592(98)00112-5.

(37) Simonin, J. P. On the Comparison of Pseudo-First Order and Pseudo-Second Order Rate Laws in the Modeling of Adsorption Kinetics. *Chem. Eng. J.* **2016**, *300*, 254–263. https://doi.org/10.1016/j.cej.2016.04.079.

(38) Brandani, S. Kinetics of Liquid Phase Batch Adsorption Experiments. *Adsorption* **2021**, *27*, 353–368. https://doi.org/10.1007/s10450-020-00258-9.

(39) Wang, J.; Guo, X. Adsorption Kinetic Models: Physical Meanings, Applications, and Solving Methods. *Journal of Hazardous Materials*. Elsevier B.V. May 15, 2020, p 122156. https://doi.org/10.1016/j.jhazmat.2020.122156.

(40) Gentry, L. E.; David, M. B.; Smith-Starks, K. M.; Kovacic, D. A. Nitrogen Fertilizer and Herbicide Transport from Tile Drained Fields. *J. Environ. Qual.* **2000**, *29* (1), 232–240. https://doi.org/10.2134/jeq2000.00472425002900010030x.

(41) Tomer, M. D.; Moorman, T. B.; Kovar, J. L.; Cole, K. J.; Nichols, D. J. Eleven Years of Runoff and Phosphorus Losses from Two Fields with and without Manure Application, Iowa, USA. *Agric. Water Manag.* **2016**, *168*, 104–111. https://doi.org/10.1016/j.agwat.2016.01.011.

(42) Song, S.-H.; Yeom, S.-H.; Choi, S.-S.; Yoo, Y.-J. Effect of Oxidation-Reduction Potential on Denitrification by Ochrobactrum Anthropi SY509. *J. Microbiol. Biotechnol.* **2003**, *13* (3), 473–476.

(43) Bock, E. M.; Coleman, B.; Easton, Z. M. Effect of Biochar on Nitrate Removal in a Pilot-Scale Denitrifying Bioreactor. *J. Environ. Qual.* **2016**, *45* (3), 762–771. https://doi.org/10.2134/jeq2015.04.0179.

(44) Ghane, E.; Fausey, N. R.; Brown, L. C. Modeling Nitrate Removal in a Denitrification Bed. *Water Res.* **2015**, *71*, 294–305. https://doi.org/10.1016/j.watres.2014.10.039.

(45) Huang, X.; Massoudieh, A.; Young, T. M. Measured and Predicted Herbicide Removal by Mulch. *J. Environ. Eng.* **2006**, *132* (8), 918–925. https://doi.org/10.1061/(asce)0733-9372(2006)132:8(918).

(46) Maxwell, B. M.; Birgand, F.; Schipper, L. A.; Christianson, L. E.; Tian, S.; Helmers, M. J.; Williams, D. J.; Chescheir, G. M.; Youssef, M. A. Drying-Rewetting Cycles Affect Nitrate Removal Rates in Woodchip Bioreactors. *J. Environ. Qual.* **2018**, *48* (1), 93–101. https://doi.org/10.2134/jeq2018.05.0199.

(47) Maxwell, B. M.; Birgand, F.; Schipper, L. A.; Christianson, L. E.; Tian, S.; Helmers, M. J.; Williams, D. J.; Chescheir, G. M.; Youssef, M. A. Increased Duration of Drying–Rewetting Cycles Increases Nitrate Removal in Woodchip Bioreactors. *Agric. Environ. Lett.* **2019**, *4* (1), 190028. https://doi.org/10.2134/ael2019.07.0028.

(48) Lynd, L. R.; Weimer, P. J.; van Zyl, W. H.; Pretorius, I. S. Microbial Cellulose Utilization: Fundamentals and Biotechnology. *Microbiol. Mol. Biol. Rev.* **2002**, *66* (3), 506–577. https://doi.org/10.1128/mmbr.66.3.506-577.2002.

(49) Dai, Y. J.; Yuan, S.; Ge, F.; Chen, T.; Xu, S. C.; Ni, J. P. Microbial Hydroxylation of Imidacloprid for the Synthesis of Highly Insecticidal Olefin Imidacloprid. *Appl. Microbiol. Biotechnol.* **2006**, *71* (6), 927–934. https://doi.org/10.1007/s00253-005-0223-3.

(50) Madhuban, G.; Debashis, D.; SK, J.; Shobhita, K.; Saumya, B.; SK, D. Biodegradation of Imidacloprid and Metribuzin by Burkholderia Cepacia Strain CH9. *Pestic. Res. J.* **2011**, *23* (1), 36–40.

(51) Ellis, P. A.; Camper, N. D. Aerobic Degradation of Diuron by Aquatic Microorganisms. *J. ENVIRON. SCI. Heal.* **1982**, *17* (3), 277–289. https://doi.org/10.1080/03601238209372319.

(52) Stasinakis, A. S.; Kotsifa, S.; Gatidou, G.; Mamais, D. Diuron Biodegradation in Activated Sludge Batch Reactors under Aerobic and Anoxic Conditions. *Water Res.* **2009**, *43* (5), 1471–1479. https://doi.org/10.1016/j.watres.2008.12.040.

(53) Strong, D. T.; Fillery, I. R. P. Denitrification Response to Nitrate Concentrations in Sandy Soils. *Soil Biol. Biochem.* **2002**, *34* (7), 945–954. https://doi.org/10.1016/S0038-0717(02)00026-3.

(54) Foglar, L.; Briški, F.; Sipos, L.; Vuković, M. High Nitrate Removal from Synthetic Wastewater with the Mixed Bacterial Culture. *Bioresour. Technol.* **2005**, *96* (8), 879–888. https://doi.org/10.1016/j.biortech.2004.09.001.

(55) Schipper, L. A.; Barkle, G. F.; Vojvodic-Vukovic, M. Maximum Rates of Nitrate Removal in a Denitrification Wall. *J. Environ. Qual.* **2005**, *34* (4), 1270–1276. https://doi.org/10.2134/jeq2005.0008.

(56) Leverenz, H. L.; Haunschild, K.; Hopes, G.; Tchobanoglous, G.; Darby, J. L. Anoxic Treatment Wetlands for Denitrification. *Ecol. Eng.* **2010**, *36*, 1544–1551. https://doi.org/10.1016/j.ecoleng.2010.03.014.

(57) Greenan, C. M.; Moorman, T. B.; Kaspar, T. C.; Parkin, T. B.; Jaynes, D. B. Comparing Carbon Substrates for Denitrification of Subsurface Drainage Water. *J. Environ. Qual.* **2006**, *35* (3), 824–829. https://doi.org/10.2134/jeq2005.0247.

(58) Robertson, W. D. Nitrate Removal Rates in Woodchip Media of Varying Age. *Ecol. Eng.* **2010**, *36* (11), 1581–1587. https://doi.org/10.1016/j.ecoleng.2010.01.008.

(59) Anhalt, J. C.; Moorman, T. B.; Koskinen, W. C. Biodegradation of Imidacloprid by an Isolated Soil Microorganism. *J. Environ. Sci. Heal. Part B* **2007**, *42* (5), 509–514. https://doi.org/10.1080/03601230701391401.

(60) Sabourmoghaddam, N.; Zakaria, M. P.; Omar, D. Evidence for the Microbial Degradation of Imidacloprid in Soils of Cameron Highlands. *J. Saudi Soc. Agric. Sci.* **2015**, *14* (2), 182–188. https://doi.org/10.1016/j.jssas.2014.03.002.

(61) Mulligan, R. A.; Tomco, P. L.; Howard, M. W.; Schempp, T. T.; Stewart, D. J.; Stacey, P. M.; Ball, D. B.; Tjeerdema, R. S. Aerobic versus Anaerobic Microbial Degradation of Clothianidin under Simulated California Rice Field Conditions. *J. Agric. Food Chem.* **2016**, *64* (38), 7059–7067. https://doi.org/10.1021/acs.jafc.6b02055.

(62) Wilber, G. G.; Wang, G. Biotransformation of Herbicides in the Presence of Various Electron Acceptors. *J. Air Waste Manag. Assoc.* **1997**, *47* (6), 690–696. https://doi.org/10.1080/10473289.1997.10463931.

(63) Seybold, C. A.; Mersie, W.; McNamee, C. Anaerobic Degradation of Atrazine and Metolachlor and Metabolite Formation in Wetland Soil and Water Microcosms. *J. Environ. Qual.* **2001**, *30* (4), 1271–1277. https://doi.org/10.2134/jeq2001.3041271x.

(64) Mandal, A.; Singh, N. Kinetic and Isotherm Error Optimization Studies for Adsorption of Atrazine and Imidacloprid on Bark of *Eucalyptus Tereticornis* L. *J. Environ. Sci. Heal. Part B* **2016**, *51* (3), 192–203. https://doi.org/10.1080/03601234.2015.1108817.

(65) Mortensen, Z.; Kato, J.; Silveus, J.; Valdez, A.; Hall, S.; Nimmers, K.; Haffa, A. L. M. Isolation of Microbial Populations with the Ability to Use Pesticides as a Sole Carbon Source in Multichannel Woodchip Bioreactors under a Controlled Environment. In *ACS Symposium Series*; American Chemical Society, 2019; Vol. 1308, pp 475–489. https://doi.org/10.1021/bk-2019-1308.ch024.

(66) Pang, S.; Lin, Z.; Zhang, W.; Mishra, S.; Bhatt, P.; Chen, S. Insights Into the Microbial Degradation and Biochemical Mechanisms of Neonicotinoids. *Frontiers in Microbiology*. Frontiers Media S.A. May 19, 2020, p 868. https://doi.org/10.3389/fmicb.2020.00868.

(67) Leiva, J. A.; Wilson, P. C.; Albano, J. P.; Nkedi-Kizza, P.; O'Connor, G. A. Pesticide Sorption to Soilless Media Components Used for Ornamental Plant Production and Aluminum Water Treatment Residuals. *ACS Omega* **2019**, *4* (18), 17782–17790. https://doi.org/10.1021/acsomega.9b02296.

(68) Spark, K. M.; Swift, R. S. Effect of Soil Composition and Dissolved Organic Matter on Pesticide Sorption. *Sci. Total Environ.* **2002**, *298* (1–3), 147–161. https://doi.org/10.1016/S0048-9697(02)00213-9.

(69) Aseperi, A. K.; Busquets, R.; Hooda, P. S.; Cheung, P. C. W.; Barker, J. Behaviour of Neonicotinoids in Contrasting Soils. *J. Environ. Manage.* **2020**, *276*. https://doi.org/10.1016/j.jenvman.2020.111329.

(70) Wrightwood, O. M.; Hattaway, M. E.; Young, T. M.; Bischel, H. N. Assessment of Woodchip Bioreactor Characteristics and Their Influences on Joint Nitrate and Pesticide Removal. *ACS Environ. Sci. Technol. Water* **2022**, *2* (1), 106–116. https://doi.org/10.1021/acsestwater.1c00277.

CHAPTER 3: EXPLORATION INTO THE PESTICIDE DEGRADATION CAPACITY OF MICROBIAL ESTERASES: AN ANALYSIS OF CATALYTIC ACTIVITY AND MOLECULAR INTERACTIONS

The chapter is structured as follows:

- Section 3.1 provides background on the role of enzyme treatment in bioremediation.
- Section 3.2 provides further detail on the study motivation and outlines objectives for the research discussed in this chapter.
- Section 3.3 presents materials and methods used.
- Section 3.4 summarizes and discusses results.
- Section 3.5 concludes.

3.1 Background

The use of enzymes for bioremediation of xenobiotics, among other contaminants, is a bioaugmentation technique that employs specific enzymes to a contaminated area, reactor, or sample. Enzymatic treatment of contaminated soils and waters has often been used as a "green" remediation technique, as treatment applications can be relatively more controlled and rapid than microbial augmentation, without the adverse environmental side effects of intensive chemical treatment.[1-4] Unlike microbial or phytoremediation, enzymatic treatment does not depend on the stability of a microbial or plant population to deliver treatment. Enzymatic treatment is also more specific than other chemical oxidation strategies such as ozone treatment. Enzymatic treatment can be tailored to specific contaminants by understanding the inherent specificity of enzymes and enzyme classes (i.e., the addition of specific enzymes for targeted purposes). Treatment enzymes can also be introduced in a variety of ways to improve their performance, including in the presence

of cofactors, coenzymes, and/or cosubstrates, as well as with means of immobilization to enhance enzyme stability and recovery.[5,6]

Two of the most thoroughly explored enzyme classes (ECs) for bioremediation purposes are oxidoreductases (EC 1) and hydrolases (EC 3).[7] Oxidoreductases are typically used for their ability to oxidize aromatic structures, especially those with reactive oxygen species and metals;[8] while hydrolases break a variety of aliphatic bonds depending on the enzymes' specificity. Hydrolases contain several subclasses, including esterase and lipase subclasses, both of which have been identified as enzyme groups able to transform organophosphate and pyrethroid pesticide classes.[9] While several mammalian gut enzymes[10] and insect enzymes[11] have also been explored for their potential to degrade xenobiotics, the vast majority of enzymes harnessed for bioremediation purposes are from environmental microbes. Many microorganisms isolated from contaminated soils and waters, and/or from wastewater samples,[12,13,14] have adapted and evolved in conditions favoring xenobiotic-[co]metabolism.

Advances in techniques to characterize enzymes has enabled identification of new enzymes capable of degrading target contaminants. Genome sequencing offers detailed annotation of amino acid sequences critical to catalysis, and, following this, sequence homology has led to the identification of candidate enzymes for screening assays against various xenobiotics. Through careful activity assays, novel and specific degradation pathways have been discovered for xenobiotics (e.g., degradation of malathion via novel carboxylesterase[15] and of beta cypermethrin by *Bacillus cerus*[16]). A step further, gene clusters and enzymes have been engineered for use in specific scenarios and treatment trains. For instance, Zuo et al. (2015)[17] were able to combine both an organophosphate-degrading gene and a carboxylesterase capable of pyrethroid degradation onto a plasmid transformed into a soil bacterium, and saw degradation of both compound classes. While

degradation of xenobiotics using genetically engineered microbial products can improve mineralization efficiency, concerns over the impact of introducing engineered genes and/or enzymes into treatment trains or uncontained environments for treatment raises possible concerns. Concerns include horizontal gene transfer among indigenous microbial communities that may thwart existing ecological dynamics.[18,19] Moreover, it is generally preferable from the perspective of ecological resiliency to maintain species diversity in remediation schemes to avoid overdependence on one species and to encourage interspecies symbiosis. However, to better understand enzymatic treatment strategies, a systematic understanding of how classes of enzymes interact with classes of contaminants is needed. Additional "-omics" tools can help to expand general understanding of protein roles and gene dynamics involved in various environments and sub-environments.[20] There is still much work to be done in bioinformatics mining to discover additional enzymes and enzyme characteristics to obtain a comprehensive toolkit.

3.2 Motivation

3.2.1 Ex vivo and in silico screening approaches for assessment of catalytic competency

The bulk of existing research that assesses wild-type enzymes and related gene(s) focuses on isolate species. While this workflow limits the number of enzymes characterized at one time, it is useful for several reasons: 1) the three-dimensional crystal structures of isolated proteins can be crystallized for database submission, sometimes under multiple experimental conditions, and utilized in computational simulations; 2) enzyme activities toward specific ligands can be associated with protein database entries; 3) degradation pathways are more easily parsed in monocultures and/or single enzyme assays, as compared to consortium-derived degradation profiles. Such detailed information is important for furthering the understanding of specific

molecular features and their functionality. Class-based activity screening—both by enzyme class and by xenobiotic class—offers a high-level assessment of the variance of activity and interactions between sets of potential substrate/enzyme pairs. I hypothesized that *in silico* class-based screening will highlight binding patterns associated with activity, and that ligands may exhibit preferences to [a] specific enzyme subclass(es). *Ex vivo* studies are required here to confirm activities of enzyme/ligand pairs that have not been previously assessed. As both homologous enzyme and ligand structures can share similar biochemical activities,[21] these class-based screening approaches provide information on the extent to which this is true and can therefore inform more targeted xenobiotic remediation.

The current study employs a screening approach to better characterize the esterase class of enzymes (EC 3.1; hydrolases acting on ester bonds) in terms of catalytic activity against a selection of pyrethroids. Specifically, I aim to elucidate the substrate specificity and capacity of wild-type microbial esterases to degrade pyrethroids, structurally similar "alternative esters", and known esterase and lipase substrates. Esterases belong to the α/β hydrolase fold family and contain a highly conserved catalytic triad, typically a serine, histidine, and either glutamic or aspartic acid. The serine is organized in a Gly-X-Ser-X-Gly sequence,[21] making for a consistent nucleophile position across all enzyme candidates, where 'X' is replaceable by other amino acids variable between individual enzymes. Additionally, the well-preserved oxyanion hole of the active site helps to stabilize the acyl intermediate of the esterase catalytic pathway.[22] Ligand orientation with respect to the nucleophile and oxyanion hole residues should therefore serve as an indicator of catalytic competency, specifically in cases where (1) the amine groups of the oxyanion hole residues can form hydrogen bonds with the carbonyl oxygen of the ligand, and (2) the nucleophile oxygen of the receptor is within attacking distance of the carbonyl carbon. In this work, I use a

combination of experimental assays and molecular docking simulations to highlight molecular features and interactions that can aid in the prediction of catalytic competency of esterases toward pyrethroids and alternative esters.

3.3 Materials and methods

3.3.1 Bioinformatics and Molecular Docking Workflow

Enzyme candidates for the degradation of targeted compounds were identified by an initial bioinformatics review followed by constrained molecular docking simulations.

3.3.1.1 Enzyme Selection

Pyrethroids applied and found in agricultural drainage water in Moss Landing, CA were each entered into the Biocatalysis/Biodegradation Database Pathway Prediction System also known as EnviPath[23] developed and maintained by EAWAG. EnviPath provides biodegradation pathway predictions based on structural similarities with compounds with experimentally observed transformation pathways, some citing specific enzymes. I grouped pesticides by common first step in the returned pathway predictions. Most groups identified corresponded with the pesticide class because pesticide classes share functional groups that are likely to be involved in the first step of biodegradation.

Pesticides with predicted ester group hydrolysis, represented primarily by pyrethroids, were selected for the remainder of this study. I then searched the enzymes used in EnviPath's predicted pathways for pyrethroids within ExPASy[24] and determined them to belong to the esterase group, E.C. 3.1.1.-. I obtained a complete list of E.C. 3.1.1. microbial esterases with resolved crystal structures in RCSB's Protein Data Bank from the UniProtKB database (~10^3 structures).[25]

Using CDHit Suite[26] (Weizhong Lab, UCSC), I removed redundant entries from the PDB list by defining a 70% amino acid sequence similarity threshold (~50 structures). Finally, using the PDB entries for each remaining structure, I removed structures exhibiting low validation scores from the list, leaving 14 candidate enzymes.[27-40] The selected enzymes are listed in Table B1.

3.3.1.2 Selection of alternative ligands

Compounds with overall structure as well as substructure similarities to targeted pyrethroids were obtained to populate a ligand list for screening against the 14 selected enzymes. A list of about 400 structurally similar compounds to targeted pyrethroids was obtained using KEGG's SIM- and SUBCOMP Tools, with no similarity index cutoff. Based on product availability the final list of pyrethroids and alternative esters (designated from here forward as Group 1) were limited to: cypermethrin (CYP), bifenthrin (BIF), esfenvalerate (ESF), deltamethrin (DEL), azoxystrobin (AZO), bensulfuron-methyl (BEN), 2-hydroxyphenylacetic acid (2-HYD), and phenyl salicylate (PS). In addition to the eight pesticides and alternative esters, six known esterase/lipase substrates were added as potential positive controls, designated as Group 2: 4-nitrophenyl acetate (4-NPA), 4-nitrophenyl butyrate (4-NPBu), 4-nitrophenyl benzoate (4-NPBe), 4-nitrophenyl palmitate (4-NPP), 4-nitrophenyl octanoate (4-NPO), and 4-methylumbelliferyl butyrate (4-MUBu).[41]

3.3.1.3 Acquisition of Additional Ligand and Enzyme Characteristics

Additional ligand chemical characteristics were computed using DataWarrior (v 5.5.0). DataWarrior employs several established methods for calculating compound properties based on the SMILES structure of each ligand. For this study, cLogP,[43] clogS (water solubility), Total

Surface Area, Relative Polar Surface Area, Topological Polar Surface Area (based on Ertl et al., 2000),[43] Druglikeness, Molecular Shape Index, Molecular Flexibility, Molecular Complexity, and Globularity were calculated from the SMILES structure, and Ligand Efficiency from the PubChem IDs. The average solvent-accessible surface area (SASA) was calculated for each of the selected enzymes using PyMOL (version 4.6). The selected ligands and chemical characteristics are listed in Table B2.

3.3.1.4 Induced Fit Docking Screening Workflow with Glide

Schrödinger's (2021-3 release) Maestro (version 12.9) and accompanying applications were used for all docking processes.[44-46] The 3D protein structures for the 14 selected enzymes were imported using the 'Get PDB' tool in the Maestro workspace for structure preparation. For multimer structures, only Chain A (i.e., monomer) was kept. Ions (e.g., metals, nitrate, sulfate) were kept so long as they were not positioned in the binding pocket of the enzyme. Non-water solvents and ligands were deleted. The 'One-step Protein Preparation' application was used to prepare the enzyme structures in batch with default parameters including the following: fill in disulfide bonds with 'Prime'; fill in missing loops; delete waters beyond 5 Å from het groups; generate het states; run H-bond assignments using pH 7; run restrained minimization. The 3D Conformer structures (SDF format) of the 14 substrates of interest were downloaded from PubChem and prepared in Maestro using the 'LigPrep' application using default parameters.

The 'Induced Fit Docking' (IFD) application[47] was used in extended sampling mode without positional constraints to dock both groups of ligands to the 14 selected enzymes. The center of the docking space was set to the centroid of the nucleophile (i.e., Ser, or Asp199 in the case of PDB 1QJV) residue of the enzyme. Refinement of residue positions were set to within 5 Å

of the bound ligand. A grid with internal (core) dimensions of 10x10x10 Å and outer dimensions of 30x30x30Å was used in each case. The generous grid box size was used to allow ligands the flexibility to dock where most favorable without forcing constraints that may be unlikely. Remaining parameters were kept at default. Three IFD runs using co-crystalized ligands of PDBs 3RLI, 1HQD, and 1Q0R were performed to ensure accuracy and reproducibility of the workflow with known ligands. Post docking, the Interaction Fingerprint (IFP) of each produced pose was calculated with the 'Interaction Fingerprint' Maestro application for further analysis, described below.

3.3.2 Docking Output Data Preprocessing and Analysis

Each distribution of poses generated for each ligand/receptor pair was analyzed in two main ways to assess the main characteristics of interactions. Distributions for each ligand/enzyme pair typically comprised 20 and 80 poses, yielding hundreds of poses per enzyme. First, the interaction fingerprints (IFPs) of each docked pose were obtained and exported from Maestro for analysis. IFPs are vectors that code interactions between ligands and specific residues of a receptor,[48] in this case our set of enzymes. Each interaction is binarily coded, where 0 indicates "no interaction", and 1 indicates "interaction present". The Glide platform codes interactions between the ligand and each residue within several categories: "contact", "backbone", "sidechain", "polar", "hydrophobic", "acceptor", "donor", "aromatic", and "charged." IFP codes provide additional information about the nature of the interaction, and therefore which types of interactions dominate ligand binding.[49,50] For the present analysis, the category "contact" was not considered, as it is collinear with several other factors and confounds downstream analyses.[51] A principal component analysis (PCA) was performed on each of the respective IFP datasets using prcomp()

(R Statistical Package) to highlight differences and similarities among ligands in terms of the types and extents of interactions with each receptor. Prior to running the PCAs, the average was taken for each IFP category in each ligand/receptor pair. Factors with a variance of 0 (e.g., all 0's or all 1's) were removed. The frequency of IFP "hits" for each IFP category were calculated and compared between ligands to further identify residues and interaction types important to catalytic activity and/or ligand binding.

Second, the position of each ligand pose with respect to residue atoms essential to catalysis were determined. Specifically, the distance between the nucleophile's oxygen and the ligand's carbonyl carbon, and the distance between the oxyanion hole residue(s)' amine nitrogen(s) and the ligand's carbonyl oxygen atom were both measured. Distance measurements were obtained to gauge how many of the docked poses land in positions amenable to esterase catalysis, and how those compare to the experimentally observed activities. The Schrödinger script "distance_to_smarts.py" was modified[c] to include a 'complex' argument, which allows for differentiation of the ligand and receptor in the IFD output filetype in which they are merged. The script was employed in a command line interface (CLI) where each of the appropriate enzymes' nucleophile and oxyanion atoms were identified by atom number, and the ligands' carbonyl carbons and oxygens were identified by SMARTS patterns: "[C,c]C(=O)O[C,c]" for unionized ligands and "[O-]C(=O)Cc" for ionized/carboxylate ligands. Table B3 contains the specific atom and residue numbers used for each enzyme.

3.3.3 Enzyme Production and Purification for Experimental Activity Assays

The plasmids for each of the enzymes (Twist Bioscience) were produced and purified according to previously published protocols as described below.[43,44] Green fluorescent protein

[c]Thank you to Schrödinger engineer Jeff Saunders for modifying the original script.

(GFP) was also produced as a positive expression control, and to serve as a negative control in the activity assay. Each plasmid was transformed into BL21(DE3) competent cells by combining the stocks in a 42°C water bath for 90 seconds, then allowed to recover in terrific broth (TB; ThermoFischer Scientific) at 37°C for 45 minutes. The cells (200uL) were then plated on luria broth (LB; ThermoFischer Scientific) plates containing 50 µg/mL of kanamycin and grown overnight at 37°C. Colonies were harvested and grown in 2mL in TB containing 50 µg/mL kanamycin and 10 µg/mL of tetracycline, then expanded in TB containing 50 µg/mL kanamycin. After reaching exponential phase, 1mM of isopropyl ß-D-1-thiogalactopyranoside (IPTG) was added to each of the cultures and left for expression for 20 hours at 18°C. The cells were collected by centrifuging at 4700 rpm for 10 min at 4°C, washed for one cycle in PBS, then resuspended in 40mL of PBS. The cells were lysed via sonication alternating 30 seconds on, 30 seconds off at 10,000 watts for 5 minutes. The lysed cells were centrifuged at 4700 rpm for 1 hour at 4°C. The lysate was purified on 500 µL of NiNTA (His-tag) beads, washed with PBS with 20 mM imidazole (pH 7.5), then eluted with PBS with 200 mM imidazole (pH 7.5). A final buffer exchange was performed to remove the imidazole from the protein storage buffer, to prevent any interference to the enzymes' activities. The exchange was performed using a Zeba™ Spin Desalting Columns (7K MWCO, 5 mL; ThermoFischer Scientific), leaving the enzymes in PBS. The A280 enzyme concentration was measured using a multi-mode microplate reader (Synergy™ H1; Biotek®). Esterase activity was confirmed qualitatively by letting 150 µL of protein stock react with 10 µL of 1000 mg/L 4-nitrophenyl acetate (4-NPA) for 5 minutes; photos of the wells were taken at 2 and 5 minutes to document the colorimetric reaction and compared to 3 PBS-only controls (Figure B1).

3.3.4 Group 1 Activity Assays

3.3.4.1 Description of Group 1 Activity Assays

Each of the Group 1 substrates were dissolved in MS-grade ethanol, then diluted in PBS at least 10-fold to between 24 and 300 µM. The enzyme stocks were diluted 10-fold in PBS and were tested in both their undiluted (1x) and diluted (10x) concentrations. The assays were initiated by adding 20 µL of substrate dilution to 30 µL of enzyme solution in a 96-well plate; a no-enzyme control was run for each row of the plate (PBS instead of enzyme solution), and three GFP controls were run at both 1x and 10x GFP dilutions for each substrate. The assay concentrations of the substrates ranged between 120 and 1500 µM, and the assay concentrations of the enzymes (1x) ranged between 0.27 and 5.15 mg/mL. The plates were allowed to sit for 22 hours at room temperature, and in the dark to avoid substrate photodegradation. After 22 hours, the reactions were quenched with 150 µL of 70% acetonitrile containing 1.8 µg/mL of the following substrate mixture: chlorpyrifos d10, fipronil, diclofenac, imidacloprid, metolachlor, and sulfamethoxazole. The plates were centrifuged at 4000 rpm for 1 hour at 4°C, and the supernatants (150 µL) were transferred to 2mL autosampler vials. This protocol was performed twice for the four pyrethroids, as recoveries were inconsistent in the first round. The samples being analyzed for bifenthrin, esfenvalerate, cypermethrin, and deltamethrin were diluted to 1.5 mL in ethyl acetate. The samples being analyzed for azoxystrobin, phenyl salicylate, bensulfuron-methyl, and 2-hydroxyphenylacetic acid were diluted to 1 mL with Optima water.

Following measurements of pyrethroids via gas chromatography coupled with electron capture detector (GC-ECD), a solvent exchange was performed for the analysis of esterase transformation products: the ethyl acetate extracts were exchanged to methanol by the addition of

300 µL of methanol, and evaporation to 200 µL. Subsequently, samples were brought up to 1mL with Optima water.

3.3.4.2 Group 1 Activity Sample Analyses

Internal standards were added to each sample and calibration standard to account for instrument variability: imidacloprid d4, MCPA methyl d3, dimethoate d6, and methomyl d3 (LC); and DBOFB (GC). The pyrethroids were quantified via GC-ECD (Agilent 6890), with a slightly modified EPA (no. 552.3) method[55] for haloacetic acids in drinking water: the initial oven temperature was 100°C for 1 minute, then ramping to 200 at 15°C/minute, followed by two ramps at 3.80°C/minute until 290°C, and 10.00°C/minute until 300°C. A J&W DB-5ms capillary column was used (model #122-5532). Azoxystrobin was analyzed and quantified using liquid chromatography quadrupole time of flight mass spectrometry (LC-QTOF-MS) in positive electrospray ionization mode (ESI+) as described in Moschet et al. (2016).[56] Bensulfuron-methyl, 2-hydroxyphenylacetic acid, and phenyl salicylate were analyzed and quantified with LC-QTOF-MS in negative electrospray ionization mode (ESI-) (Agilent 1260 Infinity HPLC coupled to an Agilent 6530 QTOF-MS with a Zorbax Eclipse Plus C18 column; 100 mm, 2.5 mm, 1.8 µm, Agilent Technologies, Inc.). Data acquisition methodology was adapted from Moschet et al. (2016).[56] Example parent and qualifier chromatograms are in Figures B2.A-C. The solvent-exchanged pyrethroid extracts were analyzed using LC-QTOF-MS (ESI-), further described in the next section.

3.3.4.3 Pyrethroid Transformation Product Detection via Suspect Screening

A suspect screening approach was used to screen for the esterase products of each of the pyrethroids: the MassHunter PCDL Manager (v 7.00) was used to curate a personal compound

database library (PCDL) of the esterase products (i.e., the alcohol and acid groups) of the investigated pyrethroids. Because the recovery of the more hydrophobic pyrethroids was less precise, the detection of their respective esterase-specific transformation products was used as a metric by which to assess activity as a semi-quantitative mass balance check. MassHunter Workstation for Qualitative Analysis (v 10.0) was used to screen the acquired all-ions MS spectra of each of the solvent-exchanged samples against the curated PCDL using the Find by Formula algorithm, default settings, and ion adducts set to those present in PBS. Product identities were further confirmed against the spectra of analytical standards for the case of TFP acid and permethric acids. The TFP and permethric acid standards were also detected using the same suspect screening workflow. The acid products were readily detected using this method, and their responses relative to the ISTD were used to estimate relative concentrations.

3.3.5 Group 2 Activity Assays

To ground-truth enzymatic activity and compare docking analyses, six additional substrates (Group 2 compounds shown in Table B2) were analyzed kinetically with each of the above-described enzymes. The esterase and lipase substrates used were 4-nitrophenyl butyrate, 4-nitrophenyl octanoate, 4-nitrophenyl benzoate, 4-nitrophenyl acetate, 4-nitrophenyl palmitate, and 4-methylumbelliferyl butyrate. The substrates were assayed at four concentrations (0.5, 1, 2 and 5 ug/mL) in duplicate, and enzymes were assayed between 0.5-5 mg/mL. A microplate reader (Synergy™ H1; Biotek®) was used to measure the production of the 4-nitrophenol group (absorbance at 405 nm[57]), and fluorescence of 4-methylumbelliferone production (excitation energy 380 nm, emission at 454 nm[58]). Assays were run for 1h at 37°C, and measurements were taken every 90 seconds. The resulting transformation rates for each enzyme/substrate pair were determined for each of the substrate starting concentrations by the linear region of the

transformation curve. The rate information in relation to starting concentration was used to determine activity: from fundamental enzyme kinetics, as starting substrate concentration increases while enzyme concentration is kept constant, so should the substrate transformation rate. A linear regression (rate ~ initial substrate concentration) was run in R (R Project for Statistical Computing) and compared against a naïve model, assessed statistically using an F-test.

3.4 Results and discussion

3.4.1 Assay Results

3.4.1.1 Group 1 Assay Results: Pesticides and Alternative Esters

The relative recovery of parent compounds as compared to assay no-enzyme controls (C/C_{NE}) are illustrated in Figures B3.A and B3.B for assay rounds 1 and 2, respectively. Recovery of parent compounds varied widely, especially for the more hydrophobic pyrethroid class, as noted by recoveries well over 1 as compared to no-enzyme control samples. Moreover, losses in the GFP controls were sizable, especially for cypermethrin (Figure B3.B). This speaks to the general difficulty of conducting assays with hydrophobic substrates in salt buffers without the addition of detergents/surfactants to aid solubility, many of which may compromise enzyme activity. Additionally, it is possible that losses of hydrophobic pesticides occurred by nonspecific associations with proteins rather than by enzymatic transformation.[59] For this reason, confident designations of esterase activity of pesticides and alternative esters were decided based on a parent compound recovery as compared to GFP controls of the same enzyme concentration (with $C/C_{GFP} < 0.70$ in at least one dilution replicate). The enzyme and ligand combinations selected as candidates for further study are presented in Figure B4. Figure B4 displays relative recoveries of

parent compounds to respective controls, and detection of corresponding transformation products, for each candidate pair.

The relative abundance of esterase transformation products in the pyrethroid extracts compared to controls provided a secondary assessment of activity in each assay (Figure B4). Three carboxylic acid esterase pyrethroid products were observed, while none of the pyrethroid alcohol products were detected in ESI- mode. The esterase product of cypermethrin, permethric acid (m/z 206.998), was detected in the activity assay for both dilutions of the 1CUG enzyme and was not detected in any of the no-enzyme or GFP controls. Permethric acid shared spectral similarity with spectra deposited in MassBank.[60] The esterase product of esfenvalerate, (RS)-fenvaleric acid (m/z 211.054), was detected in both dilutions of the 3RLI enzyme assay and not detected in any no-enzyme or GFP controls. Unfortunately, (RS)-fenvaleric acid had no comparable LC-MS spectral database entries against which to screen for further confirmation. The esterase product of bifenthrin, TFP acid (m/z 241.026), was detected in several bifenthrin-containing assay extracts. However, TFP was also detected in some control extracts and other pyrethroid assay extracts. Because of this, only bifenthrin assay samples in which the relative response of TFP acid was greater than the most abundant of the other extracts (i.e., for both controls and other pyrethroid assays) were considered. Additionally, permethric acid and TFP acid were both identified in standard mixtures via the suspect screening approach, and targeted MS/MS spectra were acquired for TFP acid confirmation (Figure B5.A-C.).

3.4.1.2 Group 2 Assay Results: Esterase and Lipase Substrates

Kinetic curves of esterase and lipase substrates transformed by the present proteins were used to assess activity of each substrate/enzyme pair. The most recalcitrant of these substrates was

the most hydrophobic, 4-nitrophenyl palmitate (4-NPP; C16; $\log K_{ow}$ 8.8), as well as that with a benzene functional group, 4-nitrophenyl benzoate (4-NPBe). Due to limited esterase plasmid stock, some esterase and lipase substrates were not assessed. Additionally, PDB codes 4CCY and 4ZWN precipitated during the esterase/lipase screening, rendering absorbance readings unusable. Examples of "inactive" and "active" absorbance curves are presented in Figure B6. All kinetic parameters obtained are presented in Table B4.

3.4.1.3 Activity Designations

Activity designations from both Group 1 and Group 2 assays are presented in Table B5, where "Ac" denotes esterase active, and "In" denotes inactive. Activity confirmation of Group 1 substrates (pesticides and alternative esters) was defined by clear parent compound loss as compared to both the no-enzyme and GFP controls, with enzyme dose dependency. For the pyrethroids, detection of carboxylic acid product in the extract (Figure B4) was also used for determining activity. Pairs denoted with the light green (Active) designation refer to combinations in which parent compound loss and/or transformation product formation did not follow the expected dose dependency pattern, or in which insufficient, though promising data were acquired (e.g., transformation product not detected, though parent compound exhibited expected patterns). The (Active) and examples of Inactive pairs are shown in Figures B7 and B8, respectively.

Group 2 activity was based on F-statistic results at the 90% and 95% confidence levels: pairs designated as Active fell within the 95% CI (i.e., F-stat > 98.5); pairs designated as (Active) fell within the 90% CI (i.e., 18.5 < F-stat < 98.5); and Inactive pairs were those outside of the 95% CI (i.e., F-stat < 18.5). Full regression results are presented in Table B4. Unmeasured combinations are denoted by "NA", and those with confounding precipitation are denoted by "P".

The activity patterns yielded from the Group 2 assays highlighted that several enzymes have a greater affinity toward shorter chain substrates. 4-NPP (C16) was among the least active substrates, for which two enzymes isolated from *Streptomyces spp.*, 1Q0R and 5MAL, were the only two to exhibit distinct activity. Furthermore, the reported preference of 4KRX toward 4-NP esters up to C8[27] was consistent with our results, as 4KRX did not hydrolyze the lipid substrate 4-NPP.

Activity designations determined from the Group 1 assays highlighted several candidates for the ester hydrolysis of pyrethroids: 1CUG, 1Q0R, 3D2B, 3RLI, 4CCY, and to a lesser extent, 4KRX and 1UZA. These enzymes represent a variety of lipases (3RLI, 3D2B, 1CUG), carboxylesterases (4CCY) and a methylesterase (1Q0R). Moreover, the Group 1 activities showed an overall preference for carboxylester substrates (i.e., pyrethroids and phenyl salicylate) rather than methylesters (i.e., azoxystrobin and bensulfuron-methyl) or carboxylic acids (i.e., 2-hydroxyphenylacetic acid). The two methylesterases representatives, 1Q0R and 1QJV, however, did not show activity toward the two methylester substrates of Group 1. This may be explained by their respective affinities toward methyl esters of pectin polymers, further discussed in the subsequent section. This leaves phenyl salicylate as the alternative ester with the most substrate potential across the present suite of enzymes, showing the most overlap in activity with the studied pyrethroids.

3.4.2 Induced Fit Docking (IFD)

Assessment of the induced docking workflow via the redocking of known ligands or ligand analogues that were co-crystalized with 1HQD, 1Q0R, and 3RLI yielded root mean square deviation (RMSD) values primarily under 2Å, with the interquartile ranges all below 2Å (Figure

B9). This confirms that the pose distributions obtained from the IFD workflow are relatively accurate.

The docking scores of the pose distributions generated by the IFD workflow for all ligands (pesticides, alternative esters, and esterase/lipase substrates) yielded low correlation with activities. This is to be expected, as docking scores are not intended to be predictors of catalytic activity. Instead, docking scores rank pose favorability in terms of surrounding interaction energies. It is therefore important to investigate the nature of specific interactions, particularly those with residues at the catalytic site,[61] as discussed in subsequent sections.

3.4.2.1 Activity Patterns with Respect to Distances to Nucleophiles and Oxyanion Hole Residues

Each distribution of poses generated by the induced fit docking screening was plotted based on their position relative to the enzymes' nucleophile and oxyanion hole residues. The distance distribution boxplots of three enzymes (3D2B, 1CUG, and 1QJV) are displayed in Figure B10. A distance of 3.5Å radius around the crucial nucleophile and oxyanion hole atoms is indicated on each plot to denote a common contact distance threshold required for activity. The distance of 3.5 was chosen based on the maximum hydrogen bond distance, with variance for O-H or N-H bond length accommodation.[62]

Of the examined enzymes, two enzymes stood out as displaying distance relationships corresponding most closely with activity. First, the 3D2B distance plots show that active substrates largely exhibited little positional variance and fell near or below the 3.5Å radius around the crucial nucleophile and oxyanion hole atoms. Conversely, inactive substrates generally fell farther from the crucial atoms, with more spatial variability. Furthermore, when investigating the proportion of poses that fell within the 3.5Å radius of both the nucleophile *and* an oxyanion hole residue (further

increasing the likelihood of catalysis source), this proportion was significantly greater for substrates designated as Active (56.6±16.6%) than for those designated as Inactive (12.8±8.8%).

Upon visual inspection of the 3D2B poses, we also highlighted a putative second oxyanion hole residue, isoleucine (Ile) 12. Ile 12 not only shows the expected distance relationships with respect to the carbonyl oxygen atoms of [primarily] active substrates (Figure B10.A-C.), but also yielded a greater proportion of donor contacts among substrates (Figure B11.D).

The second enzyme showing a similar activity and position patterns is 1CUG. However, substrate poses for 1CUG generally exhibited more positional variance than poses for 3D2B, regardless of their activity designation. This distinction between 3D2B and 1CUG variances may be because 1CUG generally has a more accessible binding site; the bulk solvent-accessible surface area (SASA) for 3D2B (chain A) is 7,498.7 $Å^2$, compared to 8445.1 $Å^2$ of 1CUG. This may simply allow ligands more flexibility to their poses corresponding to more diverse distributions.

In contrast with PDBs 3D2B and 1CUG, the pectin methylesterase 1QJV exhibited little activity with the selected substrates. While 1QJV exhibited no activity toward the methylester substrates, a second methylesterase represented, namely alacinomycin methylesterase (1Q0R), exhibited activity with a larger set of substrates (Figure B12). Activity was observed for 1Q0R with all the Group 2 substrates, as well as deltamethrin and esfenvalerate, though the distances to crucial residues did not offer a clear association with activity. 1Q0R and 1QJV share similarities in the structure of their preferred substrates ester (i.e., a methyl ester), but their binding pockets differ significantly in size and accessibility. 1QJV contains a large cleft as a binding pocket, in many ways resembling Pac Man (Figure B13.A). Perhaps the shape of the binding pocket helps to explain why average distances from all ligands (though especially active ligands) to the nucleophile and oxyanion hole residues were relatively large compared to enzymes 3D2B and

1CUG (Figure B10.H-I). To contrast, 1Q0R harbors a narrower canal to the catalytic site, lined with hydrophobic residues that can help accommodate proper ligand orientation with respect to the catalytic site. This makes intuitive sense given the characteristics of each enzymes' native ligand. The distinction between 1QJV and 1Q0R highlights the need for enzyme-specific parameterization of docking conditions. Instances where an enzyme has a large binding site may benefit from a smaller grid box size. That said, in the case of 1QJV, having relatively fewer active Group 1 and 2 substrates may simply be a reflection of its greater specificity for longer polysaccharide ligand surfaces.

The remaining enzymes with complete activity data for both Group 1 and Group 2 substrates (5MAL, 1Q0R, 1UZA, 1QOZ, and 4KRX) exhibited less-clear relationships between distances to crucial residues and activity (Figure B12). The substrates that proved to be most recalcitrant in the activity assays (namely azoxystrobin and bensulfuron-methyl) are often among the farthest from the crucial active site residues (Figure B12), an observation that was consistent across all of these enzymes.

3.4.2.2 Identification of Binding Patterns and Driving Residue Interactions from PCAs and Factor Analyses

The following sections discuss the results of the interaction fingerprint analysis using principal component analysis (PCA) as well as the breakdown of each type of interaction with respect to the set of ligands. The PCAs display the variability of interactions between the set of ligands and each enzyme and can be used to highlight similarities among ligands in terms of their binding behavior. Because the PCAs were built from averaged IFP distributions, the subsequent investigation of each interaction individually allows for a finetuned look at the frequency with

which residue interactions occur by each ligand/ligand group. Focus will again be put on PDBs 1CUG, 3D2B, and 1QJV.

Each of the PCAs generated for each enzyme are presented in Figure B14. It is generally clear from the resulting biplots that there is little correlation between the principal components and the activity designations of the ligands. In the case of 3D2B, for instance, there is considerable overlap between the 90% CI ellipses of each of the activity designations in the first two principal components (Figure B14.K-L), as is true of most of the generated PCAs. Viewing with a third principal component axis did not separate the activity groups. From this, it is apparent that using interaction fingerprints is insufficient for delimiting activity levels, at least using this workflow.

Instead, ligands with similar physicochemical characteristics tended to be more closely located among the IFP components. For instance, cypermethrin and deltamethrin (ligand numbers 2 and 3, respectively), the most structurally similar among the pyrethroids tested, shared more similar IFPs as compared to bifenthrin and esfenvalerate (i.e., their PCA coordinates were near one another). Similarly, the two nitrophenyl substrates with the shortest chains, 4-NPA and 4-NPBu, (ligand numbers 9 and 10, respectively) shared similar IFPs as compared to the longer chain nitrophenyl substrates (e.g., 4-NPP/ligand 13). To contrast, bensulfuron-methyl, one of the more dissimilar ligands based on 2D structure and polar surface area, often fell far from other ligands (Figure B14). This is consistent with the distance measurement patterns described earlier.

Last, the PCAs did highlight for each enzyme the set of residue interactions that described the bulk of the variance of ligand PCA coordinates. The most driving factors in the first two principal components were generally represented by interactions with residues adjacent to crucial catalytic site residues, and in some instances, the crucial residues themselves. For example, the PCA performed on 1CUG IFPs highlighted residue numbers 120, 42, and 121, the enzyme's

nucleophile and oxyanion residues, respectively, as well as adjacent residues numbered 189, 43, and 44. While interactions with these residues are important to catalysis, disparities between active and inactive ligands were not split along these terms (as visible from the PCA biplots). This is likely simply because all ligands were subject to the same grid box centered on the catalytic site, and therefore would all likely have contacts with the same residues. This prompted an investigation of other residues that may have differential interactions with ligands based on activity or other ligand characteristics, and is discussed in the following section.

A detailed look into the frequencies of specific interaction types allowed for the distinction of residue interactions that were most common, and interactions that differ between ligands based on ligand characteristics, and sometimes activity designations. These will be discussed for enzyme 3D2B.

In the case of lipase 3D2B, there are several interactions that are clearly drivers of ligand binding regardless of ligand identity. As is the case with the other screened enzymes, the most interactive residues of 3D2B were typically those adjacent to catalytic residues (i.e., the catalytic triad and oxyanion hole residues). Residues lining the binding pocket have long been recognized as important to ligand binding, as well as influencing ligand selectivity.[63]

While there were no apparent interaction disparities between active and inactive substrates, several residues exhibit a much greater frequency of interaction with bifenthrin than with its Type II pyrethroid counterparts: the backbone structures of residues Gly13 and Ile135 exhibited contacts with 88% of bifenthrin poses, where the Type II pyrethroids showed contacts with <20% and <38% of poses, respectively. Similarly, the hydrophobic sidechains of leucine residues A108 and A140 had contacts with 79% and 80% of bifenthrin poses, and contacts comprising <29% and <19% of Type II pyrethroid pose distributions.

Finally, a high proportion of ligand interactions occurred with residue Ile12. Given the position of Ile12 with respect to the carbonyl oxygen of the ligand, as well as the relatively high proportion of polar/donor interactions (Figure B10), it appears likely that Ile12 contributes to oxyanion stabilization of the acyl intermediate of the acyl-enzyme complex (Figure B15). While this is a very specific observation in the scope of the present work, it highlights that investigation of residue interactions from a high/overview level can help to identify residues critical to catalysis, that can later be probed with mutation and heterologous expression experimentation.

3.5 Conclusion

The present work screened a list of representative microbial esterases against a set of ligands comprised of pyrethroid pesticides, alternative esters, and a set of designed esterase/lipase ligands. Overall, enzymes 1CUG, 1Q0R, 3D2B, 3RLI, and 4CCY showed signs of esterase activity toward some of the pyrethroids. Generally, this set of enzymes preferred ligands with carboxylester groups rather than carboxylate or methyl ester groups; phenyl salicylate was the only alternative ester from the Group 1 ligands that exhibited activity with the enzyme set. This suggests that there is overlap in catalytic competence between pyrethroids and phenyl salicylate. Previously reported selectivity with Group 2 substrates (e.g., preferences of 4KRX toward substrates $\leq$C8[27]) were also seen in this study.

The low solubility of the pyrethroids posed experimental obstacles resulting in a relatively high recovery error, evident from Figure B3. While this may be able to be improved with the addition of detergents such as Triton X-100,[64,65] such optimization was outside the scope of this exploratory study. In this case, the detection of esterase transformation products provided better confidence in pyrethroid activity designations. However, development of robust

pyrethroid/enzyme turnover assays will be beneficial for future development of enzyme-based pyrethroid remediation strategies.

The induced fit docking workflow for screening ligands against enzymes with degradation potential yielded mixed results. In terms of post-docking analysis, the use of distances to nucleophile and oxyanion hole residues proved to be somewhat successful in delineating active versus inactive substrates. However, the IFD workflow was only useful for certain enzymes (e.g., 3D2B and 1CUG). Tightening docking parameters to be more enzyme-specific in terms of grid box positioning and additional positional constraints may improve this pattern. Though, in the current screening workflow, such additional parameterization would defeat the purpose of 'easy identification' of catalytically competent pairs.

The use of PCA clustering and factor analysis was useful in identifying important residue interactions, some of which were differential based on ligand characteristics. While this did not prove to be useful in clustering ligands by activity, this avenue could be used to inform docking constraints for a more specific predictive workflow. Moreover, running the induced fit docking workflow followed by residue interaction analysis is more efficient than visually inspecting each pose, of which there are dozens per enzyme/ligand pair, to narrow down targets for more specific docking workflows.

3.5 References

(1) Ruggaber, T. P.; Asce, M.; Talley, J. W. Enhancing Bioremediation with Enzymatic Processes: A Review. https://doi.org/10.1061/ASCE1090-025X200610:273.

(2) Sharma, B.; Dangi, A. K.; Shukla, P. Contemporary Enzyme Based Technologies for Bioremediation: A Review. *Journal of Environmental Management*. Academic Press March 15, 2018, pp 10–22. https://doi.org/10.1016/j.jenvman.2017.12.075.

(3) Okino-Delgado, C. H.; Zanutto-Elgui, M. R.; do Prado, D. Z.; Pereira, M. S.; Fleuri, L. F. Enzymatic Bioremediation: Current Status, Challenges of Obtaining Process, and Applications; Springer, Singapore, 2019; pp 79–101. https://doi.org/10.1007/978-981-13-7462-3_4.

(4) Speight, J. G. *Chapter 8 - Biological Transformations, In: Reaction Mechanisms in Environmental Engineering: Analysis and Prediction*; Butterworth-Heinemann, 2018. https://doi.org/https://doi.org/10.1016/C2013-0-16045-X.

(5) Mateo, C.; Palomo, J. M.; Fernandez-Lorente, G.; Guisan, J. M.; Fernandez-Lafuente, R. Improvement of Enzyme Activity, Stability and Selectivity via Immobilization Techniques. *Enzyme and Microbial Technology*. **2007**, pp 1451–1463. https://doi.org/10.1016/j.enzmictec.2007.01.018.

(6) Ho, C. T.; Kang, S.; Hur, H. G. Enzymatic Properties of Atrazine Chlorohydrolase Entrapped in Biomimetic Silica. *J. Appl. Biol. Chem.* **2008**, *51* (4), 143–147. https://doi.org/10.3839/JABC.2008.024.

(7) Gianfreda, L.; Rao, M. A.; Scelza, R.; De La Luz Mora, M. Role of Enzymes in Environment Cleanup/Remediation. In *Agro-Industrial Wastes as Feedstock for Enzyme Production: Apply and Exploit the Emerging and Valuable Use Options of Waste Biomass*; Elsevier Inc., 2016; pp 133–155. https://doi.org/10.1016/B978-0-12-802392-1.00006-X.

(8) Karigar, C. S.; Rao, S. S. Access To. *Res. Enzym. Res.* **2011**, *2011*, 11. https://doi.org/10.4061/2011/805187.

(9) Gangola, S.; Sharma, A.; Bhatt, P.; Khati, P.; Chaudhary, P. Presence of Esterase and Laccase in Bacillus Subtilis Facilitates Biodegradation and Detoxification of Cypermethrin. *Sci. Reports 2018 81* **2018**, *8* (1), 1–11. https://doi.org/10.1038/s41598-018-31082-5.

(10) Koppel, N.; Rekdal, V. M.; Balskus, E. P. Chemical Transformation of Xenobiotics by the Human Gut Microbiota. *Science* **2017**, *356* (6344), 1246–1257. https://doi.org/10.1126/SCIENCE.AAG2770/ASSET/7F3BFA3D-4441-425F-A5E7-A8C2BB8E8AEF/ASSETS/GRAPHIC/356_AAG2770_F4.JPEG.

(11) Zhang, Y.; Li, S.; Xu, L.; Guo, H. F.; Zi, J.; Wang, L.; He, P.; Fang, J. Overexpression of Carboxylesterase-1 and Mutation (F439H) of Acetylcholinesterase-1 Are Associated with Chlorpyrifos Resistance in Laodelphax Striatellus. *Pestic. Biochem. Physiol.* **2013**, *106* (1–2), 8–13. https://doi.org/10.1016/J.PESTBP.2013.03.002.

(12) Silva, E.; M. Fialho, A.; Sá-Correia, I.; G. Burns, R.; J. Shaw, L. Combined Bioaugmentation and Biostimulation To Cleanup Soil Contaminated with High Concentrations of Atrazine. *Environ. Sci. & Technol.* **2003**, *38* (2), 632–637. https://doi.org/10.1021/es0300822.

(13) Silva, V. P.; Moreira-Santos, M.; Mateus, C.; Teixeira, T.; Ribeiro, R.; Viegas, C. A. Evaluation of Arthrobacter Aurescens Strain TC1 as Bioaugmentation Bacterium in Soils Contaminated with the Herbicidal Substance Terbuthylazine. *PLoS One* **2015**, *10* (12), e0144978. https://doi.org/10.1371/journal.pone.0144978.

(14) Mandelbaum, R.; Wackett, L. P.; Allan, D. Soil Bacteria Rapidly Hydrolyze Atrazine to Hydroxyatrazine. *Environ. Sci. Technol.* **1993**, *27*, 1943–1946.

(15) Sirajuddin, S.; Khan, M. A.; Qader, S. A. U.; Iqbal, S.; Sattar, H.; Ansari, A. A Comparative Study on Degradation of Complex Malathion Organophosphate Using of Escherichia Coli IES-02 and a Novel Carboxylesterase. *Int. J. Biol. Macromol.* **2020**, *145*, 445–455. https://doi.org/10.1016/J.IJBIOMAC.2019.12.192.

(16) Narayanan, M.; Kumarasamy, S.; Ranganathan, M.; Kandasamy, S.; Kandasamy, G.; Gnanavel, K. Enzyme and Metabolites Attained in Degradation of Chemical Pesticides ß Cypermethrin by Bacillus Cereus. *Mater. Today Proc.* **2020**, *33*, 3640–3645. https://doi.org/10.1016/J.MATPR.2020.05.722.

(17) Zuo, Z.; Ting, G.; You, C.; Ruihua, L.; Ping, X.; Hong, J.; Chuanling, Q.; Cunjiang, S.; Chao, Y. Engineering Pseudomonas Putida KT2440 for Simultaneous Degradation of Organophosphates and Pyrethroids and its Application in Bioremediation of Soil. *Biodegradation.* **2015**, 26(3), 223-233. https://doi.org/10.1007/s10532-015-9729-2.

(18) Sayler, G. S.; Ripp, S. Field Applications of Genetically Engineered Microorganisms for Bioremediation Processes. *Current Opinion in Biotechnology*. Current Biology Ltd June 1, 2000, pp 286–289. https://doi.org/10.1016/S0958-1669(00)00097-5.

(19) Urgun-Demirtas, M.; Stark, B.; Pagilla, K. Use of Genetically Engineered Microorganisms (GEMs) for the Bioremediation of Contaminants. *Critical Reviews in Biotechnology*. Taylor & Francis September 1, 2006, pp 145–164. https://doi.org/10.1080/07388550600842794.

(20) Singh, D. P.; Prabha, R.; Gupta, V. K.; Verma, M. K. Metatranscriptome Analysis Deciphers Multifunctional Genes and Enzymes Linked with the Degradation of Aromatic Compounds and Pesticides in the Wheat Rhizosphere. *Front. Microbiol.* **2018**, *9* (JUL), 1331. https://doi.org/10.3389/fmicb.2018.01331.

(21) Lockridge, O.; Quinn, D. M.; Radić, Z. Esterases. In *Comprehensive Toxicology: Third Edition*; Elsevier Inc., 2018; Vol. 10–15, pp 277–307. https://doi.org/10.1016/B978-0-12-801238-3.01970-X.

(22) Aranda, J.; M. F. S. A. Cerqueira, N.; A. Fernandes, P.; Roca, M.; Tuñon, I.; J. Ramos, M. The Catalytic Mechanism of Carboxylesterases: A Computational Study. *Biochemistry* **2014**, *53* (36), 5820–5829. https://doi.org/10.1021/bi500934j.

(23) Wicker, J.; Lorsbach, T.; Gütlein, M.; Schmid, E.; Latino, D.; Kramer, S.; Fenner, K. EnviPath--The Environmental Contaminant Biotransformation Pathway Resource. *Nucleic Acids Res.* **2016**, *44* (D1), D502–D508. https://doi.org/10.1093/NAR/GKV1229.

(24) Swiss Institute of Bioinformatics. *Expasy*. https://www.expasy.org/ (accessed Jun 2, 2020).

(25) EMBL-EBI; Protein Information Resource; Swiss Institute of Bioinformatics. *UniProt*. UniProtKB; https://www.uniprot.org/uniprotkb?query=* (accessed Jun 2, 2020).

(26) Fu, L.; Niu, B.; Zhu, Z.; Wu, S.; Li, W. CD-HIT: Accelerated for Clustering the next-Generation Sequencing Data. *Bioinformatics* **2012**, *28* (23), 3150–3152. https://doi.org/10.1093/BIOINFORMATICS/BTS565.

(27) Schiefner, A.; Gerber, K.; Brosig, A.; Boos, W. Structural and Mutational Analyses of Aes, an Inhibitor of MalT in Escherichia Coli. *Proteins* **2014**, *82* (2), 268–277. https://doi.org/10.1002/PROT.24383.

(28) Rozeboom, H. J.; Godinho, L. F.; Nardini, M.; Quax, W. J.; Dijkstra, B. W. Crystal Structures of Two Bacillus Carboxylesterases with Different Enantioselectivities. *Biochim. Biophys. Acta* **2014**, *1844* (3), 567–575. https://doi.org/10.1016/J.BBAPAP.2014.01.003.

(29) Jenkins, J.; Mayans, O.; Smith, D.; Worboys, K.; Pickersgill, R. W. Three-Dimensional Structure of Erwinia Chrysanthemi Pectin Methylesterase Reveals a Novel Esterase Active Site. *J. Mol. Biol.* **2001**, *305* (4), 951–960. https://doi.org/10.1006/JMBI.2000.4324.

(30) Aschauer, P.; Rengachari, S.; Lichtenegger, J.; Schittmayer, M.; Padmanabha Das, K. M.; Mayer, N.; Breinbauer, R.; Birner-Gruenberger, R.; Gruber, C. C.; Zimmermann, R.; Gruber, K.; Oberer, M. Crystal Structure of the Saccharomyces Cerevisiae Monoglyceride Lipase Yju3p. *Biochim. Biophys. Acta* **2016**, *1861* (5), 462–470. https://doi.org/10.1016/J.BBALIP.2016.02.005.

(31) Rengachari, S.; Bezerra, G. A.; Riegler-Berket, L.; Gruber, C. C.; Sturm, C.; Taschler, U.; Boeszoermenyi, A.; Dreveny, I.; Zimmermann, R.; Gruber, K.; Oberer, M. The Structure of Monoacylglycerol Lipase from Bacillus Sp. H257 Reveals Unexpected Conservation of

the Cap Architecture between Bacterial and Human Enzymes. *Biochim. Biophys. Acta* **2012**, *1821* (7), 1012–1021. https://doi.org/10.1016/J.BBALIP.2012.04.006.

(32) Luić, M.; Tomić, S.; Leščić, I.; Ljubović, E.; Šepac, D.; Šunjić, V.; Vitale, L.; Saenger, W.; Kojić-Prodić, B. Complex of Burkholderia Cepacia Lipase with Transition State Analogue of 1-Phenoxy-2-Acetoxybutane: Biocatalytic, Structural and Modelling Study. *Eur. J. Biochem.* **2001**, *268* (14), 3964–3973. https://doi.org/10.1046/J.1432-1327.2001.02303.X.

(33) Ahmad, S.; Kamal, M. Z.; Sankaranarayanan, R.; Rao, N. M. Thermostable Bacillus Subtilis Lipases: In Vitro Evolution and Structural Insight. *J. Mol. Biol.* **2008**, *381* (2), 324–340. https://doi.org/10.1016/J.JMB.2008.05.063.

(34) Longhi, S.; Czjzek, M.; Lamzin, V.; Nicolas, A.; Cambillau, C. Atomic Resolution (1.0 Å) Crystal Structure of Fusarium Solani Cutinase: Stereochemical Analysis. *J. Mol. Biol.* **1997**, *268* (4), 779–799. https://doi.org/10.1006/jmbi.1997.1000.

(35) Vincent, F.; Charnock, S. J.; Verschueren, K. H. G.; Turkenburg, J. P.; Scott, D. J.; Offen, W. A.; Roberts, S.; Pell, G.; Gilbert, H. J.; Davies, G. J.; Brannigan, J. A. Multifunctional Xylooligosaccharide/Cephalosporin C Deacetylase Revealed by the Hexameric Structure of the Bacillus Subtilis Enzyme at 1.9 Å Resolution. *J. Mol. Biol.* **2003**, *330* (3), 593–606. https://doi.org/10.1016/S0022-2836(03)00632-6.

(36) Hakulinen, N.; Tenkanen, M.; Rouvinen, J. Three-Dimensional Structure of the Catalytic Core of Acetylxylan Esterase from Trichoderma Reesei: Insights into the Deacetylation Mechanism. *J. Struct. Biol.* **2000**, *132* (3), 180–190. https://doi.org/10.1006/JSBI.2000.4318.

(37) McAuley, K. E.; Svendsen, A.; Patkar, S. A.; Wilson, K. S. Structure of a Feruloyl Esterase from Aspergillus Niger. *Acta Crystallogr. D. Biol. Crystallogr.* **2004**, *60* (Pt 5), 878–887. https://doi.org/10.1107/S0907444904004937.

(38) Jansson, A.; Niemi, J.; Mäntsälä, P.; Schneider, G. Crystal Structure of Aclacinomycin Methylesterase with Bound Product Analogues: Implications for Anthracycline Recognition and Mechanism. *J. Biol. Chem.* **2003**, *278* (40), 39006–39013. https://doi.org/10.1074/JBC.M304008200.

(39) Leščić Ašler, I.; Štefanić, Z.; Maršavelski, A.; Vianello, R.; Kojić-Prodić, B. Catalytic Dyad in the SGNH Hydrolase Superfamily: In-Depth Insight into Structural Parameters Tuning the Catalytic Process of Extracellular Lipase from Streptomyces Rimosus. *ACS Chem. Biol.* **2017**, *12* (7), 1928–1936. https://doi.org/10.1021/ACSCHEMBIO.6B01140.

(40) Zhiqiang, L.; Yuying, G.; Baker, P.; Ravee, Y.; Lu, Z.; Alemu, G.; Li, H.; Butterfoss, G.; Kong, X-P.; Gross, R.; Montclare, J. Structural and Functional Studies of Aspergillus Oryzae Cutinase: Enhanced Thermostability and Hydrolytic Activity of Synthetic Ester

and Polyester Degradation. *J. Am. Chem. Soc.* **2009**, *131* (43), 15711–15716. https://doi.org/10.1021/JA9046697.

(41) Madubuike, H.; Ferry, N. Molecules Characterisation of a Novel Acetyl Xylan Esterase (BaAXE) Screened from the Gut Microbiota of the Common Black Slug (Arion Ater). **2022**. https://doi.org/10.3390/molecules27092999.

(42) Mannhold, R.; Poda, G. I.; Ostermann, C.; Tetko, I. V. Calculation of Molecular Lipophilicity: State-of-the-Art and Comparison of Log P Methods on More than 96,000 Compounds. *J. Pharm. Sci.* **2009**, *98* (3), 861–893. https://doi.org/10.1002/JPS.21494.

(43) Ertl, P.; Rohde, B.; Selzer, P. Fast Calculation of Molecular Polar Surface Area as a Sum of Fragment-Based Contributions and Its Application to the Prediction of Drug Transport Properties. **2000**. https://doi.org/10.1021/jm000942e.

(44) Friesner, R. A.; Banks, J. L.; Murphy, R. B.; Halgren, T. A.; Klicic, J. J.; Mainz, D. T.; Repasky, M. P.; Knoll, E. H.; Shaw, D. E.; Shelley, M.; Perry, J. K.; Francis, P.; Shenkin, P. S. Glide: A New Approach for Rapid, Accurate Docking and Scoring. 1. Method and Assessment of Docking Accuracy. *J. Med. Chem.* **2004**, *47*, 1739–1749.

(45) Friesner, R. A.; Murphy, R. B.; Repasky, M. P.; Frye, L. L.; Greenwood, J. R. Halgren, T. A. Sanschagrin, P. C.; Mainz, D. T. Extra Precision Glide: Docking and Scoring Incorporating a Model of Hydrophobic Enclosure for Protein-Ligand Complexes. *J. Med. Chem.* **2006**, *49*, 6177–6196.

(46) Halgren, T. A.; Murphy, R. B.; Friesner, R. A.; Beard, H. S.; Frye, L. L.; Pollard, W. T.; Banks, J. L. Glide: A New Approach for Rapid, Accurate Docking and Scoring. 2. Enrichment Factors in Database Screening. *J. Med. Chem.* **2004**, *47*, 1750–1759.

(47) Miller, E. B.; Murphy, R. B.; Sindhikara, D.; Borrelli, K. W.; Grise-Wood, M. J.; Ranalli, F.; Dixon, S. L.; Jerome, S.; Boyles, N. A.; Day, T.; Gha-Nakota, P.; Mondal, S.; Rafi, S. B.; Troast, D. M.; Abel, R.; Friesner, R. A. A Reliable and Accurate Solution to the Induced Fit Docking Prob-Lem for Protein-Ligand Binding. **2020**.

(48) Kelly, M. D.; Mancera, R. L. Expanded Interaction Fingerprint Method for Analyzing Ligand Binding Modes in Docking and Structure-Based Drug Design. **2004**. https://doi.org/10.1021/ci049870g.

(49) Brewerton, S. C. The Use of Protein-Ligand Interaction Fingerprints in Docking. *Curr. Opin. Drug Discov. Devel.* **2008**, *11* (3), 356–364.

(50) Chupakhin, V.; Marcou, G.; Gaspar, H.; Varnek, A. Simple Ligand–Receptor Interaction Descriptor (SILIRID) for Alignment-Free Binding Site Comparison. *Comput. Struct. Biotechnol. J.* **2014**, *10* (16), 33–37. https://doi.org/10.1016/J.CSBJ.2014.05.004.

(51) Rácz, A.; Bajusz, D.; Héberger, K. Life beyond the Tanimoto Coefficient: Similarity Measures for Interaction Fingerprints. *J. Cheminform.* **2018**, *10* (1), 1–12. https://doi.org/10.1186/S13321-018-0302-Y/FIGURES/7.

(52) Han, J.; Kamber, M.; Pei, J. *Data Mining: Concepts and Techniques*, 3rd ed.; Elsevier Inc., 2012. https://doi.org/https://doi.org/10.1016/C2009-0-61819-5.

(53) Wolf, C.; Siegel, J. B.; Tinberg, C.; Camarca, A.; Gianfrani, C.; Paski, S.; Guan, R.; Montelione, G.; Baker, D.; Pultz, I. S. Engineering of Kuma030: A Gliadin Peptidase That Rapidly Degrades Immunogenic Gliadin Peptides in Gastric Conditions. **2015**. https://doi.org/10.1021/jacs.5b08325.

(54) Black, W. B.; Zhang, L.; Shun Mak, W.; Maxel, S.; Cui, Y.; King, E.; Fong, B.; Sanchez Martinez, A.; Siegel, J. B.; Li, H. Engineering a Nicotinamide Mononucleotide Redox Cofactor System for Biocatalysis. *Nat. Chem. Biol.* | **2020**, *16*. https://doi.org/10.1038/s41589-019-0402-7.

(55) USEPA. METHOD 552.2 Determination of Haloacetic Acids and Dalapon in Drinking Water by Liquid-Liquid Extraction, Derivatization and Gas Chromatography with Electron Capture Detection, Revision 1. EPA 815-B-03-002. **2003**.

(56) Moschet, C.; Lew, B. M.; Hasenbein, S.; Anumol, T.; Young, T. M. LC- and GC-QTOF-MS as Complementary Tools for a Comprehensive Micropollutant Analysis in Aquatic Systems. *Environ. Sci. Technol.* **2017**, *51* (3), 1553–1561. https://doi.org/10.1021/acs.est.6b05352.

(57) Bowers, G. N.; Mccomb, R. B.; Christensen, R. C.; Schaffer2, R. High-Purity 4-Nitrophenol: Purification, Characterization, and Specifications for Use as a Spectrophotometric Reference Material. *CLIN.CHEM* **1980**, *26* (6), 724.

(58) Sigma-Aldrich. 4-Methylumbelliferone (M1381) - Product Information Sheet.

(59) Lichtenberg, J. Y.; Ling, Y.; Kim, S. Non-Specific Adsorption Reduction Methods in Biosensing. *Sensors (Basel).* **2019**, *19* (11). https://doi.org/10.3390/S19112488.

(60) Huber, C.; Müller, E.; Schulze, T.; Brack, W.; Krauss, M. Improving the Screening Analysis of Pesticide Metabolites in Human Biomonitoring by Combining High-Throughput In Vitro Incubation and Automated LC-HRMS Data Processing. *Anal. Chem.* **2021**, *93* (26), 9149–9157. https://doi.org/10.1021/ACS.ANALCHEM.1C00972.

(61) Bertolani, S. J.; Siegel, J. B. A New Benchmark Illustrates That Integration of Geometric Constraints Inferred from Enzyme Reaction Chemistry Can Increase Enzyme Active Site Modeling Accuracy. *PLoS One* **2019**, *14* (4). https://doi.org/10.1371/JOURNAL.PONE.0214126.

(62) Kyte, J. Structure in Protein Chemistry, 2nd Ed.; Garland Science, 2006.

(63) Jansson, A.; Niemi, J.; Mäntsälä, P.; Schneider, G. Crystal Structure of Aclacinomycin Methylesterase with Bound Product Analogues: Implications for Anthracycline Recognition and Mechanism. *J. Biol. Chem.* **2003**, *278* (40), 39006–39013. https://doi.org/10.1074/JBC.M304008200.

(64) Womack, M. D.; Kendall, D. A.; MacDonald, R. C. Detergent Effects on Enzyme Activity and Solubilization of Lipid Bilayer Membranes. *Biochim. Biophys. Acta - Biomembr.* **1983**, *733* (2), 210–215. https://doi.org/10.1016/0005-2736(83)90524-2.

(65) Ramakrishna, T. R. B.; Ashton, T. D.; Marshall, S. N.; Nalder, T. D.; Yang, W.; Barrow, C. J. Effect of Triton X-100 on the Activity and Selectivity of Lipase Immobilized on Chemically Reduced Graphene Oxides. **2021**. https://doi.org/10.1021/acs.langmuir.1c01386.

CHAPTER 4: COMPARISON OF FOUR SUBSTRATES FOR THE ENRICHMENT OF AN AUTHOCTHONOUS MICROBIAL CONSORTIUM

The chapter is structured as follows:

- Section 4.1 provides motivation for the study.
- Section 4.2 presents materials and methods used.
- Section 4.3 summarizes and discusses results.
- Section 4.4 concludes.

4.1 Motivation

This brief study was designed primarily to compare substrate enrichments of a woodchip bioreactor microbial community. Varying the substrate supply to microbial communities has long been shown to influence the community composition,[1] the growth kinetics of the community, and the expression of enzymes of the community. For example, Gangola et al. (2018)[2] demonstrated that an increase in esterase and laccase expression in *Bacillus subtilis* cultures in response to cypermethrin exposure, played an essential role in cypermethrin detoxification. Such observations of microbial carboxylesterase activity against pyrethroids have been reported in many other studies, however primarily in pure culture experiments.[3,4] Given the natural promiscuity of wildtype microbial enzymes with respect to substrate specificity—particularly esterases and lipases—it is likely that the enzymes upregulated by one substrate would be catalytically compatible with a similar substrate.

In the context of woodchip bioreactor applications, the present work focuses on a microbial community isolated from a functional woodchip bioreactor. Previously, Mortenson et al. (2019)[5] isolated species from agricultural drainages and sediments that were characterized after cultivation on selective media containing common pesticides including bifenthrin, cis-permethrin, and imidacloprid. Moreover, Mortenson et al. (2019)[5] demonstrated that several of the isolated strains

were also able to perform the catalytic steps of denitrification, an important process to maintain in woodchip bioreactors.

Drawing from the conclusion of Chapter 3 experiments, the current chapter aims to provide preliminary evidence that phenyl salicylate as a substrate may enrich microbial communities in similar (or improved) ways to jump start pyrethroid degradation. While the study is limited, growth and metabolite data are reported as preliminary confirmation that native woodchip bioreactor microbes are able to metabolize two pyrethroids, as well as phenyl salicylate.

4.2 Materials and methods

4.2.1 Media and substrate solution preparation

The microbial suspension and subsequent enrichments were carried out in a minimal salt media (MSM) composed of 2.0 ppm $(NH_4)_2SO_4$, 0.2 ppm $MgSO_4 \cdot 7H_2O$, 0.01 ppm $CaCl_2 \cdot 2H_2O$, 0.001 ppm $FeSO_4 \cdot 7H_2O$, 1.5 ppm $Na_2HPO_4 \cdot 12\ h_2O$, 1.5 ppm KH_2PO_4, and adjusted to pH 7.0 ± 0.2 with concentrated NaOH (2M).[6] The four enrichment substrates, glucose (MilliporeSigma), phenyl salicylate (MilliporeSigma), bifenthrin (PESTANAL), and cypermethrin (PESTANAL), were dissolved in acetone to obtain 5000 ppm stock solutions. Bifenthrin and cypermethrin were chosen as the target pyrethroids to represent both Type I and Type II pyrethroids, and previous success in identifying esterase metabolites with current extraction/analytical protocols (see Chapter 3). The substrate stock solutions were sterilized by filtration through 0.2-micron PTFE filters (Millex).

4.2.2 Enrichment protocol

Woodchips were obtained from an operational field woodchip bioreactor (SeaMist bioreactor, Moss Landing, CA) and kept submerged in bioreactor water, and stored at 4°C until

use. Twenty grams (wet weight) of field woodchips were transferred to a baked (500°C, 4h) and autoclaved Erlenmeyer flask containing 200mL of minimal salt media and incubated at 200 rpm at 37°C for 48 hours to create a microbial suspension. Six of each treatment and control—glucose-, phenyl salicylate-, bifenthrin-, and cypermethrin-enriched, and inoculant-free controls—were prepared with 100mL of MSM in baked 125mL Erlenmeyer flasks, then autoclaved. Substrates were added to respective flasks by adding 1mL of sterilized stocks to the media (final concentration of 50ppm), then inoculated with 1mL of microbial suspension. The thirty flasks were incubated under conditions similar to Pankaj et al., (2016)[7] at 200 rpm and 37°C for a total of 15 days.

Six replicates of 3mL microbial suspension aliquots were kept for RNA extraction to obtain initial community and transcriptome profiles. Periodically throughout the incubation, microbial growth was monitored (about every 24 h) by OD600 measurement (Biowave Cell Density Meter CO8000) and confirmed with periodic CFU enumeration by the spread plate method (Standard Method 9215C).[8] Samples for substrate quantification were collected at incubation days 6, 8, 9, and 15. All samples were collected under aseptic conditions. Samples for RNA extraction were collected during log growth phase for transcriptomic analysis, where 3mL of culture were sampled and preserved in 6mL of RNAprotect Bacteria Reagent (Qiagen) as per reagent protocol and stored at -80°C until extraction. Transcriptome analysis is still underway and will not be discussed further.

4.2.3 Substrate parent compound and transformation products extraction and analysis

At each timepoint, 1mL of media was sampled from three of the six replicates, as well as the entire volume of one of the control flasks. The 1mL samples were diluted 10x in MilliQ water to allow for better-paced solid phase extraction. All samples were spiked with a surrogate mix containing imidacloprid d4, diuron d6, esfenvalerate, and boscalid d4, to monitor extraction

consistency. Samples were stored at 4°C and extracted within 24 h using Waters Oasis SPE cartridges. Cartridges were eluted with two volumes each of ethyl acetate and methanol (5mL). Sample vials were treated with Na_2SO_4 to remove residual water and extracted with 10 mL of 1:1 hexane and acetone. The hexane/acetone and ethyl acetate extracts were combined and concentrated to 1mL by N_2 evaporation. The internal standard 4,4′-Dibromooctafluorobiphenyl (DBOFB) was added to each standard and sample, then samples were analyzed using GC-NCI for pyrethroid quantification using MassHunter Workstation Quantitative Analysis (Agilent, v 10.1).

Methanol extracts were concentrated and diluted 5x in Optima water, spiked with imidacloprid as the internal standard, and analyzed with LC-QTOF-MS (Agilent 1260 Infinity HPLC coupled to an Agilent 6530 QTOF-MS with a Zorbax Eclipse Plus C18 column), in both ESI+ and ESI-. Phenyl salicylate was analyzed as described in Chapter 3. A PCDL (Agilent MassHunter PCDL Manager v 7.0) was curated with known biotransformation products of both bifenthrin and cypermethrin, along with salicylic acid and two surrogates, diuron d6 and imidacloprid d4 (Table C1). The Find by Formula suspect screening tool in MassHunter Qualitative Analysis (Agilent, v 10.0) was used, and hits with validation scores of 80 and above were retained for analysis. Transformation product abundances were normalized to ISTD and surrogates to obtain semi-quantitative estimates of relative concentrations.

4.3 Results and discussion

4.3.1 Microbial growth patterns

The woodchip suspension inoculums were able to grow on all substrates, while no growth was observed in the control flasks over the 15-day incubation period. The glucose- and phenyl salicylate-enriched flasks exhibited similar lag periods (~5 days), whereas the bifenthrin- and cypermethrin-enriched flasks showed longer lag periods, about 7 and 8 days, respectively (Figure

C1). As the lag phase is indicative of the time required for cells to produce the metabolic machinery for replication,[9] it is typically proportional to the complexity or severity of the incubation environment, including the bioavailability of nutrient sources.[9,10] As the glucose and phenyl salicylate enrichments yielded similar growth curves, the two substrates provide similarly accessible carbon sources to the consortia, as other variables were kept constant. In terms of utility as a biostimulant, smaller lag phases are desirable in order to reduce the amount of time required to reach exponential growth, and thus expedite the remediation workflow.

The longer lag phases of the bifenthrin and cypermethrin enrichments are indicative of less bioavailable and/or toxic substrates[9] and suggest a slight preference for bifenthrin. In terms of vertebrate toxicity, cypermethrin generally has a lower toxicity threshold than bifenthrin,[11] though specific toxicological studies with microbes have not been performed in great detail.

4.3.2 Substrate recovery

The change in substrate (i.e., parent compound) concentration over the course of the incubation period exhibited patterns inconsistent with consortium growth; not only were the concentrations broadly variable across treatment replicates, but the concentration measurements did not show a decrease in substrate with respect to microbial growth or over time. The bifenthrin concentrations over elapsed time did show a decrease in average concentration by day 15 as compared to day 6 (Figure C2.A.), however there was no correlation between cell density and bifenthrin concentration that we would expect from principles of cell growth and microbial stoichiometry.[12] The cypermethrin enrichments exhibited a slightly negative correlation between cypermethrin concentration and both elapsed time and cell density (Figure C3.A-B.), while the

phenyl salicylate enrichments showed an increase in phenyl salicylate concentration over time, and with cell density (Figure C4.A-B.).

The behavior of the substrate compounds' concentrations over time is likely due to the addition of substrate to concentrations well beyond their respective aqueous solubilities. The solubility of bifenthrin in water is generally reported as < 1 µg/L,[13] significantly to an average of 0.4 µg/L when measured in a 3.2%, pH 8 saline solution.[14] Cypermethrin solubility, though greater than bifenthrin solubility (2.6 µg/L),[15] also drops an order of magnitude in the same saline solution (0.7 µg/L).[14] Phenyl salicylate is reported to have an aqueous solubility of 150 µg/L.[16] The dosed concentration of each of the substrates used in this study was 50 mg/L, between two and five orders of magnitude above the above-described solubilities. Because of this, the expected decrease in substrate concentration accompanying consortium growth was not observed and led to erroneous concentration measurements due to heterogeneity of the media (Figures C2.B and C3.B). Moreover, the increase in phenyl salicylate recovery with respect to cell density suggests that with cell growth and production of extracellular biomolecules, the solubility of phenyl salicylate may increase allowing for better distribution in the treatment flasks and thus greater measured concentration. In light of this, it is preferable to assess substrate catabolism from the degradation profiles rather than substrate abatement.

4.3.3 Transformation product recovery

Of the curated PCDL used for suspect screening, fourteen bifenthrin and cypermethrin metabolite hits were found with a Find by Formula score above 80. The surrogates diuron d6 and imidacloprid d4 were accurately identified in all analyzed samples. The 14 suspects identified were further screened by retention time consistency and presence of respective qualifiers/product ions

in the obtained spectra, informed by deposited spectra available in the MassBank of North America (MoNA; Fiehn Lab, UC Davis), or predicted from the Competitive Fragmentation Modeling for Metabolite Identification (CFM-ID; Wishart Lab) [17] if no experimental spectra were available. The metabolites 3-(2-chloro-3,3,3-trifluoroprop-1-enyl)-2,2-dimethylcyclopropane-1-carboxylic acid (i.e., TFP acid), 4-propylbenzaldehyde, 3-phenoxybenzoic acid (i.e., 3-PBA), 2-methyl-3-phenylbenzoic acid, and 3-(2,2-dichlorovinyl)-2,2-dimethylcyclopropane carboxylic acid (i.e., permethric acid) were kept for further analysis.

Of the four identified pyrethroid metabolites, TFP acid, 3-PBA, and permethric acid were the most commonly detected. TFP acid, the carboxylic acid product of bifenthrin, exhibited a general increase in concentration as cell density increased, suggesting that ester hydrolysis of bifenthrin was occurring during the catabolic growth phase of the consortium. This pattern is not only predicted by biotransformation rules (e.g., EnviPath),[18] but also in several enrichment studies employing *Bacillus*, *Micrococcus*, and *Catellibacterium* strains, to name a few.[19-30] Similarly, permethric acid, the carboxylic acid product of cypermethrin, was also present in all cypermethrin-enrichment samples screened in an increasing concentration with respect to cell density. The alcohol moiety of cypermethrin also degraded to 3-PBA, a common transformation product of pyrethroids,[31] and exhibited a response proportional to the increase in permethric acid (Figure C3.C-D), further evidence of esterase activity in the cypermethrin enrichments. The 3-PBA counterpart of bifenthrin, 2-methyl-3-phenylbenzoic acid, was detected in all screened bifenthrin-enriched samples, exhibiting the same increase in abundance over time and with increasing cell density (Figures C2.C-D.). While other metabolites were detected via suspect screening, discrepancies in retention time, ion products, and inconsistency of detection among treatment replicates led them to be excluded from further analysis. Additionally, many of the smaller

aromatic pyrethroid metabolites are better detected using GC-MS-EI (e.g., 2-phenoxyphenol and 4-propylbenzaldehyde), which was not considered as part of this study.

4.4 Conclusions and future work

This study confirmed that autochthonous woodchip bioreactor microbial communities can metabolize both bifenthrin and cypermethrin as sole carbon sources. While parent compound measurements were inconsistent, likely due to heterogenous distributions throughout the minimal salt media, the detection of both the carboxylic acid and alcohol-derived 3-PBA metabolites confirmed the metabolism of the pyrethroids consistent with consortia growth. Furthermore, phenyl salicylate as a substrate produced similar growth behavior as glucose as a substrate, a desirable characteristic for biostimulants, as speed of community adaptation and growth will expedite remediation.

With evidence that this microbial community can shift to metabolize both phenyl salicylate as well as two common pyrethroids, next steps may extend in two directions: first, in order to further assess phenyl salicylate as a biostimulant, phenyl salicylate-enriched communities may be introduced to pyrethroid-containing media to assess degradation. Ideally, a pre-enriched community would ideally shorten the adaptation period in the pyrethroid media (i.e., shorten the lag phase), while expediting pyrethroid mineralization. Second, to assess the metabolic mechanisms within each enrichment, the transcriptome profiles will be compared between each of the treatment communities. Ideally, the phenyl salicylate-enriched communities will show similar transcriptome profiles as the pyrethroid-enriched communities, suggesting that phenyl salicylate can stimulate enzyme production in the native community able to mineralize pyrethroids. Of course, complete mineralization of pyrethroids involves several steps, and may be optimized by

varying other growth parameters such as co-substrates, nutrient characteristics, temperature, and incubation rpm.[3] In all, biological remediation of pyrethroids in aqueous environments is promising, though will require further experimentation to assess full feasibility.

4.5 References

(1) Mills, D. E. K.; Fitzgerald, K.; Litchfield, C. D.; Gillevet, P. M. A Comparison of DNA Profiling Techniques for Monitoring Nutrient Impact on Microbial Community Composition during Bioremediation of Petroleum-Contaminated Soils. *J. Microbiol. Methods* **2003**, *54* (1), 57–74. https://doi.org/10.1016/S0167-7012(03)00007-1.

(2) Gangola, S.; Sharma, A.; Bhatt, P.; Khati, P.; Chaudhary, P. Presence of Esterase and Laccase in Bacillus Subtilis Facilitates Biodegradation and Detoxification of Cypermethrin. *Sci. Reports 2018 81* **2018**, *8* (1), 1–11. https://doi.org/10.1038/s41598-018-31082-5.

(3) Bhatt, P.; Huang, Y.; Zhan, H.; Chen, S. Insight into Microbial Applications for the Biodegradation of Pyrethroid Insecticides. *Frontiers in Microbiology*. Frontiers Media S.A. August 2, 2019, p 1778. https://doi.org/10.3389/fmicb.2019.01778.

(4) Zhan, H.; Huang, Y.; Lin, Z.; Bhatt, P.; Chen, S. New Insights into the Microbial Degradation and Catalytic Mechanism of Synthetic Pyrethroids. *Environmental Research*. Academic Press Inc. March 1, 2020, p 109138. https://doi.org/10.1016/j.envres.2020.109138.

(5) Mortensen, Z.; Kato, J.; Silveus, J.; Valdez, A.; Hall, S.; Nimmers, K.; Haffa, A. L. M. Isolation of Microbial Populations with the Ability to Use Pesticides as a Sole Carbon Source in Multichannel Woodchip Bioreactors under a Controlled Environment. In *ACS Symposium Series*; American Chemical Society, 2019; Vol. 1308, pp 475–489. https://doi.org/10.1021/bk-2019-1308.ch024.

(6) Coleman, N. V.; Mattes, T. E.; Gossett, J. M.; Spain, J. C. Biodegradation of Cis-Dichloroethene as the Sole Carbon Source by a β-Proteobacterium. *Appl. Environ. Microbiol.* **2002**, *68* (6), 2726–2730. https://doi.org/10.1128/AEM.68.6.2726-2730.2002/ASSET/D6898C33-63DB-4951-9962-0E46BC0609F2/ASSETS/GRAPHIC/AM0622036004.JPEG.

(7) Pankaj; Sharma, A.; Gangola, S.; Khati, P.; Kumar, G.; Srivastava, A. Novel Pathway of Cypermethrin Biodegradation in a Bacillus Sp. Strain SG2 Isolated from Cypermethrin-Contaminated Agriculture Field. *3 Biotech* **2016**, *6* (1), 1–11. https://doi.org/10.1007/S13205-016-0372-3/FIGURES/6.

(8) 9215 HETEROTROPHIC PLATE COUNT - Standard Methods For the Examination of Water and Wastewater https://www.standardmethods.org/doi/10.2105/SMWW.2882.188 (accessed Sep 17, 2022).

(9) Bertrand, R. L. Lag Phase Is a Dynamic, Organized, Adaptive, and Evolvable Period That Prepares Bacteria for Cell Division. *J. Bacteriol.* **2019**, *201* (7). https://doi.org/10.1128/JB.00697-18/ASSET/753DDCF4-5339-488E-866B-829E1F43976E/ASSETS/GRAPHIC/JB.00697-18-F0007.JPEG.

(10) Nicola, L.; Bååth, E. The Effect of Temperature and Moisture on Lag Phase Length of Bacterial Growth in Soil after Substrate Addition. *Soil Biol. Biochem.* **2019**, *137*, 107563. https://doi.org/10.1016/J.SOILBIO.2019.107563.

(11) Galadima, M.; Singh, S.; Pawar, A.; Khasnabis, S.; Dhanjal, D. S.; Anil, A. G.; Rai, P.; Ramamurthy, P. C.; Singh, J. Toxicity, Microbial Degradation and Analytical Detection of Pyrethroids: A Review. *Environ. Adv.* **2021**, *5*, 100105. https://doi.org/10.1016/J.ENVADV.2021.100105.

(12) Li, Z.; Zeng, Z.; Tian, D.; Wang, J.; Fu, Z.; Wang, B.; Tang, Z.; Chen, W.; Chen, H. Y. H.; Wang, C.; Yi, C.; Niu, S. The Stoichiometry of Soil Microbial Biomass Determines Metabolic Quotient of Nitrogen Mineralization. *Environ. Res. Lett.* **2020**, *15* (3), 034005. https://doi.org/10.1088/1748-9326/AB6A26.

(13) O'Neil, M.J. *The Merck Index - An Encyclopedia of Chemicals, Drugs, and Biologicals,* 15th ed.; Royal Society of Chemistry, 2013; p. 213.

(14) Saranjampour, P.; Vebrosky, E.; Armbrust, K. Salinity Impacts on Water Solubility and *n*-octanol/water partition coefficients of selected pesticides and oil constituents. *Environ. Toxicol. Chem.* 2017, *36*, 2274-2280. https://doi.org/10.1002/etc.3784.

(15) Tomlin, C., *A World Compendium, the Pesticide Manual*. 14 ed.; British Crop Production Council, 2006.

(16) Phenyl Salicylate. *HMDB*. The Metabolomics Innovation Centre. https://hmdb.ca/metabolites/HMDB0032018 (Accessed Nov 10, 2022).

(17) Fu, L.; Niu, B.; Zhu, Z.; Wu, S.; Li, W. CD-HIT: Accelerated for Clustering the next-Generation Sequencing Data. *Bioinformatics* **2012**, *28* (23), 3150–3152. https://doi.org/10.1093/BIOINFORMATICS/BTS565.

(18) Wicker, J.; Lorsbach, T.; Gütlein, M.; Schmid, E.; Latino, D.; Kramer, S.; Fenner, K. EnviPath--The Environmental Contaminant Biotransformation Pathway Resource. *Nucleic Acids Res.* **2016**, *44* (D1), D502–D508. https://doi.org/10.1093/NAR/GKV1229.

(19) Zhan, H.; Huang, Y.; Lin, Z.; Bhatt, P.; Chen, S. New Insights into the Microbial Degradation and Catalytic Mechanism of Synthetic Pyrethroids. *Environmental Research*. Academic Press Inc. March 1, 2020, p 109138. https://doi.org/10.1016/j.envres.2020.109138.

(20) Cycon, M.; Piotrowska-Seget, Z. Pyrethroid-Degrading Microorganisms and Their Potential for the Bioremediation of Contaminated Soils: A Review. *Front. Microbiol.* **2016**, *7* (SEP). https://doi.org/10.3389/FMICB.2016.01463.

(21) Tallur, P. N.; Veena, A. E.; Megadi, B.; Harichandra, A. E.; Ninnekar, Z. Biodegradation of Cypermethrin by Micrococcus Sp. Strain CPN 1. https://doi.org/10.1007/s10532-007-9116-8.

(22) Zhao, H.; Geng, Y.; Chen, L.; Tao, K.; Hou, T. Biodegradation of Cypermethrin by a Novel Catellibacterium Sp. Strain CC-5 Isolated from Contaminated Soil. *Can. J. Microbiol.* **2013**, *59* (5), 311–317. https://doi.org/10.1139/CJM-2012-0580/ASSET/IMAGES/CJM-2012-0580TAB4.GIF.

(23) Liu, F.; Chi, Y.; Wu, S.; Jia, D.; Yao, K. Simultaneous Degradation of Cypermethrin and Its Metabolite, 3-Phenoxybenzoic Acid, by the Cooperation of Bacillus Licheniformis B-1 and Sphingomonas Sp. SC-1. *J. Agric. Food Chem.* **2014**, *62* (33), 8256–8262. https://doi.org/10.1021/JF502835N/ASSET/IMAGES/MEDIUM/JF-2014-02835N_0006.GIF.

(24) Sundaram, S.; Das, M. T.; Thakur, I. S. Biodegradation of Cypermethrin by Bacillus Sp. in Soil Microcosm and in-Vitro Toxicity Evaluation on Human Cell Line. *Int. Biodeterior. Biodegradation* **2013**, *77*, 39–44. https://doi.org/10.1016/J.IBIOD.2012.11.008.

(25) Chen, S.; Luo, J.; Hu, M.; Geng, P.; Zhang, Y. Microbial Detoxification of Bifenthrin by a Novel Yeast and Its Potential for Contaminated Soils Treatment. *PLoS One* **2012**, *7* (2), e30862. https://doi.org/10.1371/JOURNAL.PONE.0030862.

(26) Chen, S.; Geng, P.; Xiao, Y.; Hu, M. ENVIRONMENTAL BIOTECHNOLOGY Bioremediation of β-Cypermethrin and 3-Phenoxybenzaldehyde Contaminated Soils Using Streptomyces Aureus HP-S-01. https://doi.org/10.1007/s00253-011-3640-5.

(27) Chen, S.; Lai, K.; Li, Y.; Hu, M.; Zhang, Y.; Zeng, Y. ENVIRONMENTAL BIOTECHNOLOGY Biodegradation of Deltamethrin and Its Hydrolysis Product 3-Phenoxybenzaldehyde by a Newly Isolated Streptomyces Aureus Strain HP-S-01. https://doi.org/10.1007/s00253-011-3136-3.

(28) Xiao, Y.; Chen, S.; Gao, Y.; Hu, W.; Hu, M.; Zhong, G. Isolation of a Novel Beta-Cypermethrin Degrading Strain Bacillus Subtilis BSF01 and Its Biodegradation Pathway. *Appl. Microbiol. Biotechnol.* **2015**, *99* (6), 2849–2859. https://doi.org/10.1007/S00253-014-6164-Y/FIGURES/7.

(29) Guo, P.; Wang, B.; Hang, B. J.; Li, L.; Ali, S. W.; He, J.; Li, S. Pyrethroid-Degrading Sphingobium Sp. JZ-2 and the Purification and Characterization of a Novel Pyrethroid Hydrolase. *Int. Biodeterior. Biodegradation* **2009**, *63* (8), 1107–1112. https://doi.org/10.1016/J.IBIOD.2009.09.008.

(30) Lee, S.; Gan, J.; Kim, J. S.; Kabashima, J. N.; Crowley, D. E. Microbial Transformation of Pyrethroid Insecticides in Aqueous and Sediment Phases. *Environ. Toxicol. Chem.* **2004**, *23* (1), 1–6. https://doi.org/10.1897/03-114.

(31) Richards, J.; Lu, Z.; Fu, Q.; Schlenk, D.; Gan, J. Conversion of Pyrethroid Insecticides to 3-Phenoxybenzoic Acid on Urban Hard Surfaces. *Environ. Sci. Technol. Lett.* **2017**, *4* (12), 546–550. https://doi.org/10.1021/ACS.ESTLETT.7B00466/ASSET/IMAGES/LARGE/EZ-2017-00466V_0002.JPEG.

APPENDIX A: SUPPLEMENTARY INFORMATION FOR CHAPTER 2

A.1 Figures

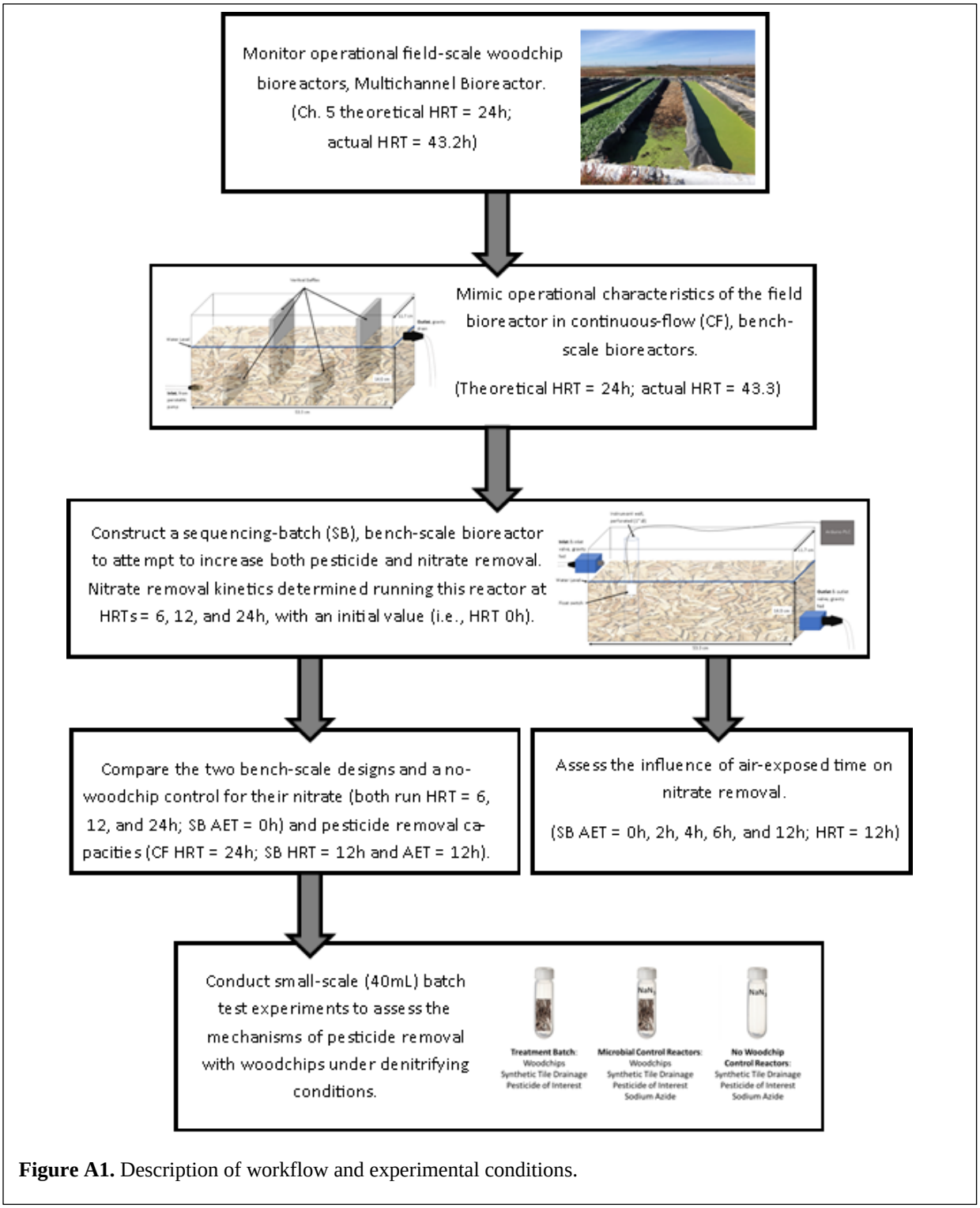

Figure A1. Description of workflow and experimental conditions.

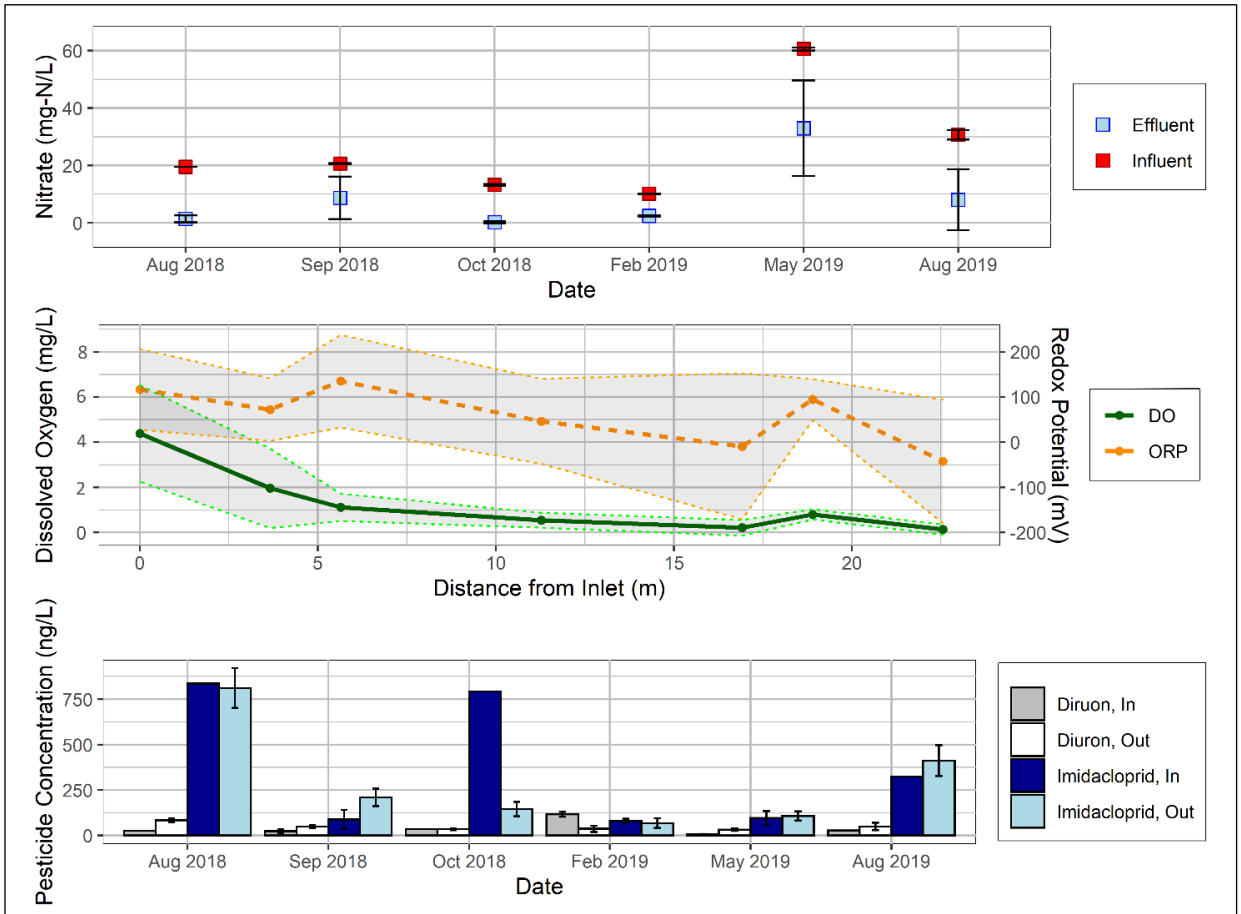

Figure A2. Nitrate concentrations at the influent and effluent of the field woodchip bioreactor, grab samples taken during six sampling events (a). Grey ribbons indicate maxima and minima for influent measurements, and standard deviation of triplicates for effluent measurements. Dissolved oxygen (DO, mg/L) and redox potential (ORP, mV) levels taken along the length of the multichannel woodchip bioreactors during the Sep 2018, Oct 2018, Feb 2019, and May 2019 sampling events (b). Grey ribbon indicates standard deviation of triplicate measurements. Nitrate influent measurement were taken in duplicate. Imidacloprid and diuron concentrations (ng/L) in the influent and effluent of field woodchip bioreactors (c). Error bars indicate standard deviations of triplicate measurements.

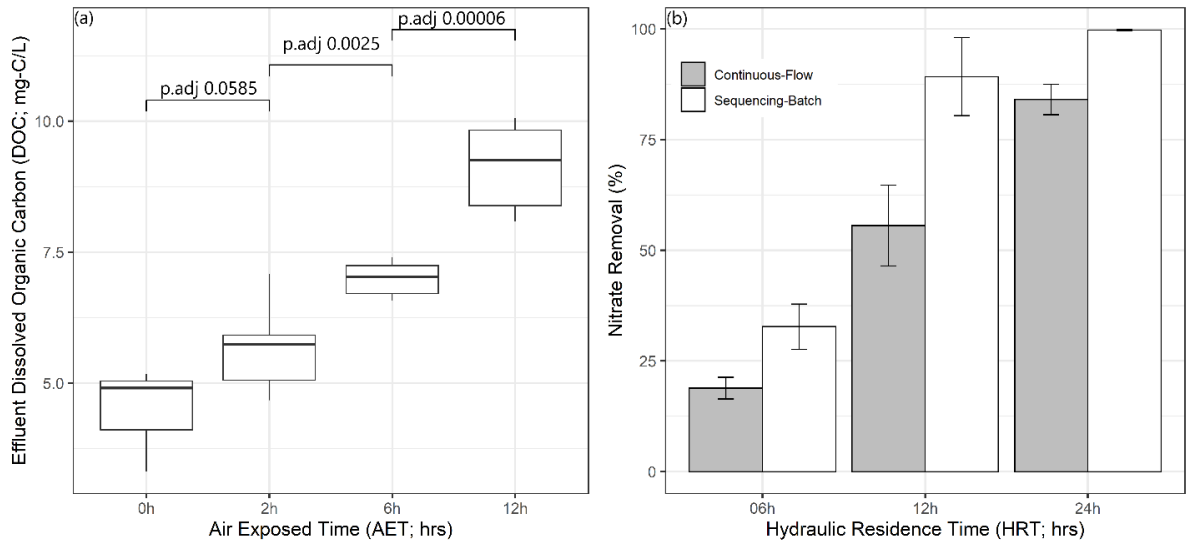

Figure A3. Dissolved organic carbon concentrations in the effluent of the sequencing-batch reactor run at a 12 h hydraulic retention time (HRT) and at four different air exposed times (AETs). The total time to drain and refill between retention times was 30 minutes. Boxes display the interquartile ranges with bolded median values, and whiskers display minima and maxima. Adjusted p-values (p.adj) are from the ANOVA post-hoc Tukey's Test (a). Comparative denitrification rates of continuous-flow and sequencing-batch style reactors. Across the three hydraulic residence times (HRTs) investigated, the batch style reactor consistently removed more nitrate than the continuous-flow reactor. Error bars indicate standard deviations (b).

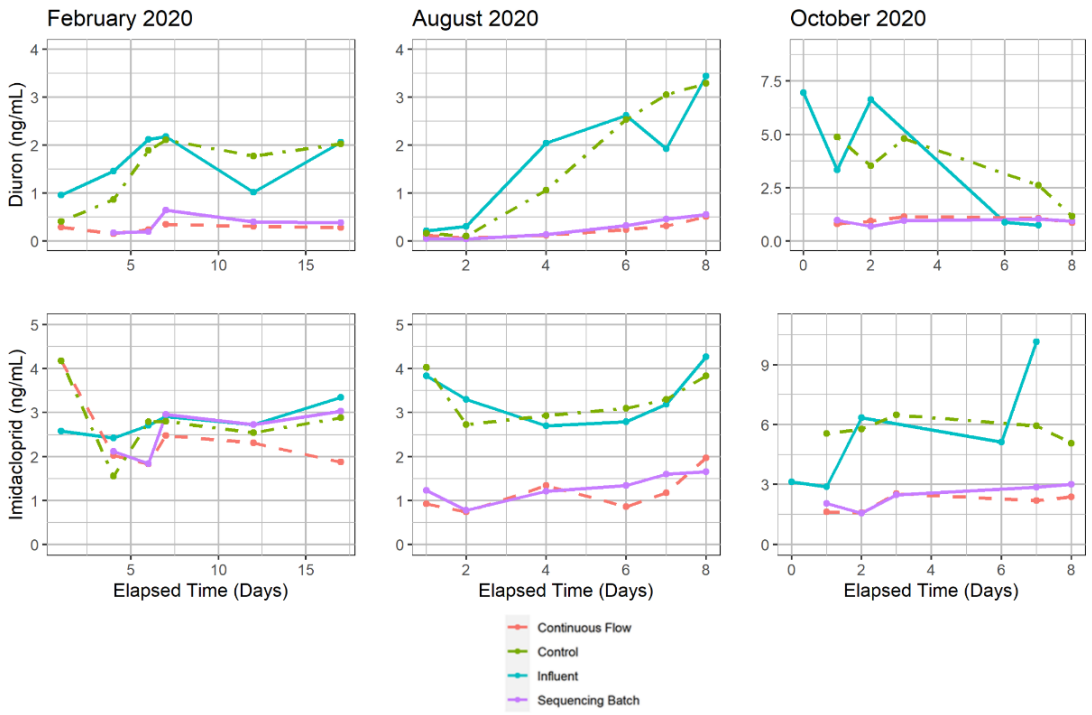

Figure A4. Pesticide concentrations in influent, no-woodchip control, continuous-flow, and sequencing-batch reactors from three side-by-side pesticide and nitrate spiking experiments. Diuron was consistently removed across both the continuous-flow and sequencing-batch bench-scale woodchip bioreactors. Imidacloprid was removed in both the August 2020 and October 2020 experiments, while removal was hindered during the February experiment due to high concentrations of imidacloprid already adsorbed to the woodchips. There was no significant difference between the continuous-flow and sequencing-batch reactors for both diuron ($p = 0.66$) and imidacloprid ($p = 0.32$).

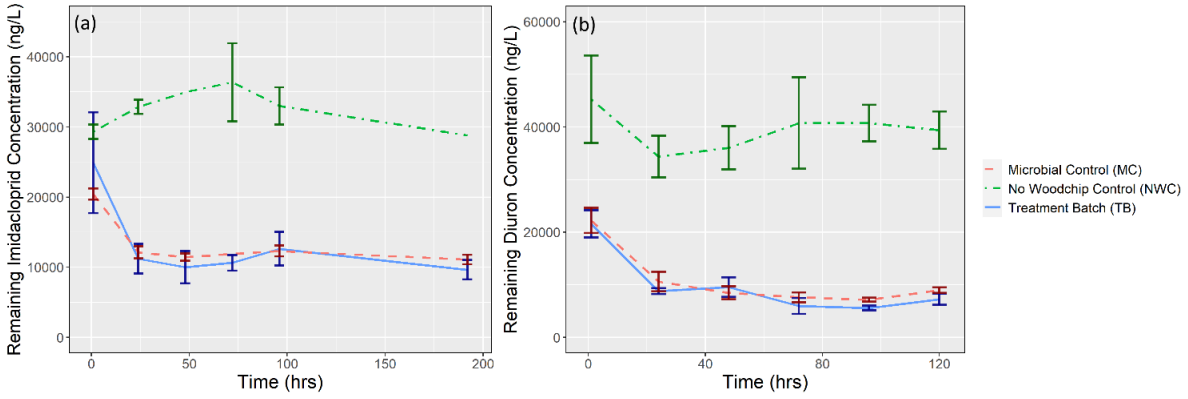

Figure A5. Remaining concentrations of imidacloprid (a) and diuron (b) across kinetic batch tests. Error bars indicate standard deviations of triplicate measurements. Points missing error bars show mean values of duplicate reactors.

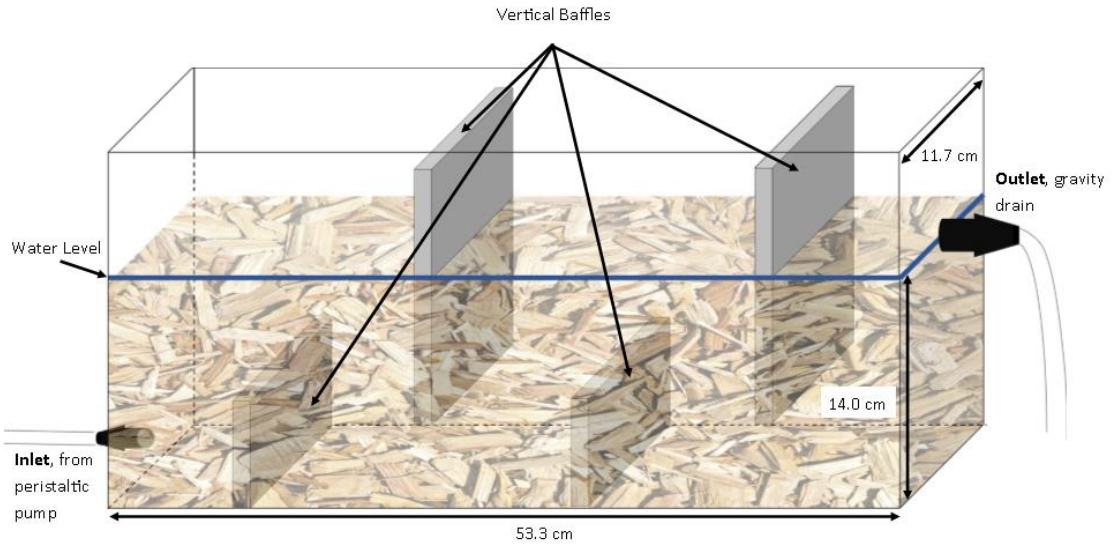

Figure A6.A. Continuous-flow bench-scale bioreactor design. The reactors were constructed from 3/8" clear cast acrylic sheets, with bulk volume dimensions 53.3cm x 11.7cm x 14.0cm (LxWxH). Because the dimension ratios differed from the field bioreactors, four vertical baffles were placed along the length of the bench-scale reactors to limit short circuiting and to achieve similar dispersion coefficient to the monitored field bioreactors.

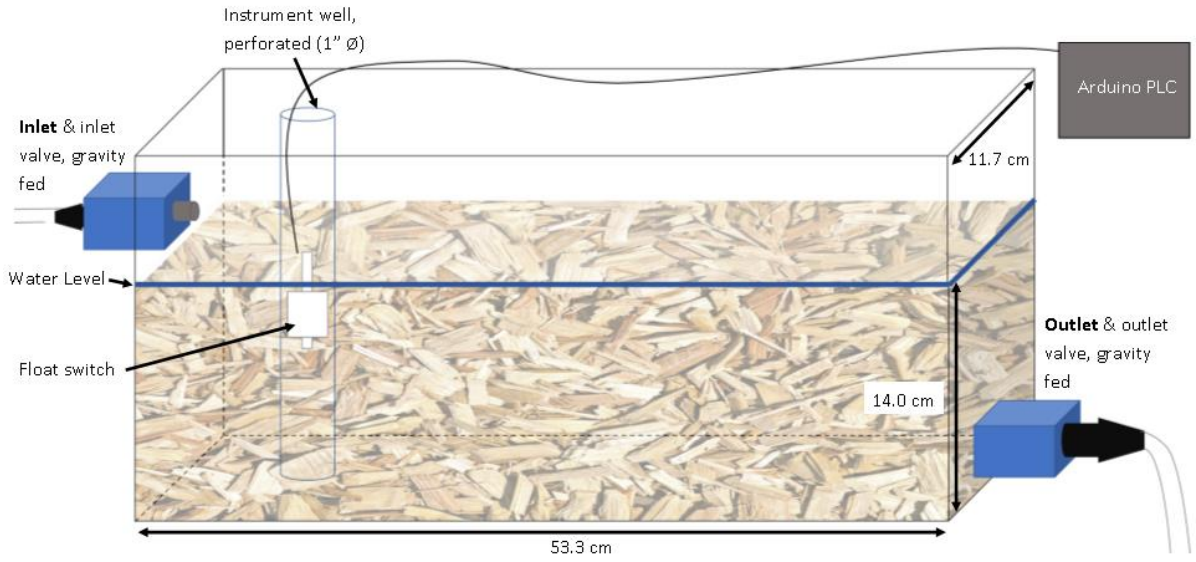

Figure A6.B. Sequencing-batch bench-scale bioreactor design. Fed with the same synthetic tile drainage as described in the Figure 1 caption, this design is gravity fed and gravity drained. Filling and draining are controlled by an Arduino program logic controller (PLC) that received signals from a float switch to indicate water level and programmed hydraulic residence and air exposed times.

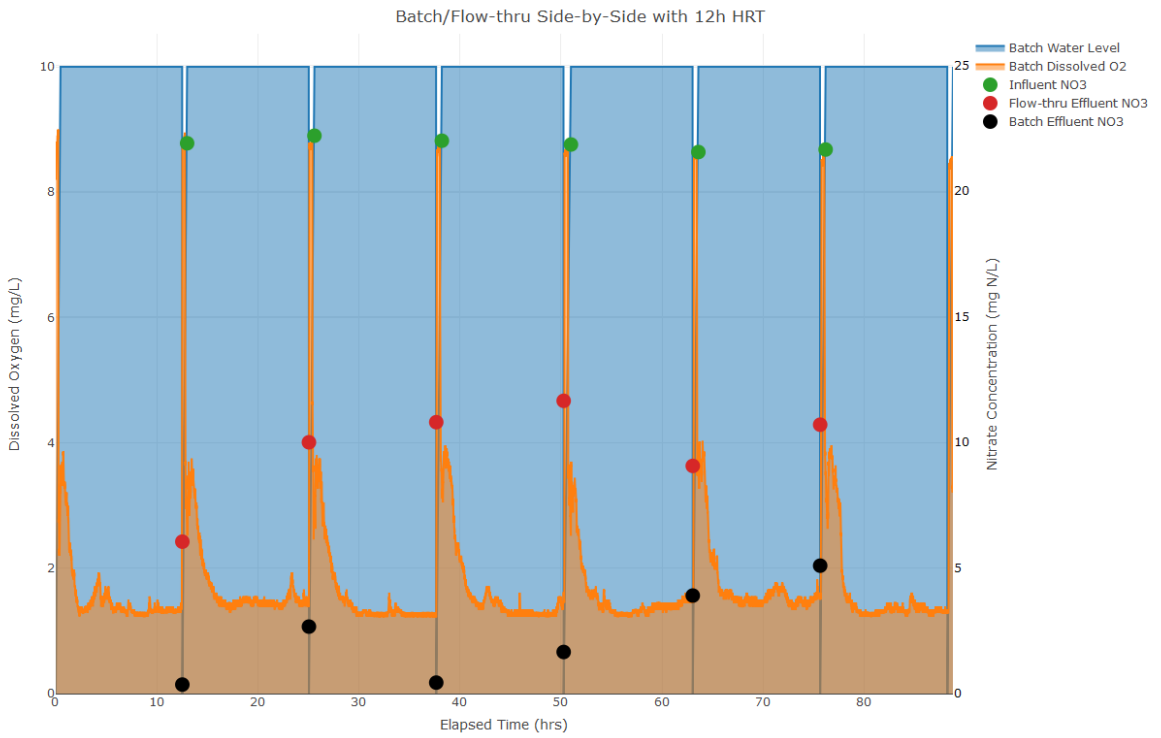

Figure A7. Profile of dissolved oxygen (DO) concentration throughout seven fill/refill cycles in the sequencing batch style reactor. Presented plot shows dynamics of operating at a 12 h HRT and 0 h AET; other HRT:AET ratios exhibited similar behavior in terms of introducing DO into the treatment cycle.

Figure A8. Photograph of PG&E Multichannel Bioreactor, Castroville, CA. There are three woodchip channels at this site, with dimensions 22.6m x 1.68m x 0.762m (LxWxH).

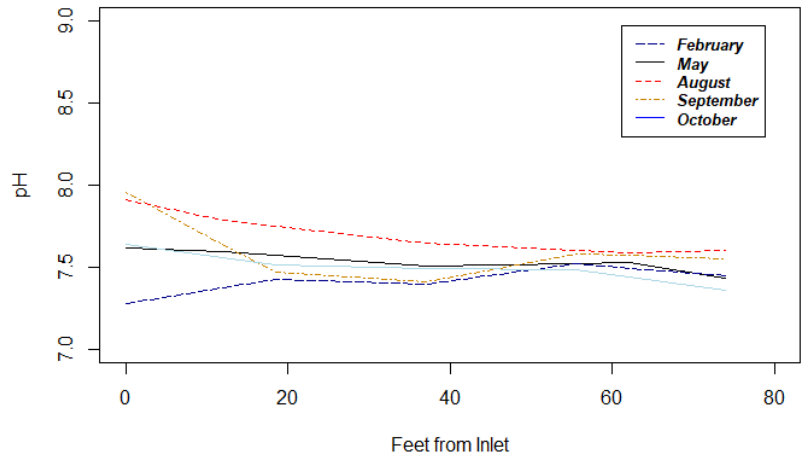

Figure A9.A. Field monitoring results of pH readings along the length of the Multichannel Bioreactor channels. Channel readings were averaged for each sampling event.

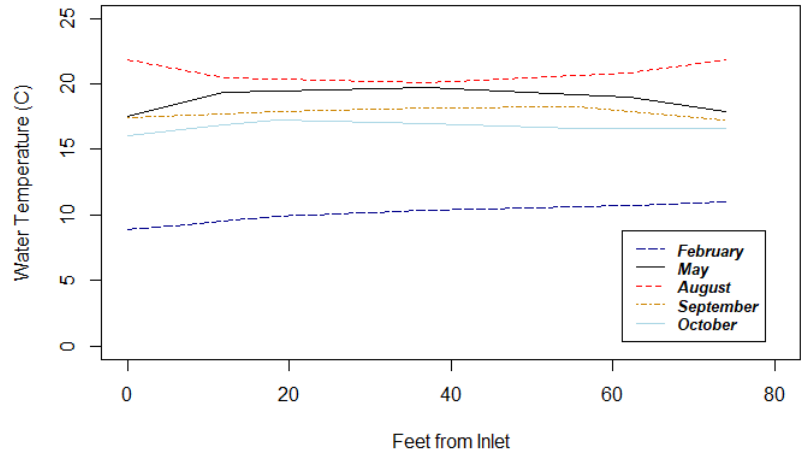

Figure A9.B. Field monitoring results of temperature readings along the length of the PG&E Multichannel Bioreactor channels. Channel readings were averaged for each sampling event.

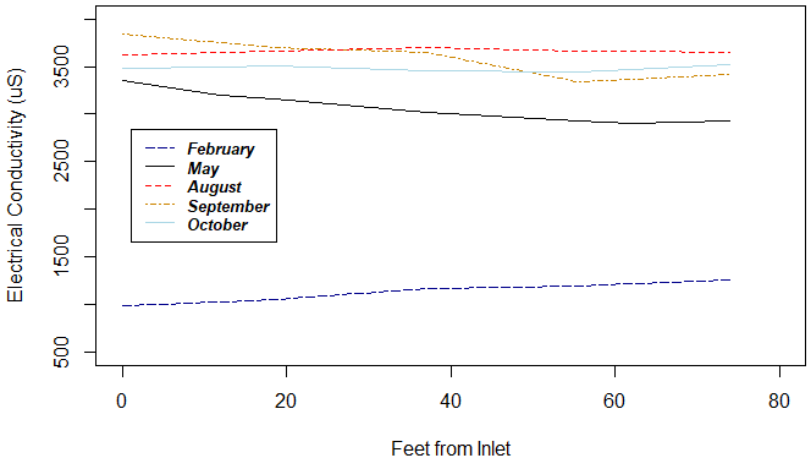

Figure A9.C. Field monitoring results of conductivity (EC) readings along the length of the PG&E Multichannel Bioreactor channels. Channel readings were averaged for each sampling event.

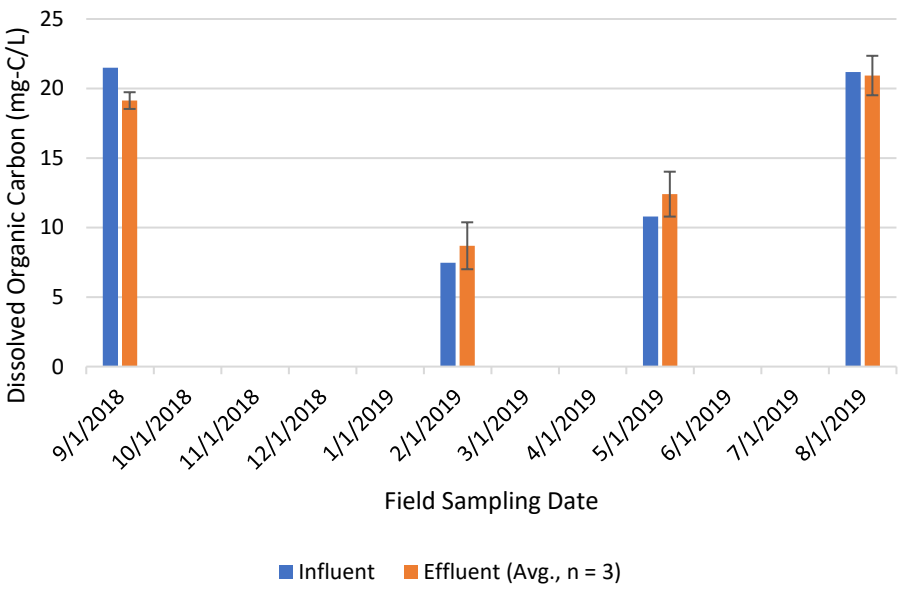

Figure A10.A. Dissolved organic carbon (DOC) concentrations at the influent and effluent of field bioreactors. Grab samples taken on listed sampling dates and analyzed at UC Davis. While seasonal differences may be attributed to irrigation patterns and storm events, there appeared to be no large difference between the influent and effluent concentrations across all sampling events. This suggests that DOC is not a limiting factor in the field bioreactors as an electron donor for microbial processes such as denitrification.

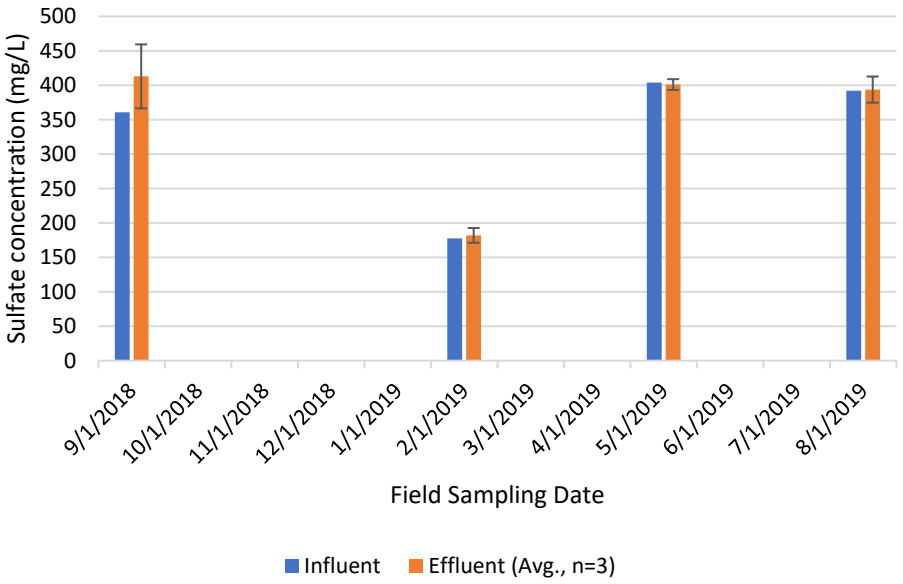

Figure A10.B. Sulfate concentrations at the influent and effluent of field bioreactors. Grab samples taken on listed sampling dates and analyzed at UC Davis. Effluent series error bars indicate standard deviation (n = 3). Apart from the February 2019 sampling event (during a storm event), concentrations remained relatively constant, showing no appreciable reduction or gain across the woodchip bioreactors.

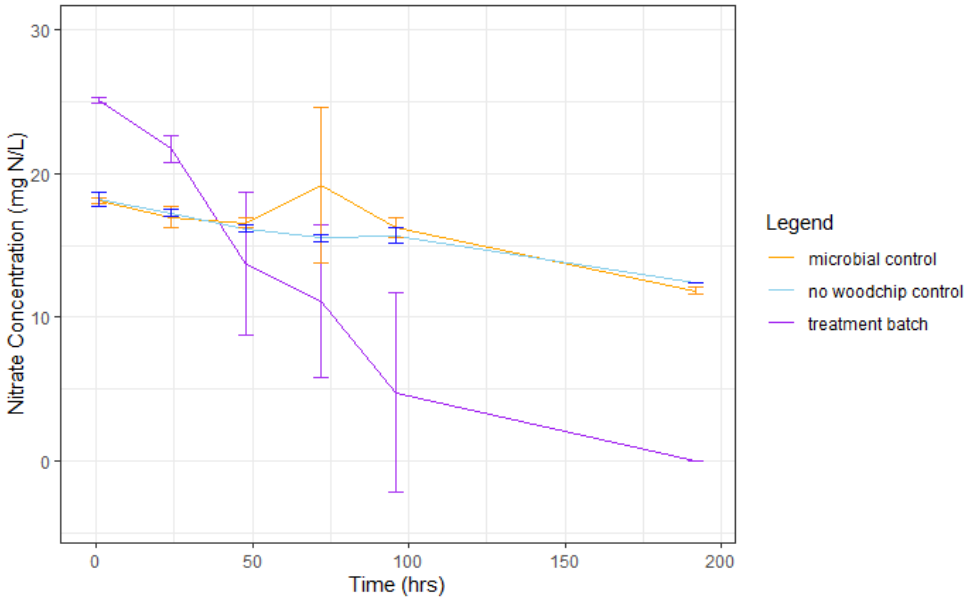

Figure A11.A. Nitrate concentration by treatment during the imidacloprid kinetic batch test. The microbial suppression of the microbial control (MC) treatment adequately suppressed denitrification, as the MC curve greatly resembles the no woodchip control curve. Nitrate was completely removed in the treatment (microbially active) batch reactors by day 8 (192hrs). Error bars represent the standard deviation of treatment triplicates.

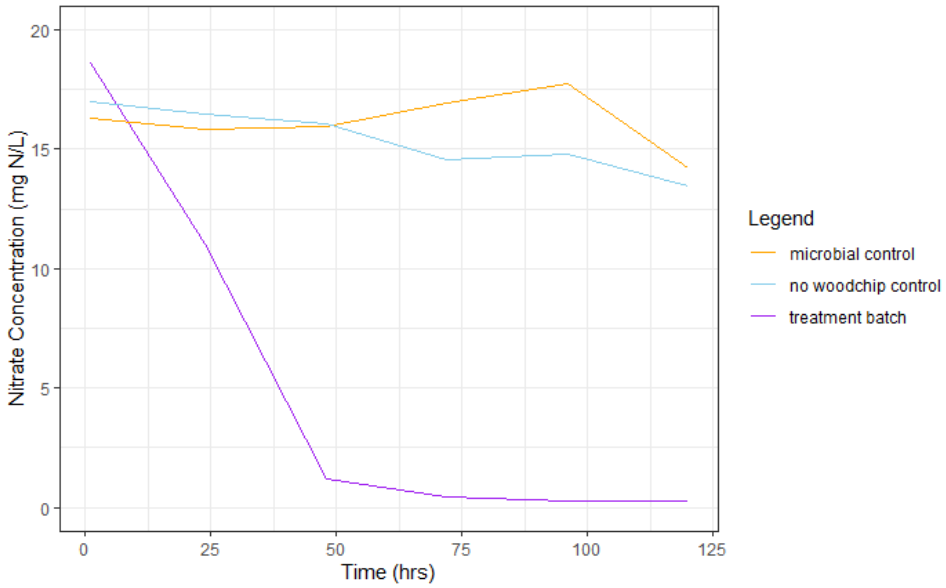

Figure A11.B. Nitrate concentration by treatment during the diuron kinetic batch test. The microbial suppression of the microbial control (MC) treatment adequately suppressed denitrification, as the MC curve greatly resembles the no woodchip control curve. Most of the nitrate was removed in the treatment (microbially active) batch reactors by day 2 (48hrs).

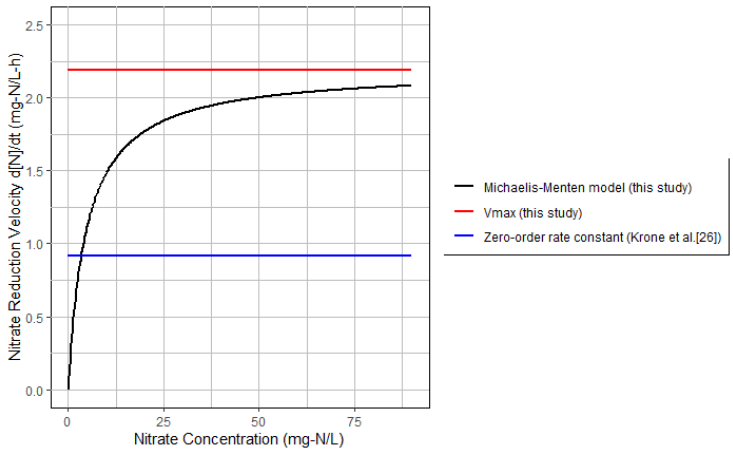

Figure A12. Plotted Michaelis-Menten model from this study alongside obtained zero-order rate constant from Krone et al. (2022) adjusted to 22°C using Krone et al.'s (2022) obtained Arrhenius constant, 1.12.

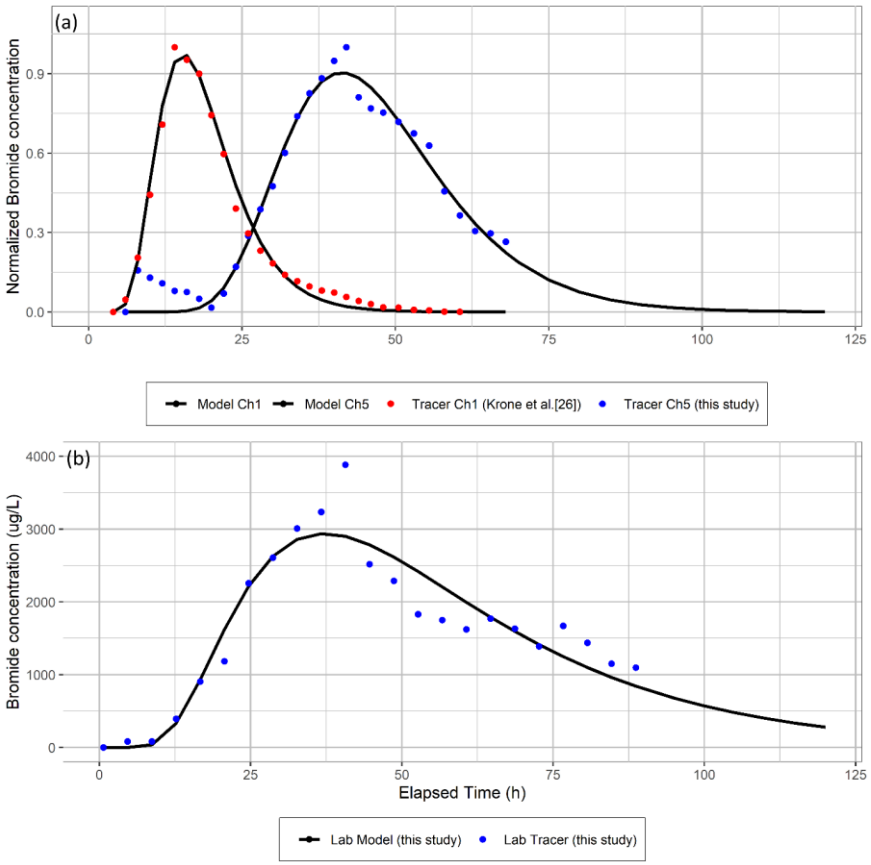

Figure A13. The results of fitting plug flow with diffusion models to the bromide tracer results from the field-scale bioreactor, Channel 5 and Channel 1 (a) and the bench-scale continuous-flow reactor (b). Fitted average HRT value from Channel 5 most closely resembled that of the bench-scale reactor. Bromide data from Krone et al. (2022) was used to fit each of the field curves.

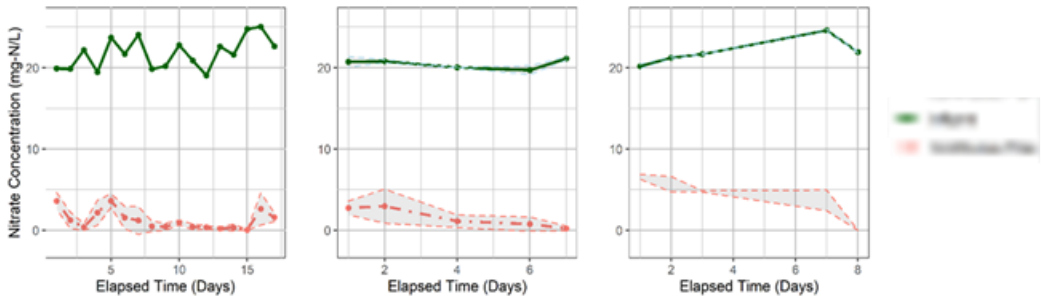

Figure A14. The denitrification efficiency of the continuous-flow reactors across three separate bench-scale operations.

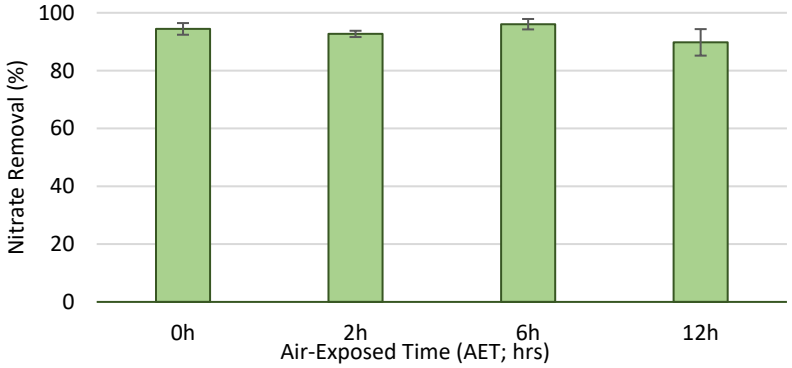

Figure A15. Results from testing the effect of air-exposed time (AET) on denitrification. Hydraulic residence time (HRT) was kept at 12 hrs for all trials. This set of experiments suggests that the air-exposed time does not substantially compromise degree of denitrification.

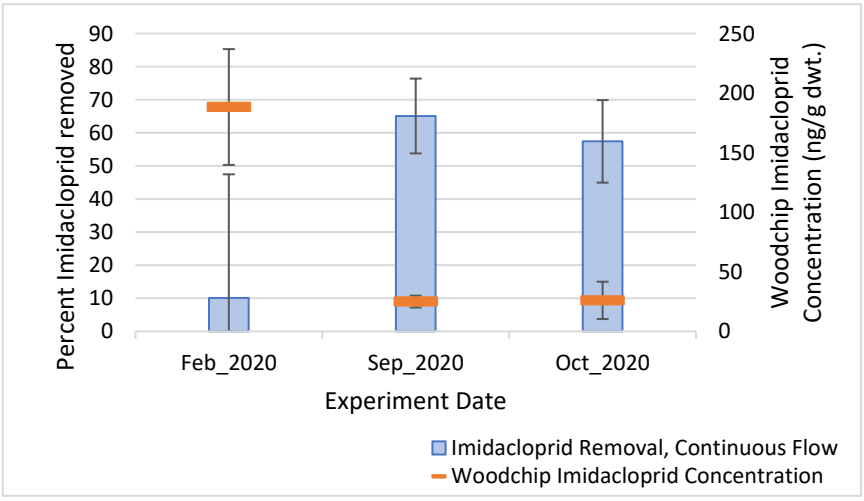

Figure A16. Inverse relationship between percent imidacloprid removal and woodchip imidacloprid concentration (ng/g dry weight). Imidacloprid extraction from each batch of woodchips was collected prior to lab experiments to obtain initial levels of imidacloprid residue. Error bars indicate standard deviations.

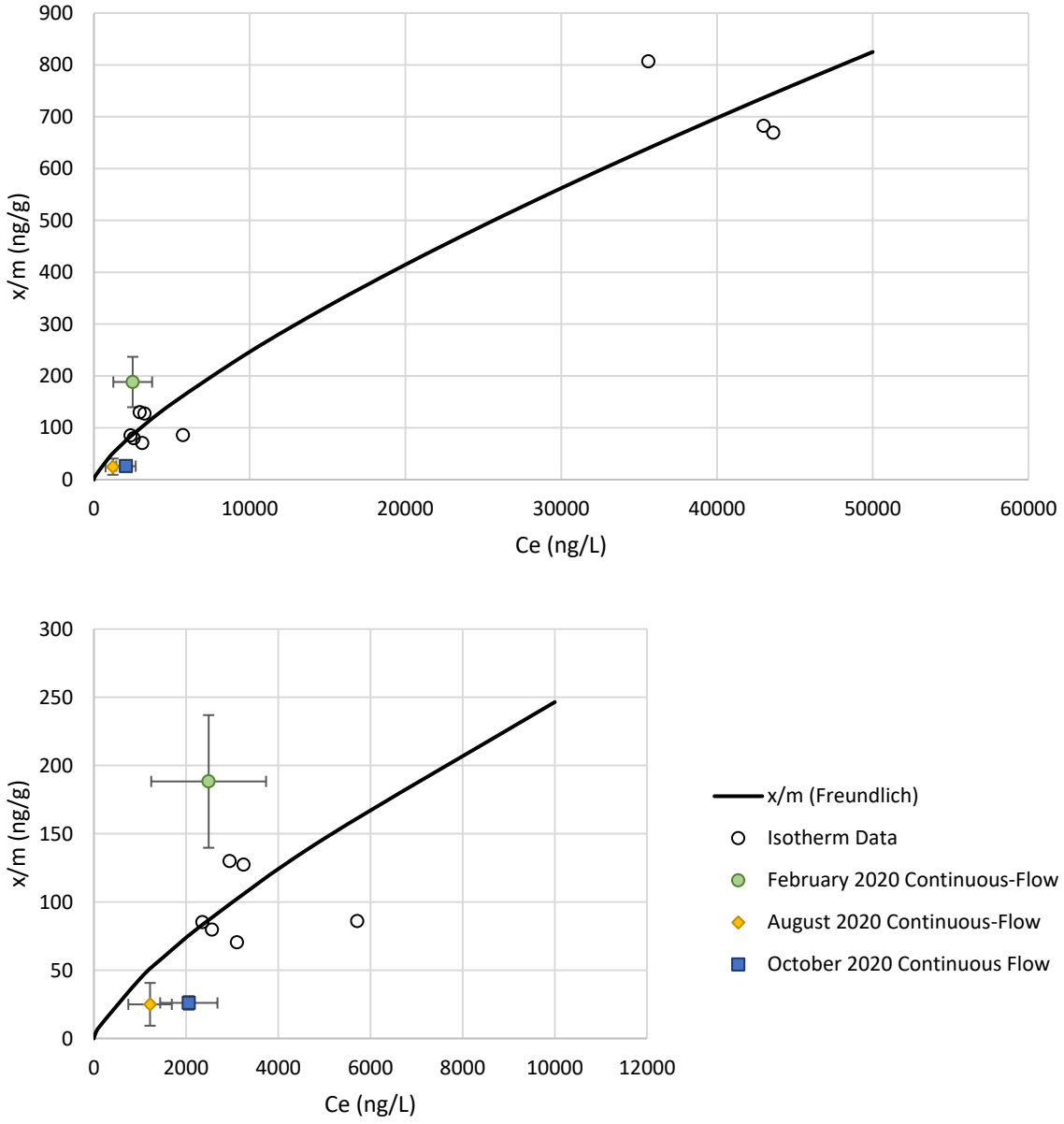

Figure A17. Imidacloprid isotherm (line) with isotherm data and Ce and x/m (qe) values from the bench scale continuous-flow reactors during the three side-by-side bench-scale experiments (i.e., February, August, and October 2020). Panel (a) displays the complete isotherm and panel (b) displays a detailed view of the lower range of the isotherm to visualize experimental data.

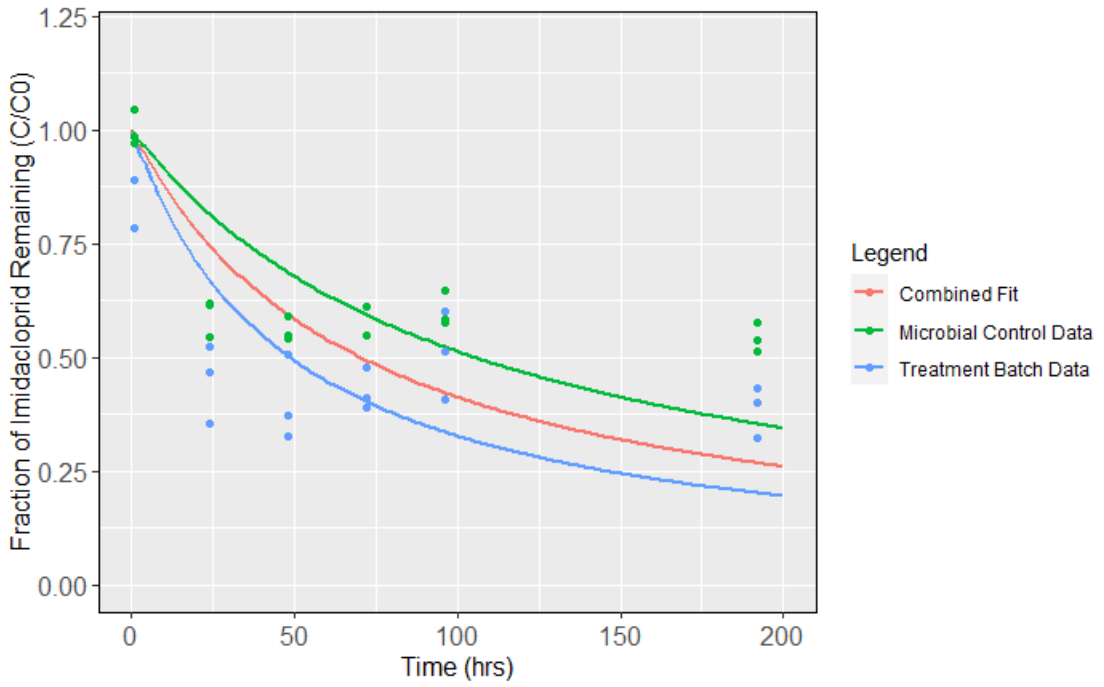

Figure A18.A. The separate and combined pseudo-second order models of imidacloprid adsorption.

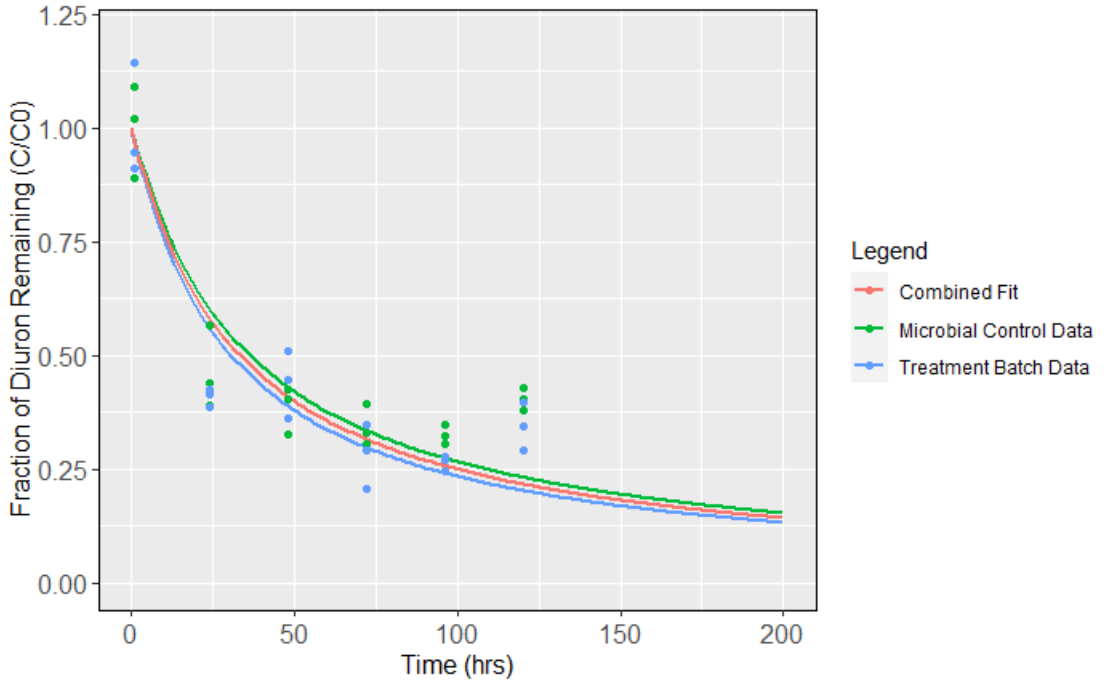

Figure A18.B. The separate and combined pseudo-second order models of diuron adsorption..

A.2 Tables

Table A1. Dispersed Flow Model (DFM) comparison for field tracer data

	$\bar{t}$	Pe	$\bar{t}$ 95% CI	Pe 95% CI
Integral Estimation/Trapezoidal Method (Ch. 5)	48.55	12.01	-	-
Nonlinear Regression Method (Ch. 1)	16.50	14.32	[16.2,16.8]	[13.2,15.4]
Nonlinear Regression Method (Ch. 5)	43.20	22.13	[42.3,44.1]	[18.8,25.4]

Table A2. Bench-scale woodchip bioreactor denitrification kinetics.

	linearized fit		fit to rate data		model parameters			
	Mult. R^{2a}	P^{b}	MSE^{c}	RSE^{d}	k (h^{-1})[e]	n^{f}	K_m[g] (mg/L)	V_{max}[h] (mg/h)
Differential Method	0.895	0.2100	0.210	0.793	0.187	0.863		
Integral Method 1st order	0.975	0.0017	1.515	1.507	0.223	1		
Michaelis-Menten	0.991	0.0622	0.054	0.401			4.774	2.193

[a] Multiple R-squared (coefficient of determination): $R^2 = 1 - \frac{\sum(y_i - \hat{y}_i)^2}{\sum(y_i - \bar{y})^2}$

[b] p-value of regression analysis F-statistic; evaluation of difference of all regression coefficients = 0.

[c] Mean squared error: $MSE = \frac{1}{n}\sum(y_i - \hat{y}_i)^2$

[d] Relative squared error: $RSE = \sqrt{\frac{1}{n-2}\sum(y_i - \hat{y}_i)^2}$

[e] Rate constant, k, for generalized rate equation: for $r = k[A]^x[B]^y \; for \; aA + bB \rightarrow cC$; First order: $r = -\frac{d[A]}{dt} = k[A]$

[f] Reaction order, n, in generalized rate law equation: $-\frac{d[A]}{dt} = k[A]^n$

[g] Michaelis constant, K_m, given by: $K_m = \frac{k_{off}+k_{cat}}{k_{on}} \; for \; enzymatic \; reaction \; [E] + [S] \overset{k_{on}/k_{off}}{\longleftrightarrow} [ES] \overset{k_{cat}}{\longrightarrow} [E] + [P]$

[h] Maximum reaction rate, V_{max}: $V_{max} = k_{cat}[E]_T \; where \; [E]_T = [E] + [ES]$

Table A3: Fitted Péclet and HRT values from tracer studies[a]

	Bench Scale		Field - Ch1		Field - Ch5	
Pe	6.422	*0.9228*	14.3161	*0.5288*	22.1344	*1.5809*
HRT (tbar)	43.43	*1.47*	16.4982	*0.132*	43.2037	*0.4272*
MDI	3.83		2.54		2.13	

[a]Fitted value with respective *standard error values*

Table A4: Pseudo-first and -second model fits of small-scale batch tests.

		First order model			Second order model		
Pesticide	**Treatment**	**MSE**	**RSE**	**k_1**	**MSE**	**RSE**	**k_2**
Imidacloprid	TB	2.28E-02	2.28E-02	1.68E-02	1.12E-02	1.09E-01	4.19E-05
	MC	2.43E-02	1.60E-01	1.47E-02	1.17E-02	1.11E-01	3.36E-05
Diuron	TB	5.15E-02	2.34E-01	1.12E-02	3.31E-02	1.87E-01	8.26E-07
	MC	3.03E-02	1.79E-01	5.84E-03	1.98E-02	1.45E-01	4.65E-07

Table A5: Model results with interaction term and combined (TB & MC) pseudo-second order.

Pesticide		**MSE**	**RSE**	**k_{22}**	**b**	**b p-value**
Imidacloprid	with int. term	2.67E-02	1.68E-01	4.19E-07	4.88E-07	1.89E-02
	combined model	3.16E-02	1.80E-01	6.28E-07		
Diuron	with int. term	1.17E-02	1.11E-01	3.75E-05	0.00E+00	1.00E+00
	combined model	1.17E-02	1.10E-01	3.75E-05		

APPENDIX B: SUPPLEMENTARY INFORMATION FOR CHAPTER 3

B.1 Figures

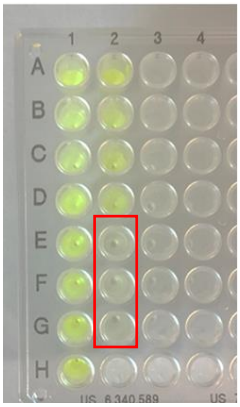

Figure B1. Confirmation of esterase activity of purified enzymes.

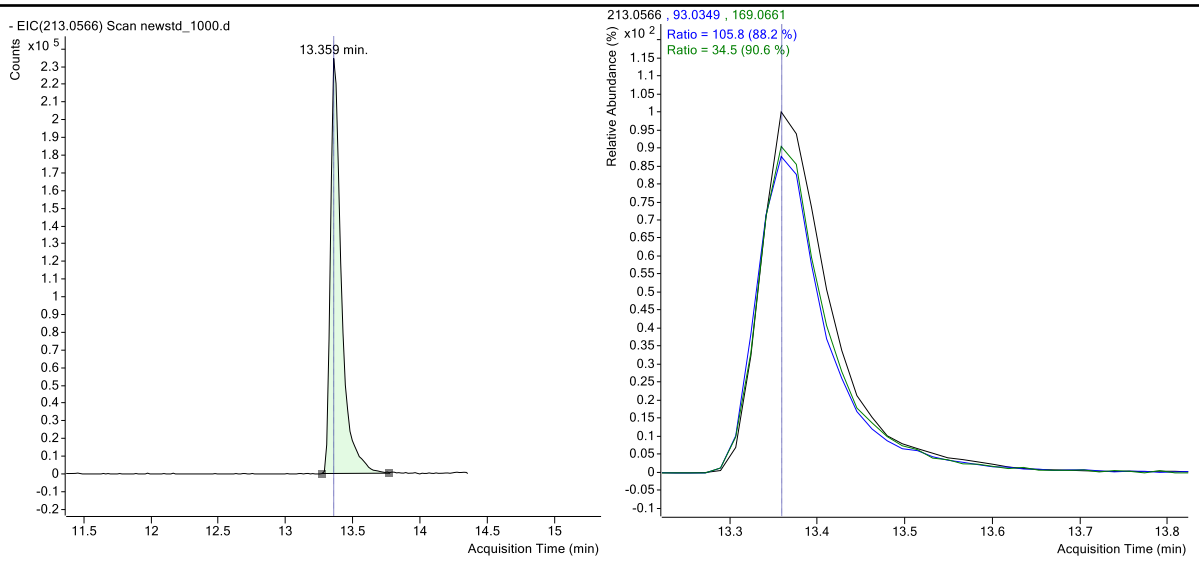

Figure B2.A. Phenyl Salicylate standard $[M-H]^-$ (m/z 213.0566) and qualifier chromatograms.

(Figure B2 continued)

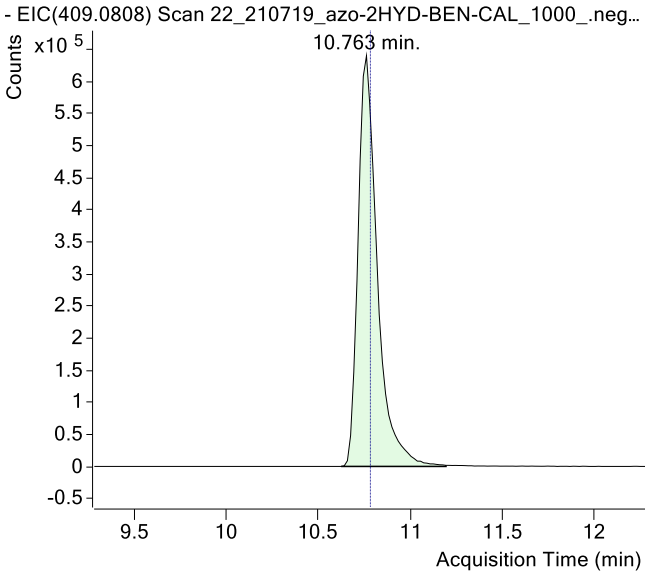

Figure B2.B. Bensulfuron-methyl standard [M-H]- chromatogram.

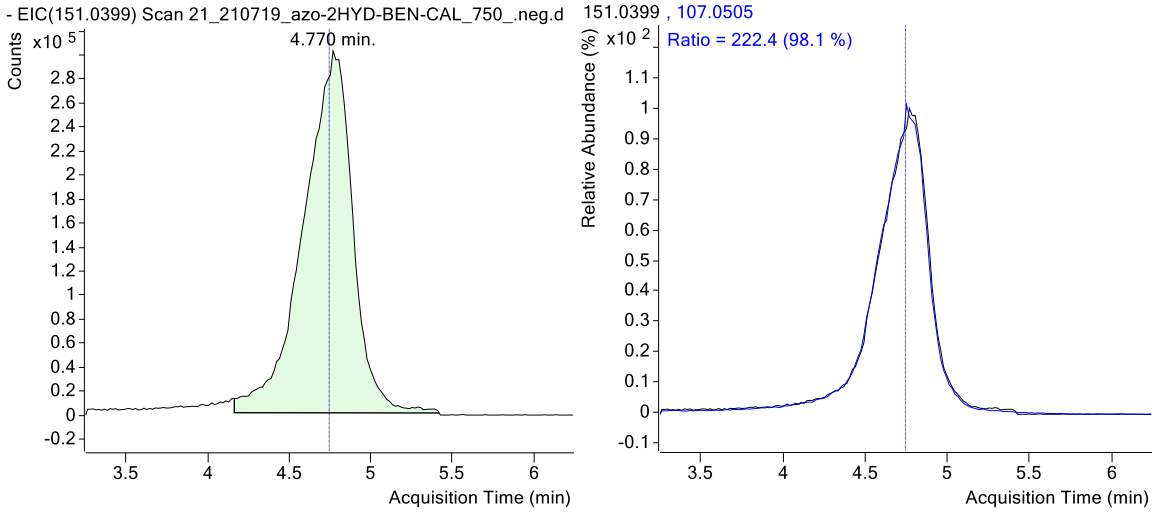

Figure B2.C. 2-Hydroxyphenylacetic Acid standard [M-H]- and qualifier chromatograms.

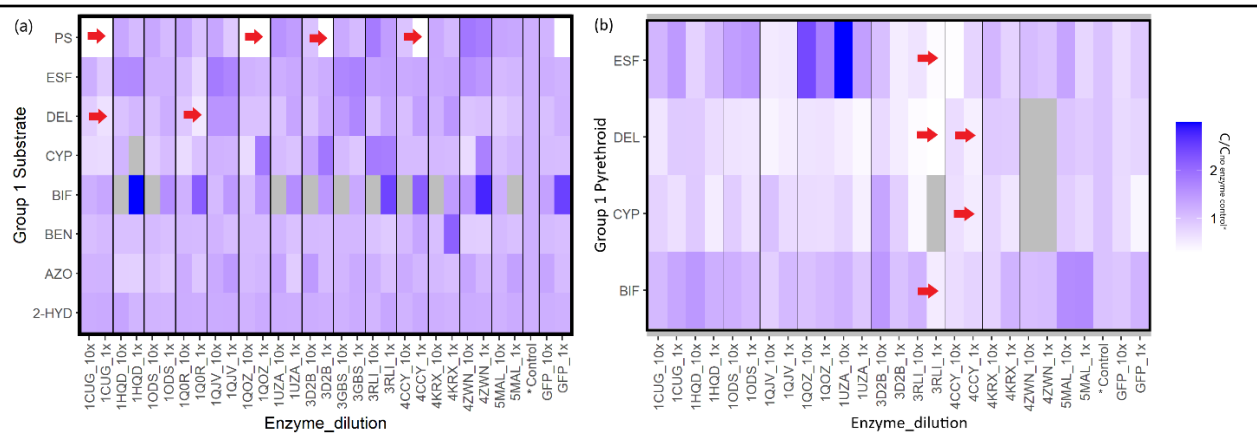

Figure B3. Parent substrate recoveries of pesticides and alternative esters as compared to no-enzyme controls ($C/C_{no\ enzyme}$) in activity assays rounds 1 (a) and 2 (b). Enzyme name abbreviations are listed in Table B1 and are appended by 10x or 1x to denote the dilution prepared. Pesticide name abbreviations are listed in Table B2. Dark blue cells illustrate a wide range of recoveries, especially among more hydrophobic pyrethroid compounds. Grey cells indicate unmeasured combinations due to low sample integrity. Red arrows indicate examples of dose dependency between 10x and 1x enzyme dilutions. Among the alternative esters, phenyl salicylate exhibited the greatest amount of parent compound loss across most enzymes.

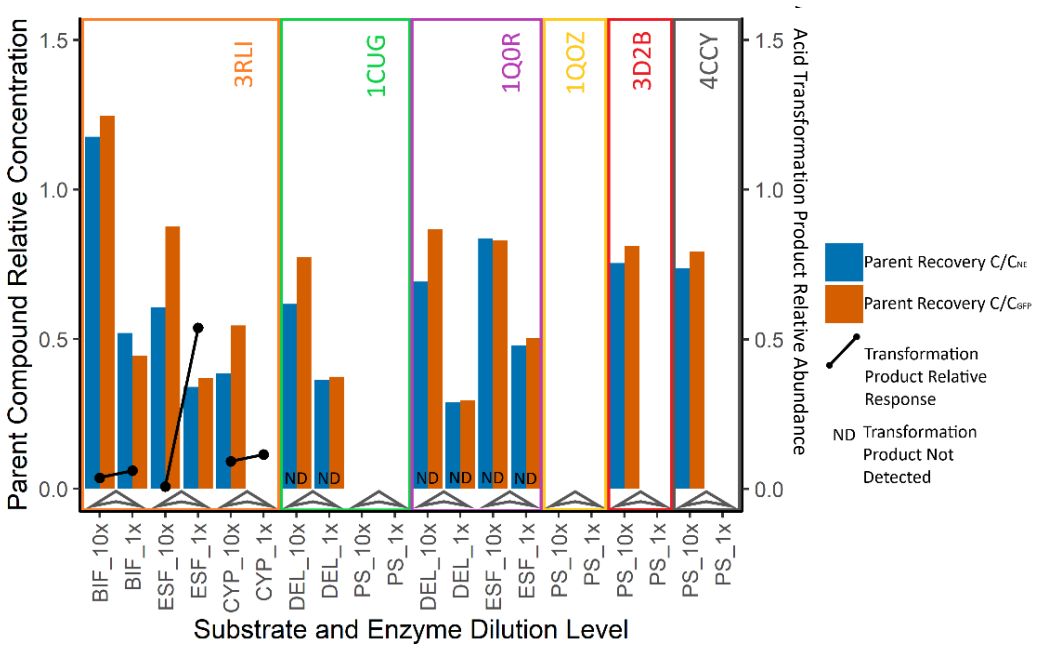

Figure B4. Selected instances of pesticide/alternative ester combinations with enzymes exhibiting parent compound recoveries ($C/C_{no\ enzyme}$) of < 0.70 as compared to GFP control in at least one dilution replicate. Instances of phenyl salicylate (PS) samples where bars are absent denote non-detection (ND).

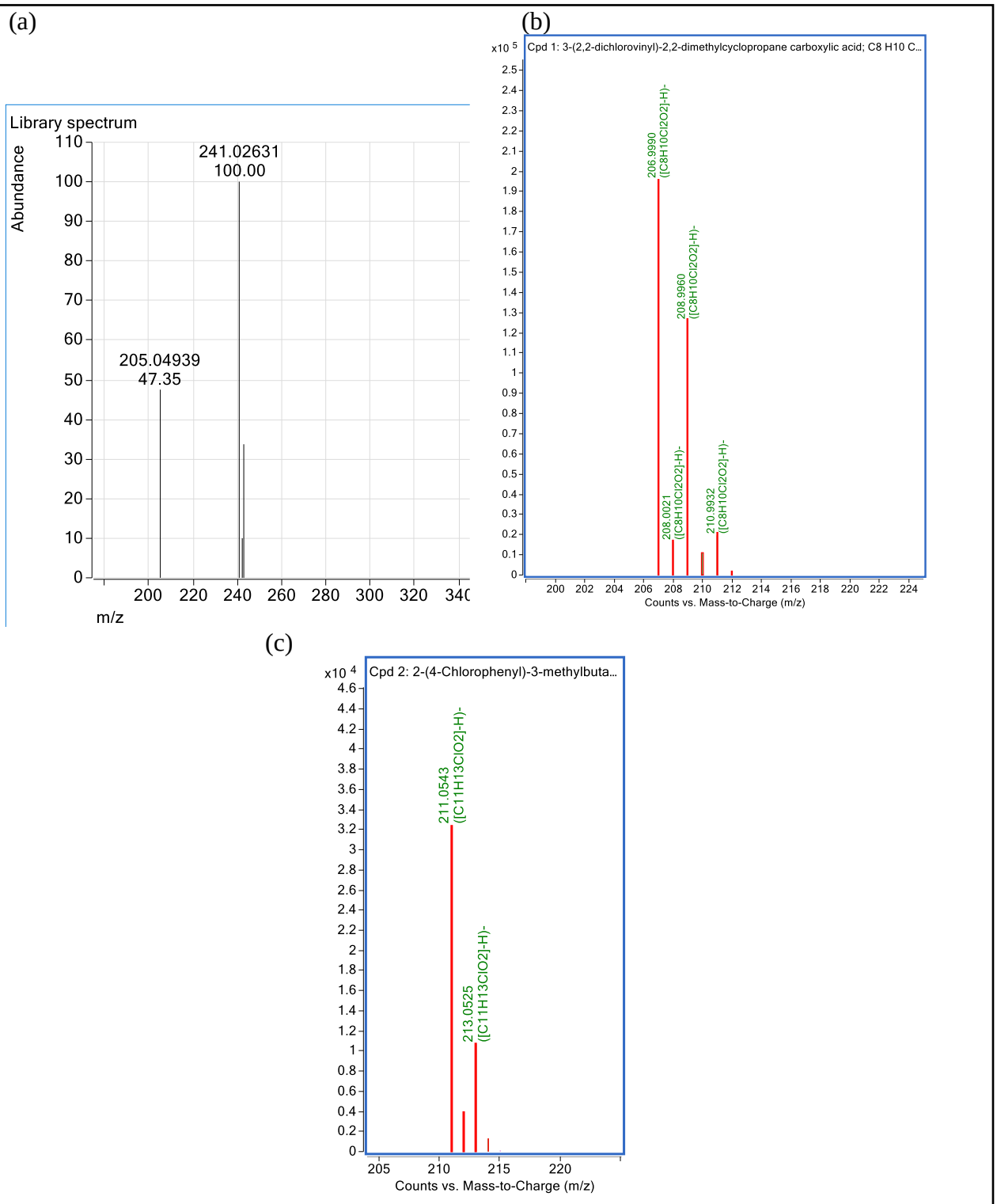

Figure B5. Spectra counts vs m/z for (a) 3-(2-Chloro-3,3,3-trifluoroprop-1-enyl)-2,2-dimethylcyclopropane-1-carboxylic acid (TFP acid) standard spectra vs. m/z; (b) (1RS)-cis,trans-3-(2,2-Dicholorovinyl)-2,2-dimethylcyclopropanecarboxylic acid (Permethric acid; cleaned from find by formula results); and (c) 2-(4-Chlorophenyl)-3-methylbutanoic acid (fenvaleric acid; cleaned from find by formula results).

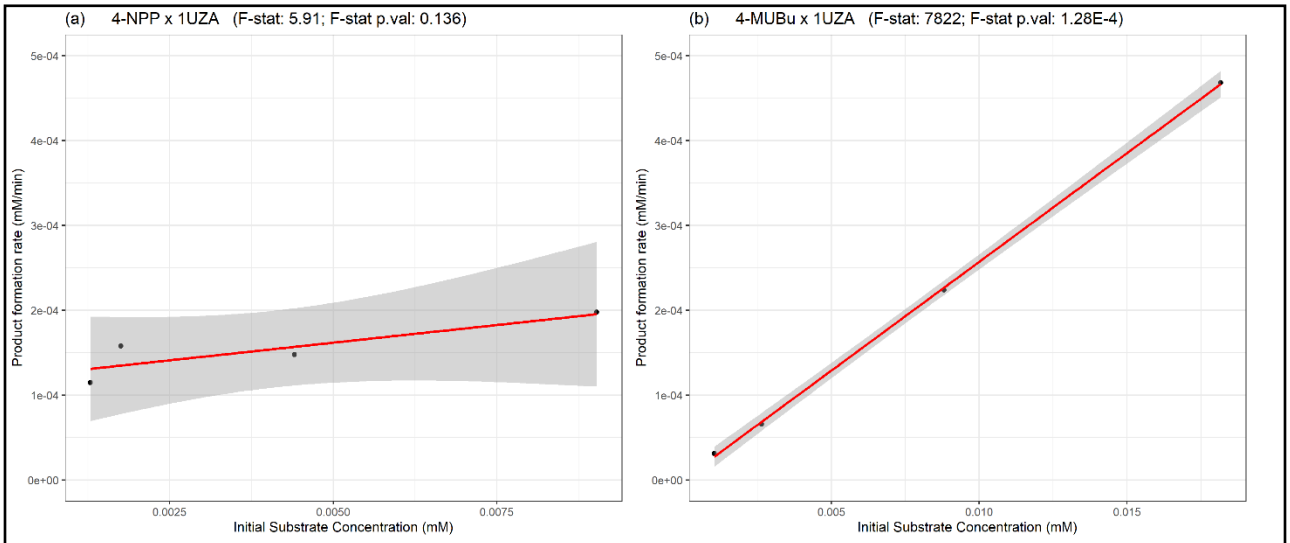

Figure B6. Examples of inactivity and activity with enzyme PDB 1UZA. Inactivity (a) characterized by weak correlation between starting substrate concentration and 4-NP production rate. Activity (b) characterized by a strong correlation between starting substrate concentration and product (4-MU) production.

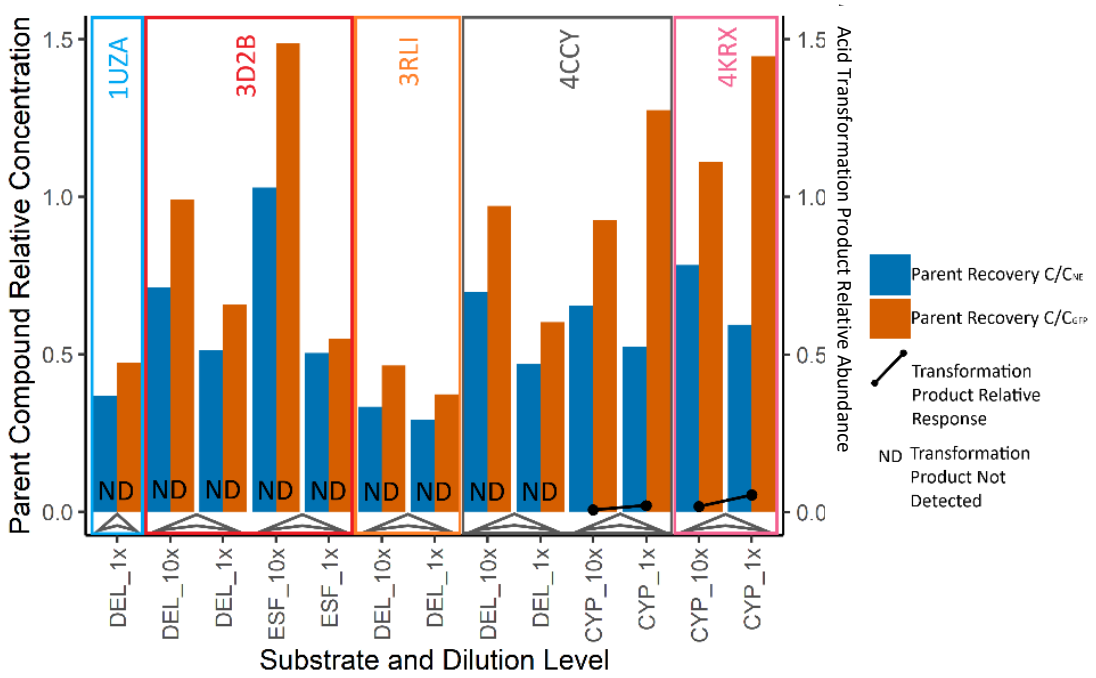

Figure B7. (Active) designation examples from substrate Group 1.

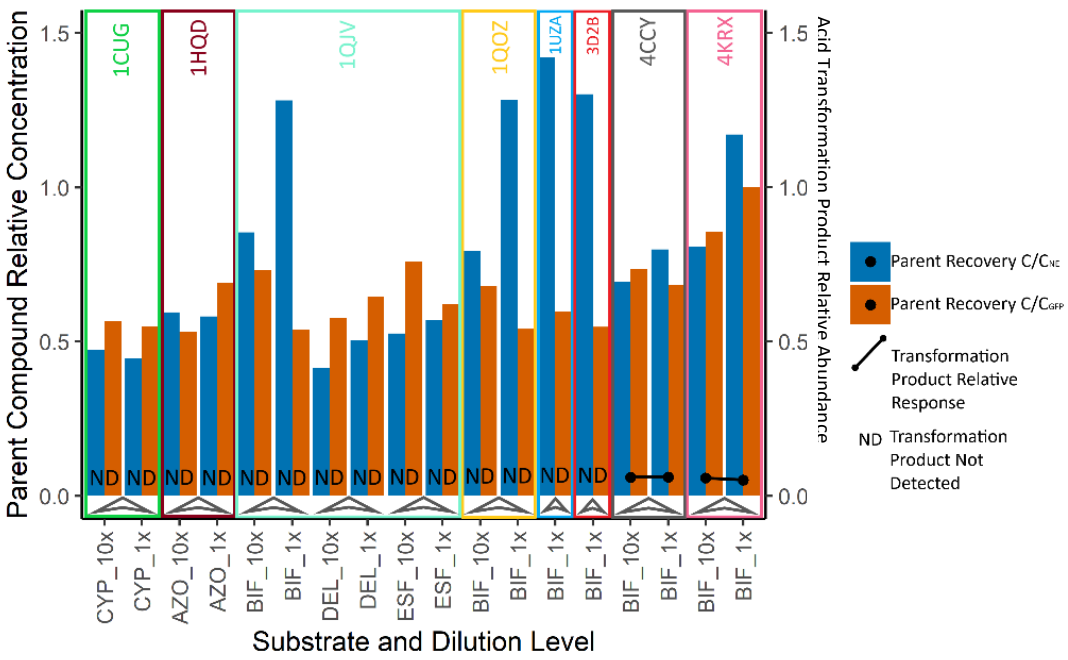

Figure B8. Inactive designation examples from substrate Group 1.

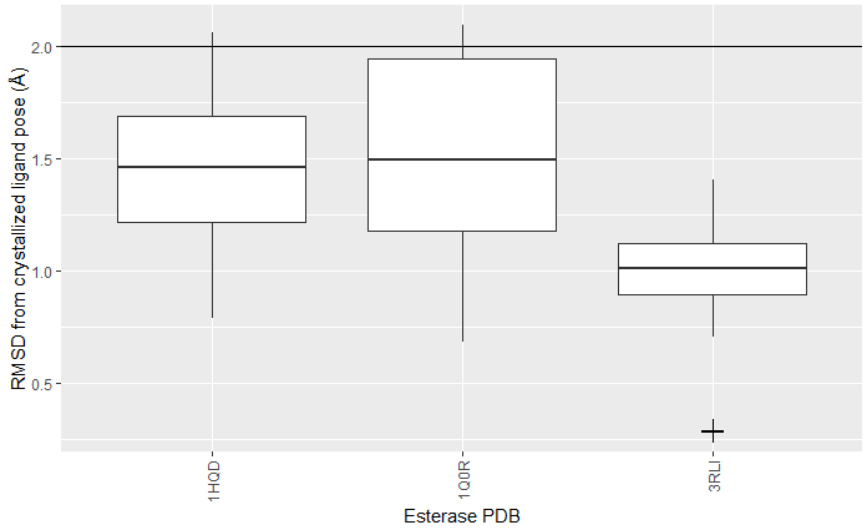

Figure B9. Root mean square deviation (RMSD) distributions of redocked co-crystalized ligands with the induced fit docking (IFD) workflow.

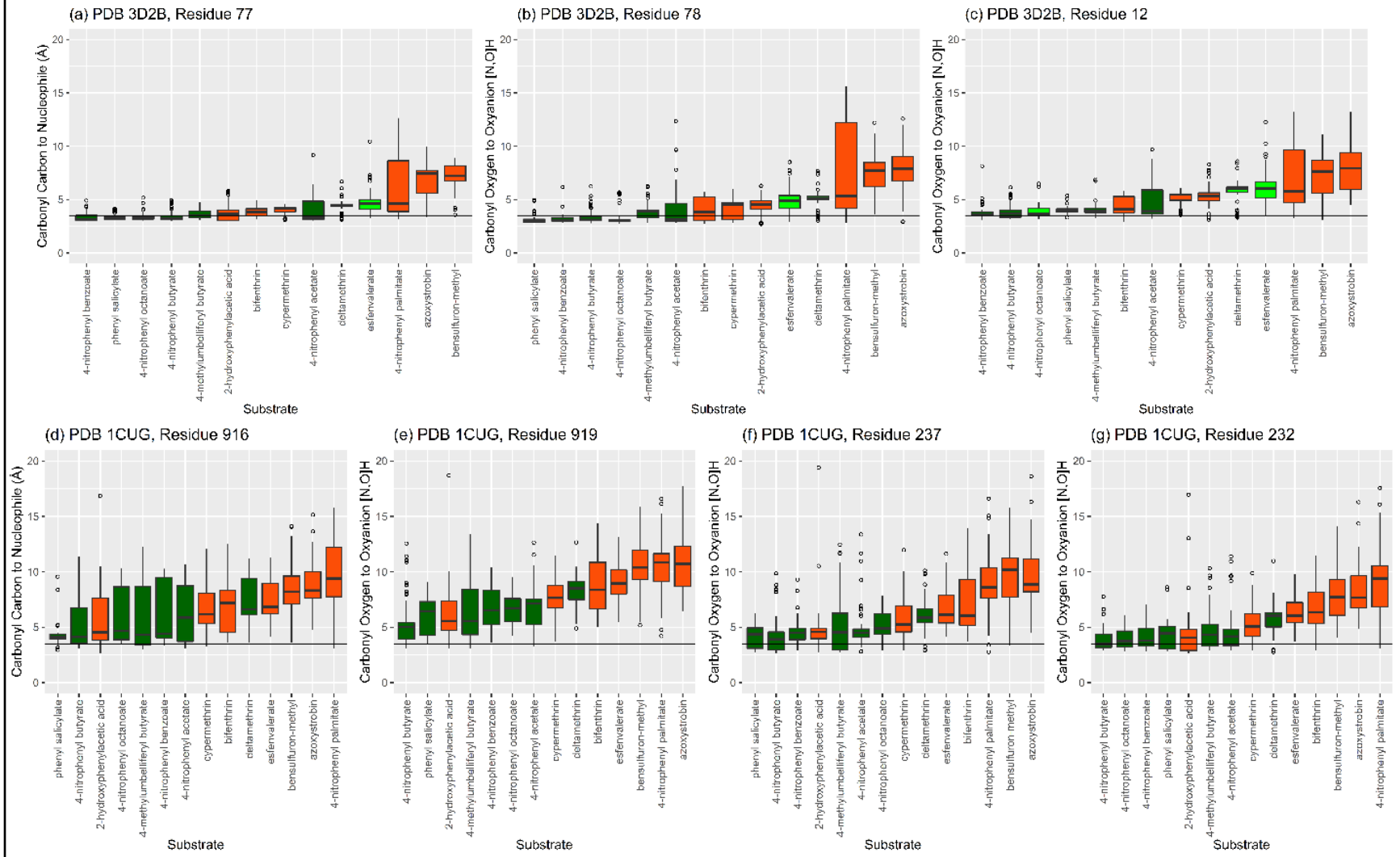

Figure B10.A-G. Distance boxplots for the pose distributions of two enzymes, PDBs 3D2B, and 1CUG.

(Figure B10 continued)

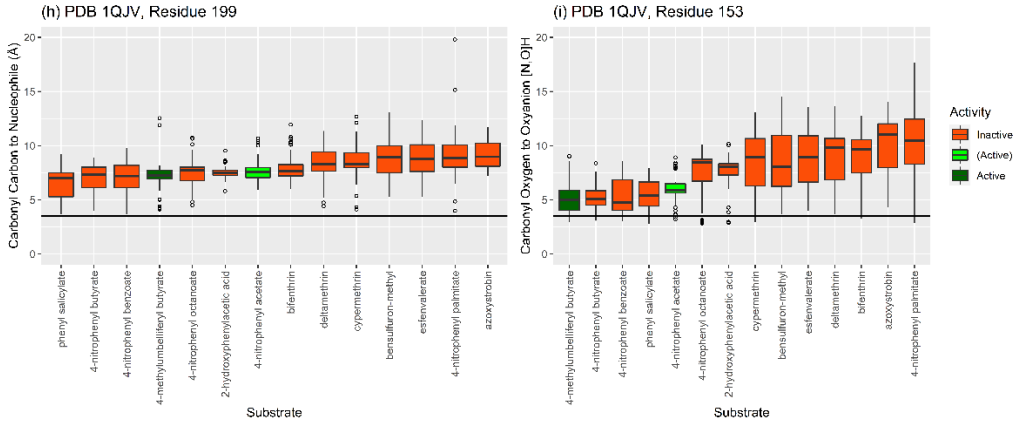

Figure B10.H-I. Distance boxplots for the pose distributions of enzyme PDB 1QJV.

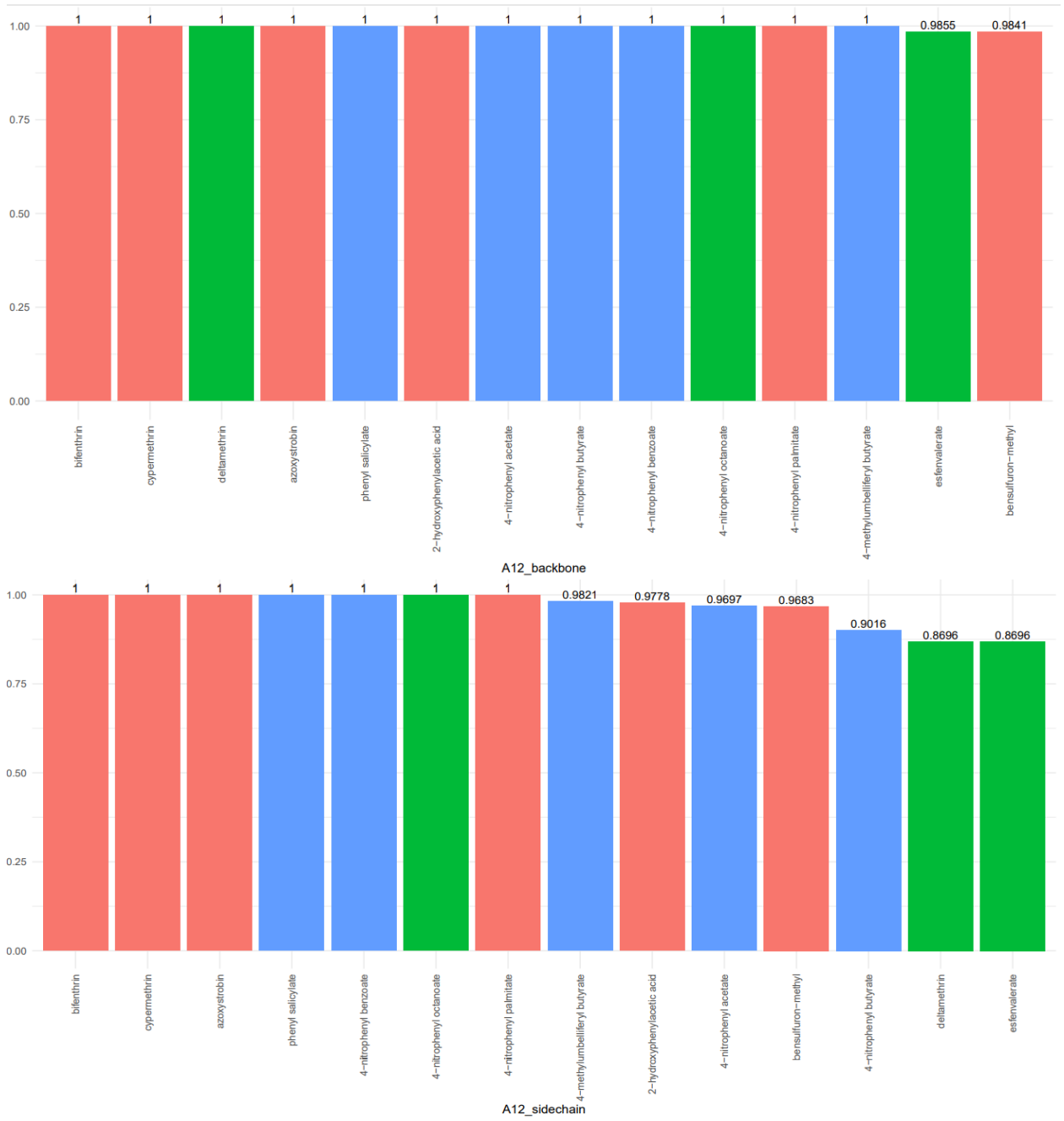

Figure B11.A-B Proportions of contacts with backbone atoms of isoleucine (Ile) 12 (a), and sidechain atoms (b).

(*Figure B11 continued)*

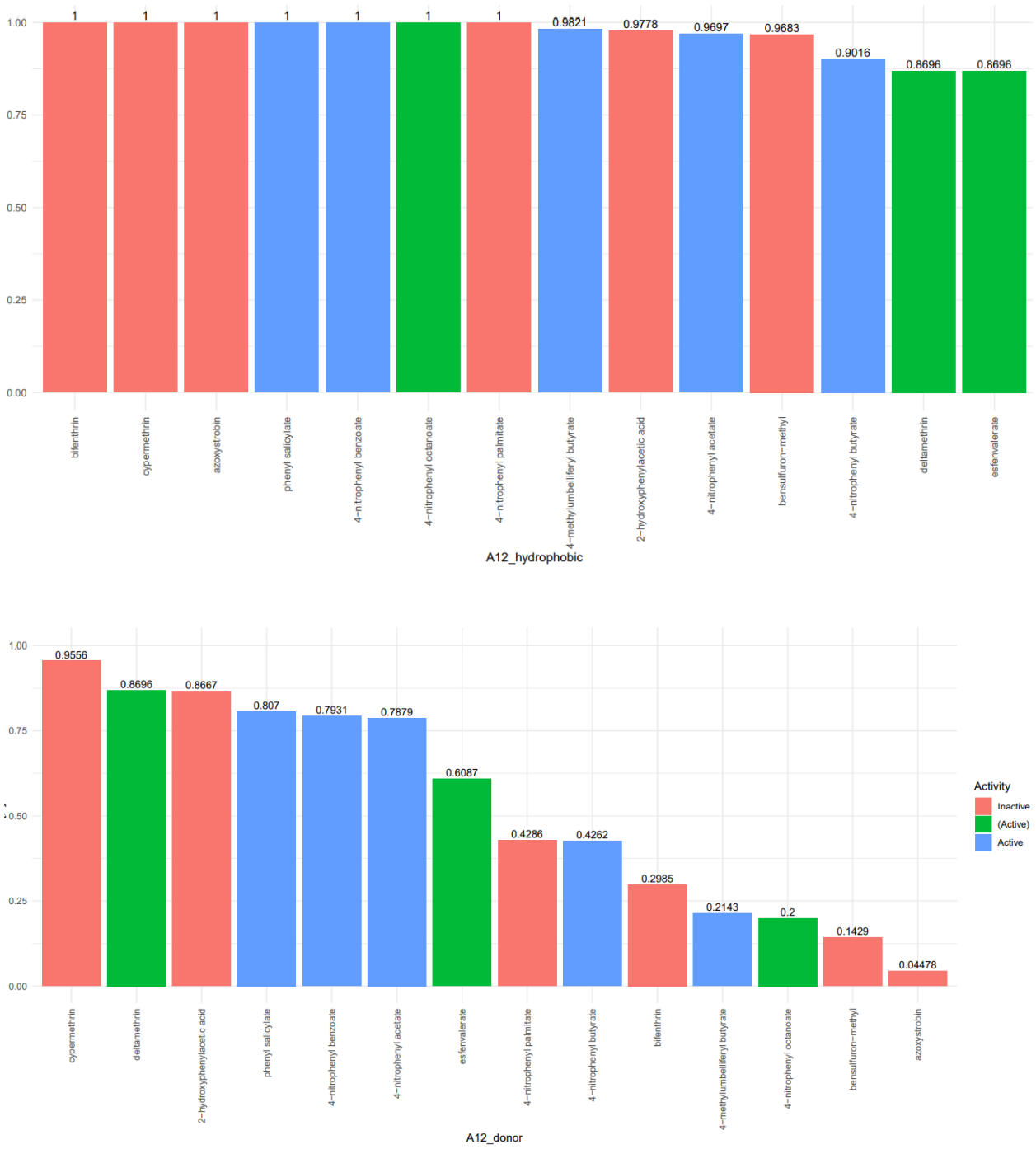

Figure B11.C-D. Proportions of hydrophobic Ile12 contacts (c), and donor interactions with Ile 12 (d).

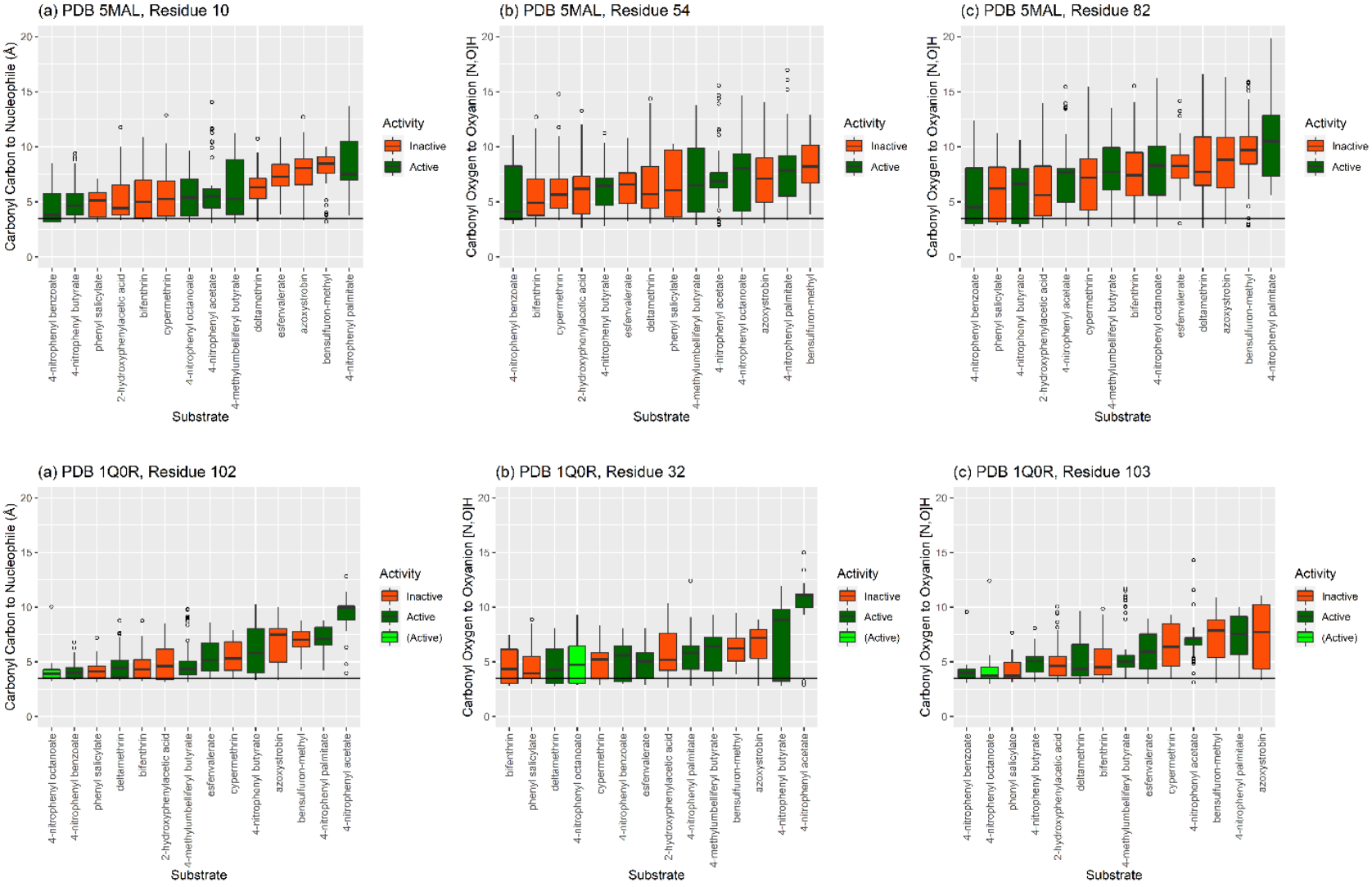

Figure B12. Distance boxplots for the pose distributions for remaining enzymes. (a) plots indicate distances from ligand carbonyl carbon to the nucleophile, while (b) and (c) plots show distances from ligand carbonyl oxygen to oxyanion hole residues.

(Figure B12 continued)

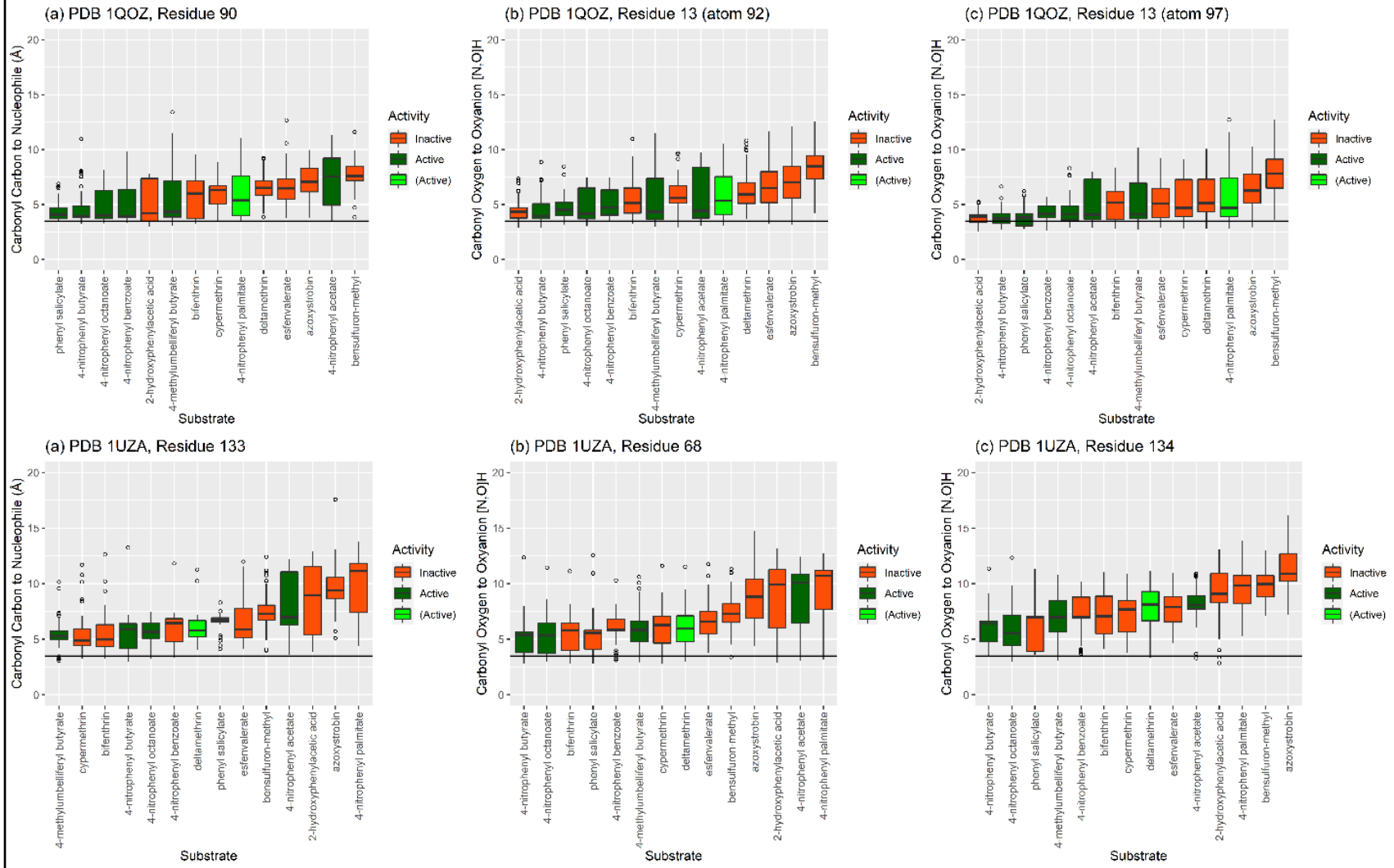

Figure B12. Distance boxplots for the pose distributions for remaining enzymes. (a) plots indicate distances from ligand carbonyl carbon to the nucleophile, while (b) and (c) plots show distances from ligand carbonyl oxygen to oxyanion hole residues.

(Figure B12 continued)

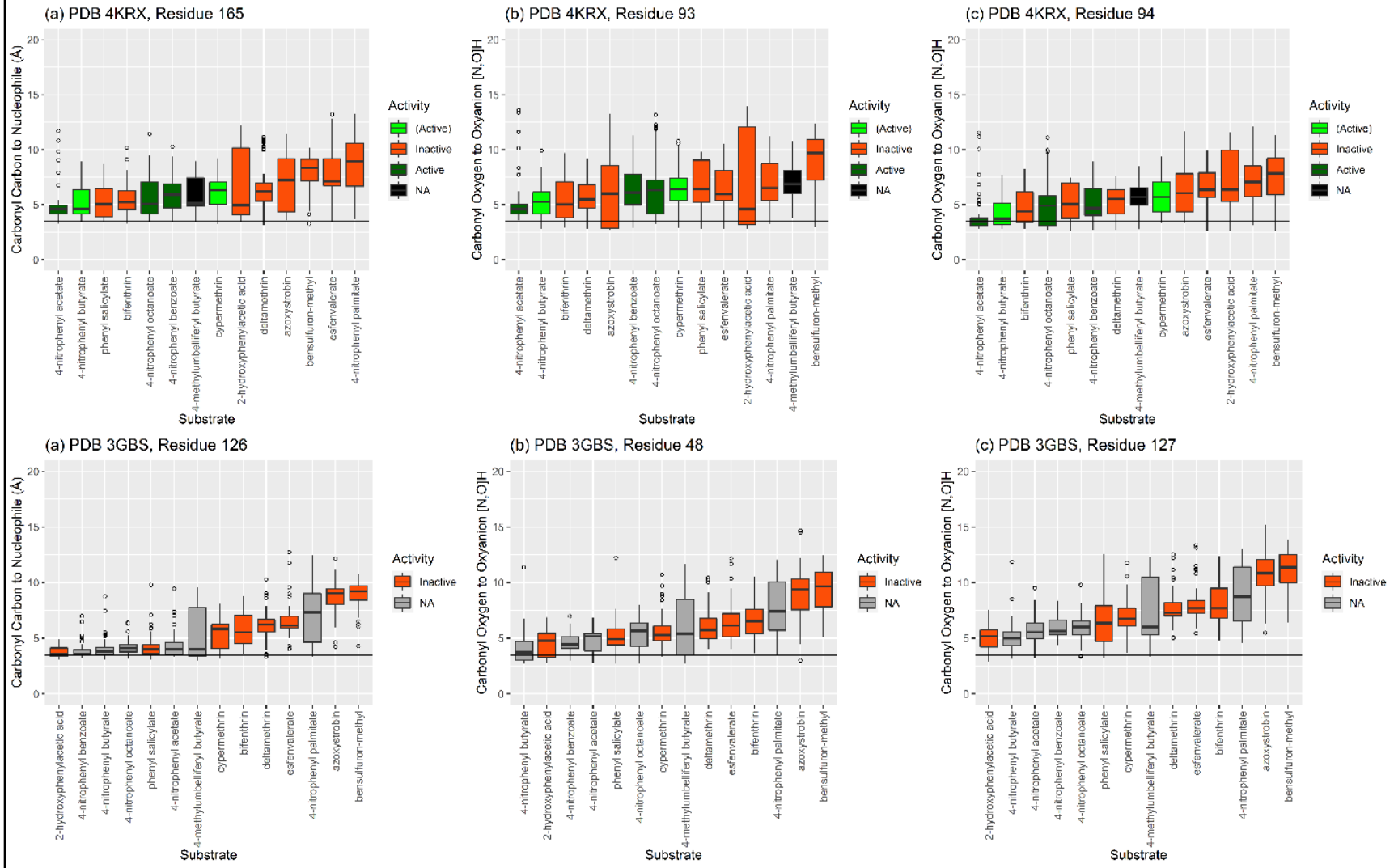

Figure B12. Distance boxplots for the pose distributions for remaining enzymes. (a) plots indicate distances from ligand carbonyl carbon to the nucleophile, while (b) and (c) plots show distances from ligand carbonyl oxygen to oxyanion hole residues.

(Figure B12 continued)

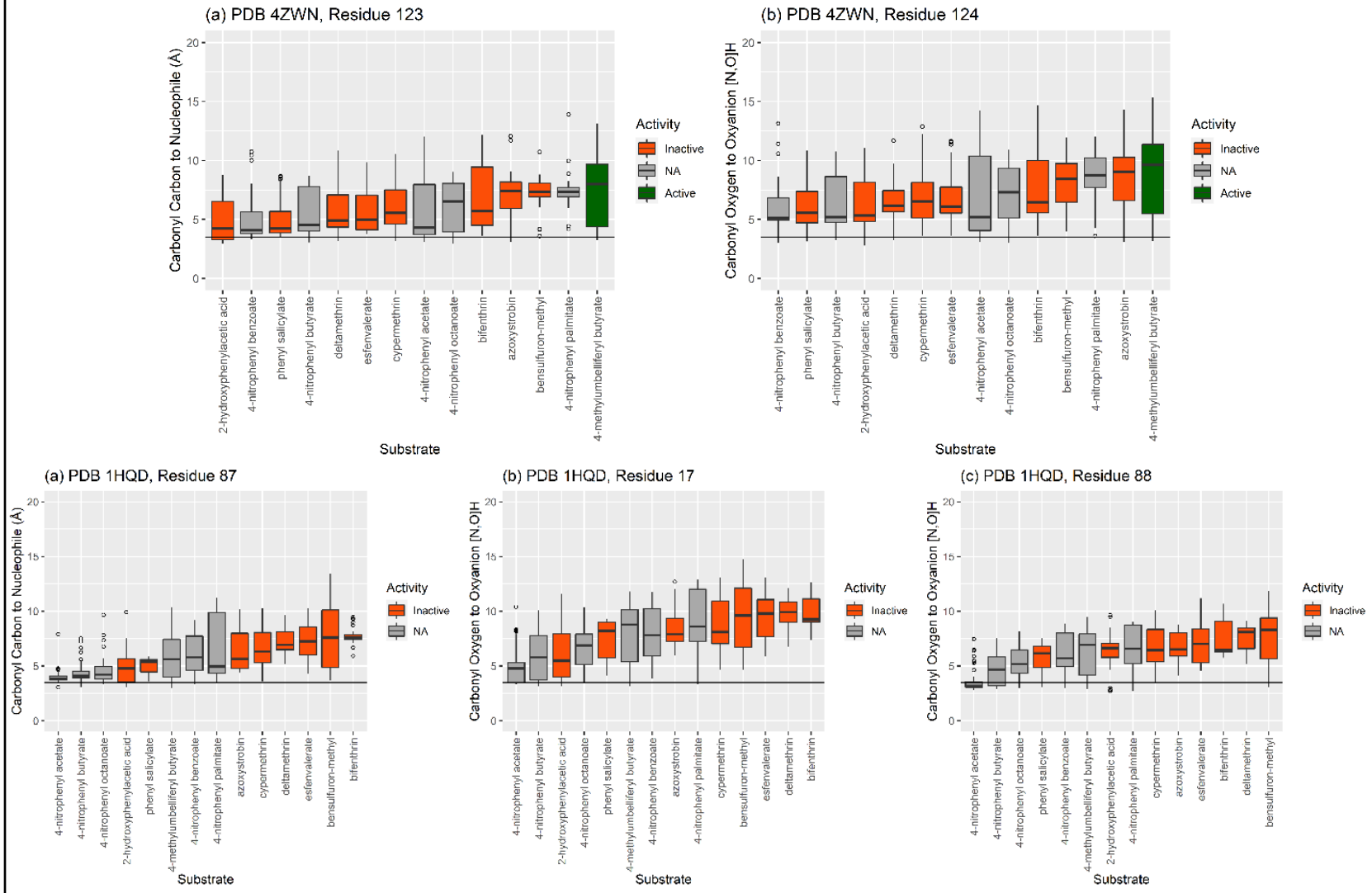

Figure B12. Distance boxplots for the pose distributions for remaining enzymes. (a) plots indicate distances from ligand carbonyl carbon to the nucleophile, while (b) and (c) plots show distances from ligand carbonyl oxygen to oxyanion hole residues.

(Figure B12 continued)

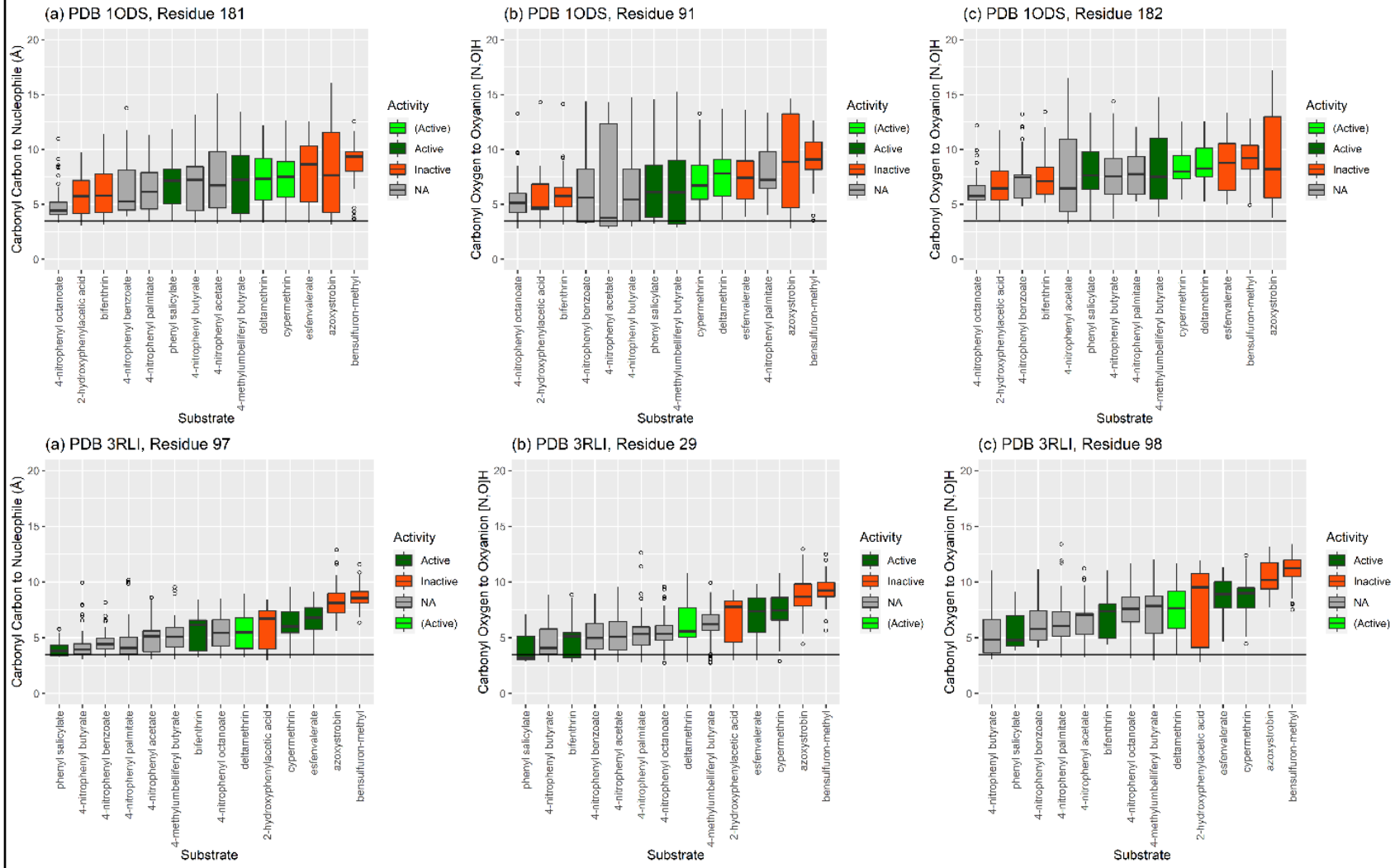

Figure B12. Distance boxplots for the pose distributions for remaining enzymes. (a) plots indicate distances from ligand carbonyl carbon to the nucleophile, while (b) and (c) plots show distances from ligand carbonyl oxygen to oxyanion hole residues.

(Figure B12 continued)

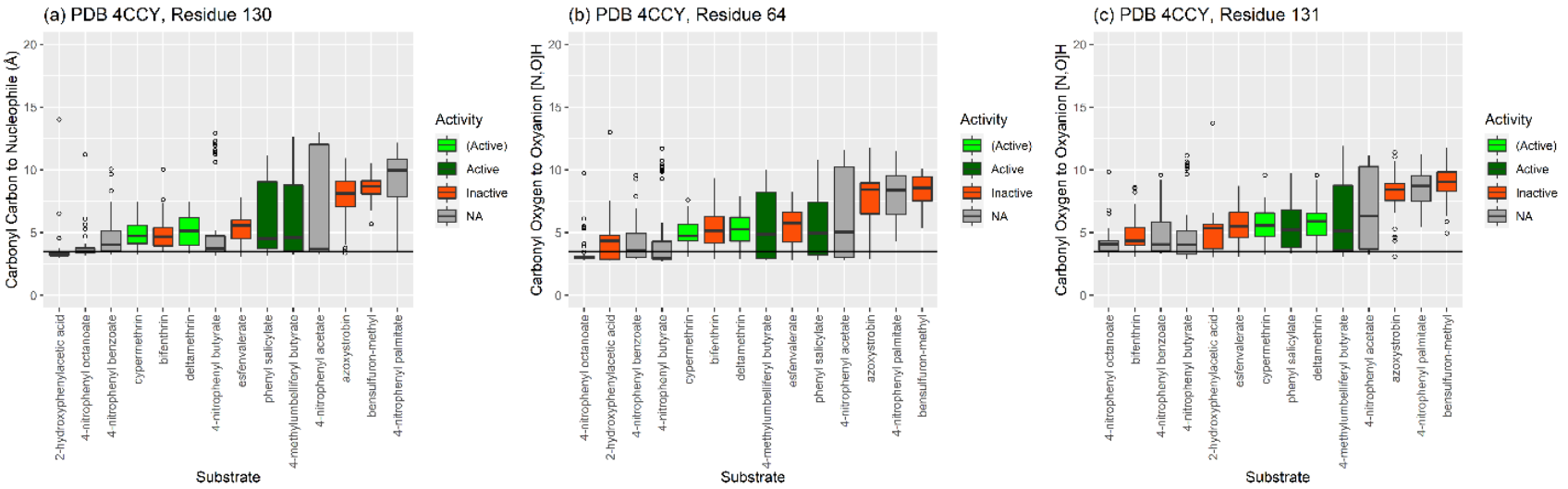

Figure B12. Distance boxplots for the pose distributions for remaining enzymes. (a) plots indicate distances from ligand carbonyl carbon to the nucleophile, while (b) and (c) plots show distances from ligand carbonyl oxygen to oxyanion hole residues.

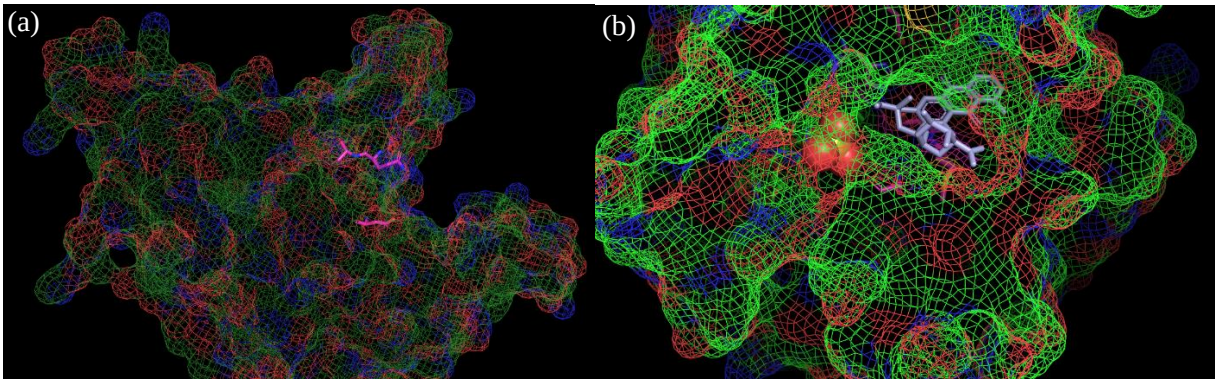

Figure B13.A-B. Surface mesh figures of PDBs 1QJV (a) and 1Q0R (b) illustrating vastly different binding sites for the methylesterases. The pink stick frame residues are the catalytic residues, while a ligand analogue for aclacinomycin[36] is in light blue to emphasize the difference in active site accessibility (b).

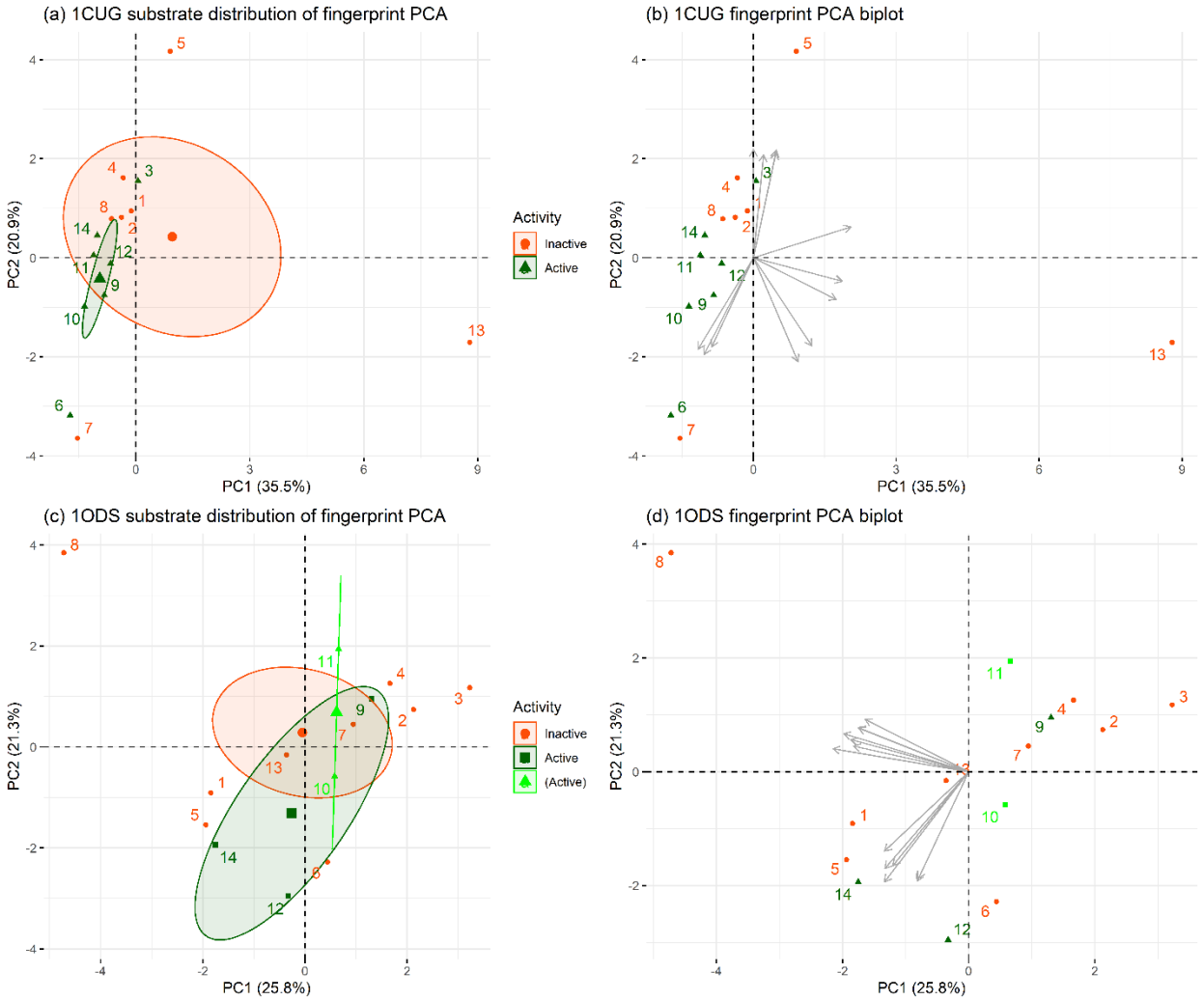

Figure B14.A-D. Individual (ligand) groups from principal component analysis, and corresponding biplots. Ligand numbers correspond to those listed in Tables B2 and B5.

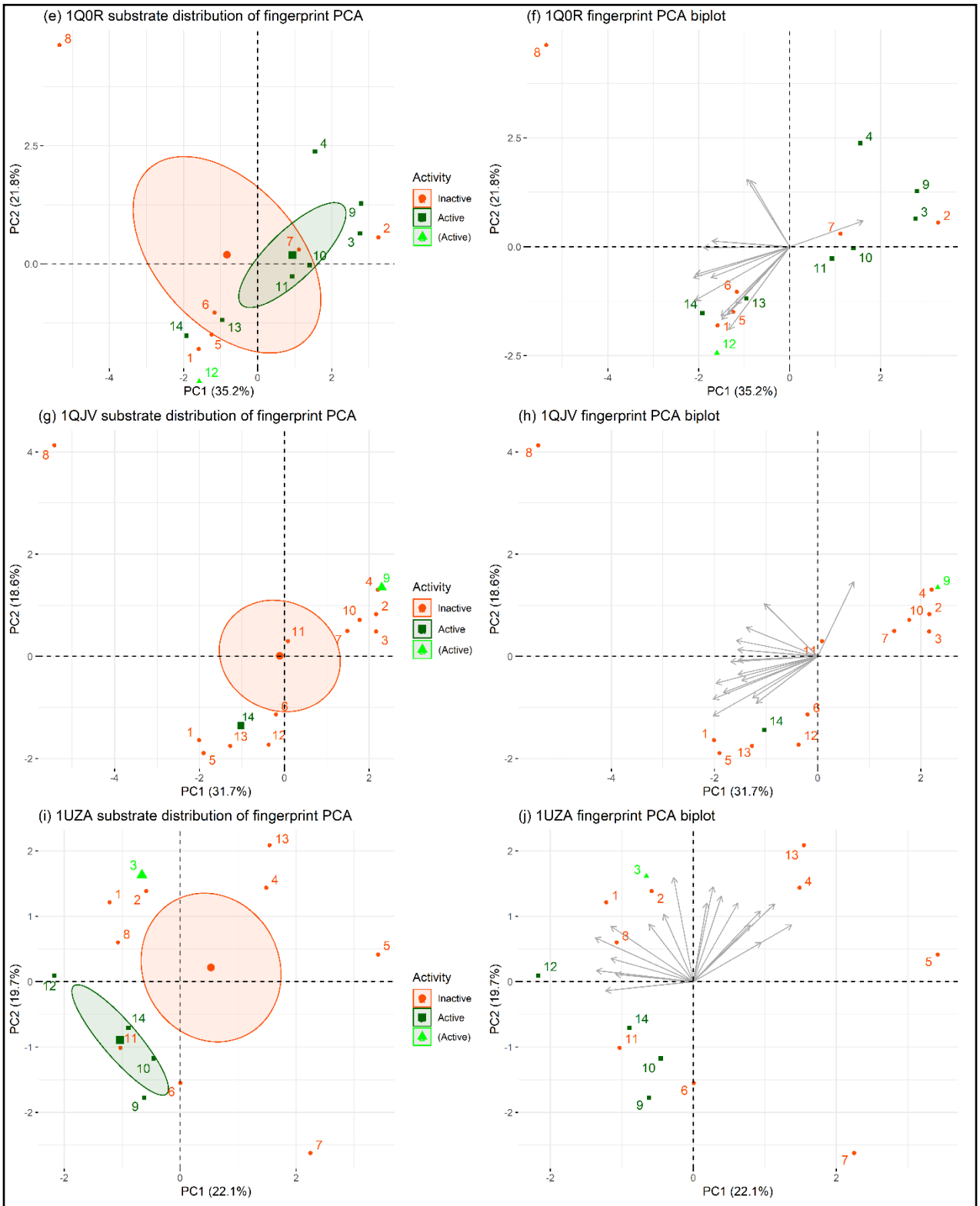

Figure B14.E-J. Individual (ligand) groups from principal component analysis, and corresponding biplots. Ligand numbers correspond to those listed in Tables B2 and B5.

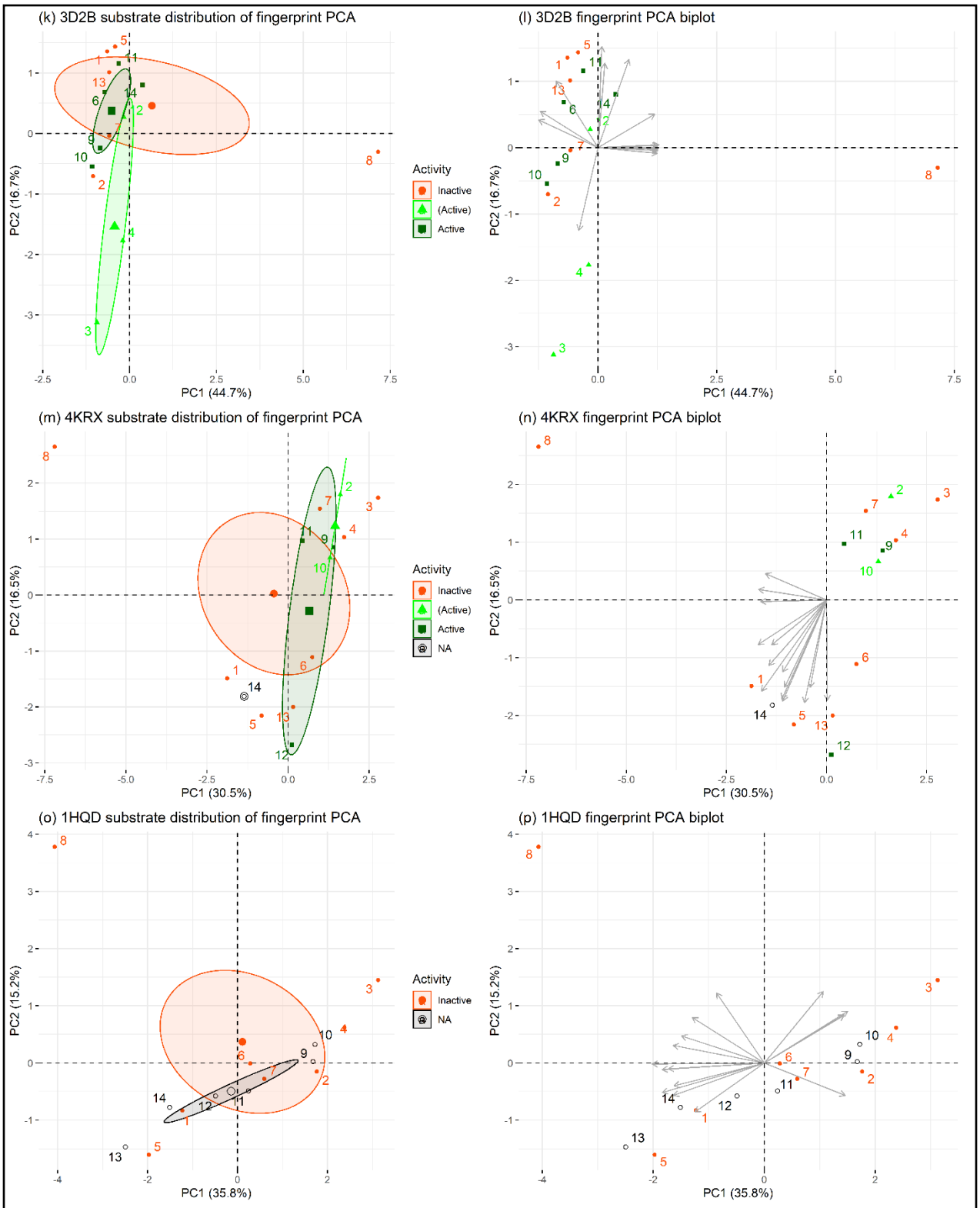

Figure B14.K-P. Individual (ligand) groups from principal component analysis, and corresponding biplots. Ligand numbers correspond to those listed in Tables B2 and B5.

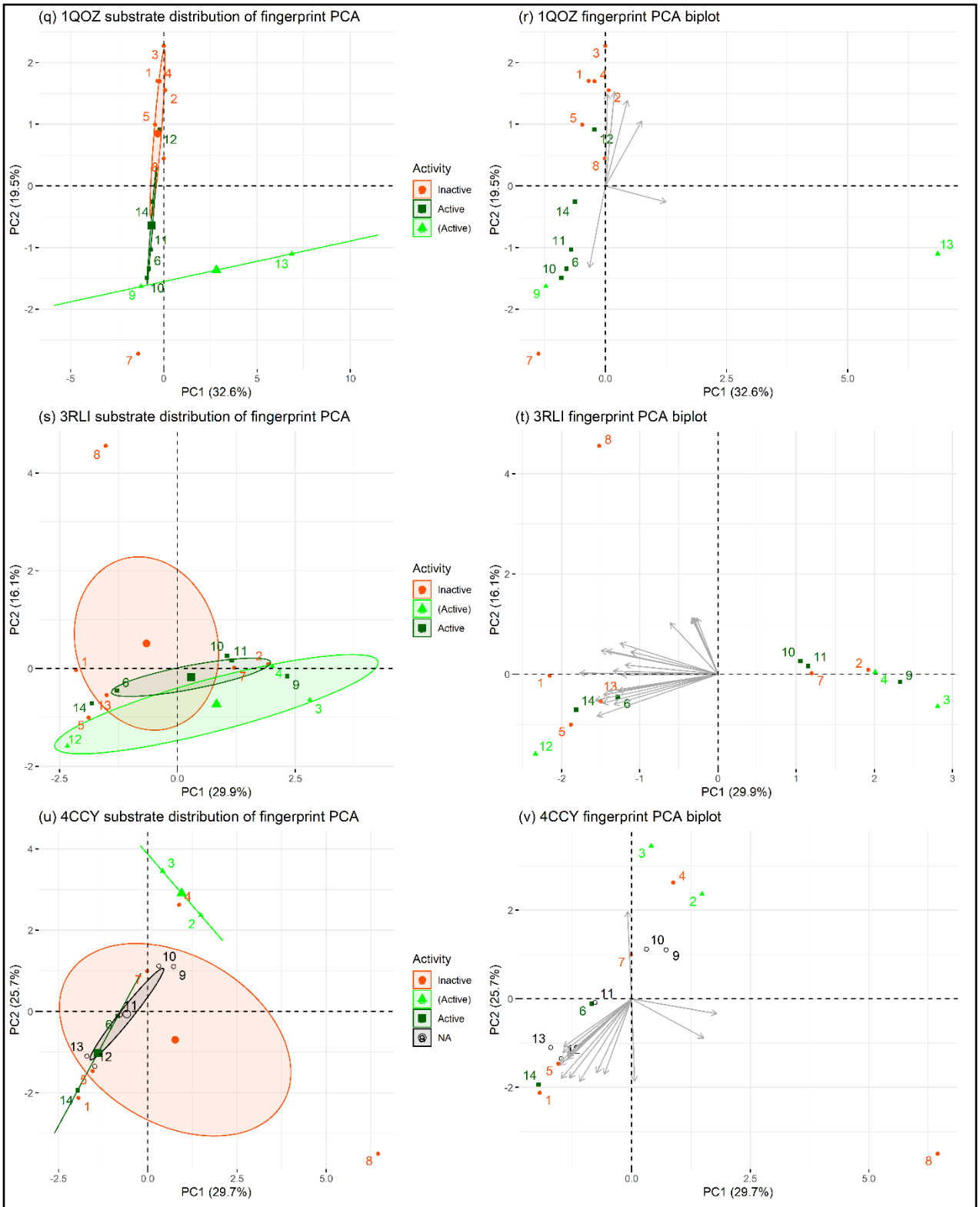

Figure B14.Q-V. Individual (ligand) groups from principal component analysis, and corresponding biplots. Ligand numbers correspond to those listed in Tables B2 and B5.

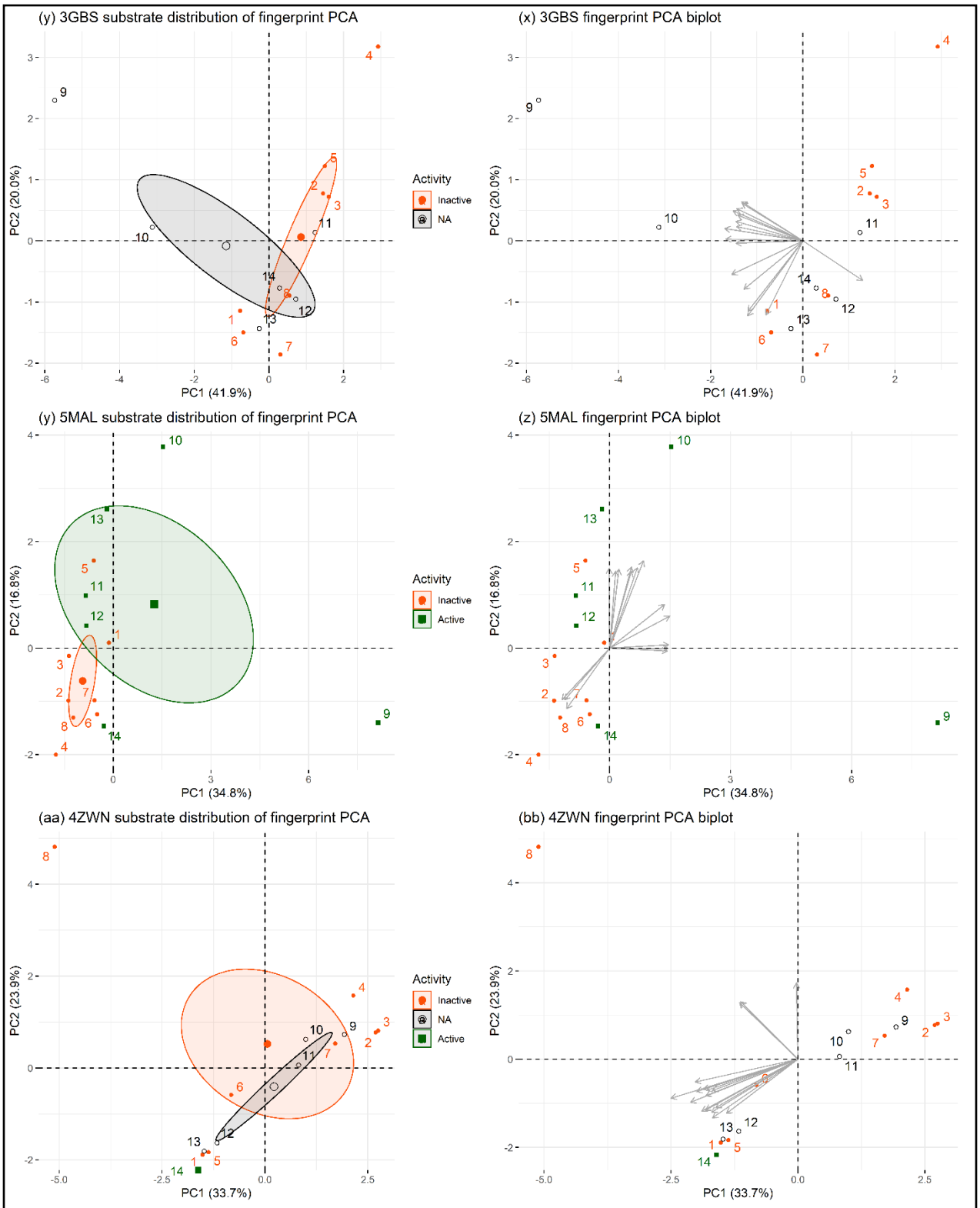

Figure B14.Y-BB. Individual (ligand) groups from principal component analysis, and corresponding biplots. Ligand numbers correspond to those listed in Tables B2 and B5.

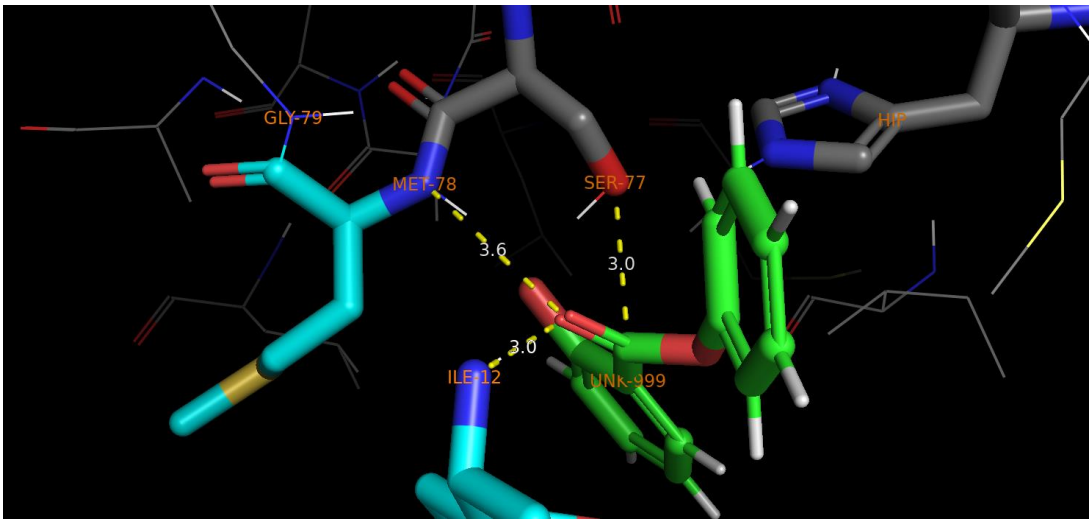

Figure B15. Active site of lipase 3D2B with bound phenyl salicylate (green carbons). Dashed yellow lines illustrate distances (Å). Catalytic serine (A77) and histidine (A156) are shown with grey carbons. Previously described oxyanion methionine residue (A78) and putative oxyanion isoleucine (Ile12) are shown with light blue carbons.

B.2 Tables

Table B1. Selected enzymes.

PDB	Name	EC	SASA Chain A	Molecular SA Chain A	SASA:Molecular SA ratio	Nucleophile relative SASA (%)	Oxyanion relative SASA (avg. %)	Classification Name	Organism	Source
4KRX	Acetyl esterase (Aes)	3.1.1.-	13499.8	32686.3	0.413	12	19	Esterase	*Escherichia coli (K-12)*	Schiefner et al. (2014)
4CCY	Carboxylesterase	3.1.1.1	12285.9	29451.5	0.417	8	12.5	Carboxylesterase	*Bacillus subtilis str. 168*	Rozeboom et al. (2014)
1QJV	Pectin methylesterase	3.1.1.11	14915.7	33548	0.445	8	18	Pectinesterase	*Dickeya chrysanthemi*	Jenkins et al. (2001)
4ZWN	Monoglyceride Lipase	3.1.1.23	13440.9	32138.9	0.418	14	19.5	Acylglycerol lipase	*Saccharomyces cerevisiae S288C*	Aschauer et al. (2016)
3RLI	Monoacylglycerol lipase	3.1.1.23	10676.1	24608.4	0.434	14	10	Acylglycerol lipase	*Bacillus H257*	Rengachari et al. (2012)
1HQD	Lipase (LipA)	3.1.1.3	13081.9	30052.9	0.435	13	16	Triacylglycerol lipase	*Pseudomonas Burkholderia cepacia*	Luic et al. (2001)
3D2B	Lipase (LipA)	3.1.1.3	7498.7	17501.9	0.428	15	14 (35.5 w/Ile12)	Triacylglycerol lipase	*Bacillus subtilis*	Ahmad et al. (2008)
5MAL	Extracellular Lipase	3.1.1.3/2	9524.3	21727.7	0.438	6	28	Triacylglycerol lipase/Arylesterase	*Streptomyces rimosus*	Asler et al. (2017)
1CUG	Cutinase	3.1.1.3/74	8445.1	18771.2	0.450	8	10.5	Triacylglycerol lipase/Cutinase	*Fusarium vanettenii*	Longhi et al. (1996)
1ODS	Cephalosporin C deacetylase	3.1.1.41/72	13443.5	32828.5	0.410	9	8.5	Cephalosporin-C deacetylase/Acetylxylan esterase	*Bacillus subtilis*	Vincent et al. (2003)
1QOZ	Acetyl xylan esterase	3.1.1.72	8918.6	19048.7	0.468	9	26	Acetylxylan esterase	*Trichoderma reesei*	Hakulinen et al. (2000)
1UZA	Feruloyl esterase	3.1.1.73	10733	25543.1	0.420	10	13	Feruloyl esterase	*Aspergillus niger*	McAuley et al. (2004)
3GBS	Cutinase	3.1.1.74	7895.4	17728.1	0.445	11	10.5	Cutinase	*Aspergillus oryzae*	Liu et al. (2009)
1Q0R	Alacinomycin methylesterase	3.1.1.95	12727.6	29063.8	0.438	25	26.5	Aclacinomycin methylesterase	*Streptomyces purpurascens*	Jansson et al. (2003)

Table B2. Selected ligands, organized by Group, with characteristics calculated from DataWarrior.

Ligand No.	Name	PubChem_ID	Formula	MW	LogKow	cLogP	cLogS	Total Surface Area	Polar Surface Area	Relative PSA	Druglikeness	LE from PubChem ID	Shape Index	Molecular Flexibility	Molecular Complexity	Globularity Vol
GROUP 1: Pesticides & Alternative Esters																
1	Bifenthrin (BIF)	6442842	C23H22ClF3O2	422.9	6	6.3407	-7.096	302.81	26.3	0.076	-7.120	0.104	0.552	0.494	0.79818	0.68288
2	Cypermethrin (CYP)	2912	C22H19Cl2NO3	416.3	6.6	5.3412	-6.688	306.96	59.32	0.152	-4.504	0.271	0.571	0.522	0.78821	0.72111
3	Deltamethrin (DEL)	40585	C22H19Br2NO3	505.2	6.2	5.6032	-6.972	313.38	59.32	0.149	-9.445	0.215	0.571	0.522	0.78821	0.68123
4	Esfenvalerate (ESF)	10342051	C25H22ClNO3	419.9	6.2	5.6229	-7.095	329.68	59.32	0.141	-5.926	0.091	0.567	0.526	0.78115	0.69134
5	Azoxystrobin (AZO)	3034285	C22H17N3O5	403.4	2.5	2.9412	-7.072	318.99	103.56	0.278	-6.600	0.115	0.500	0.504	0.82887	0.68475
6	Phenyl Salicylate (PS)	8361	C13H10O3	214.22	3.8	2.7444	-2.79	167.12	46.53	0.216	-1.598	0.435	0.625	0.356	0.60067	0.78152
7	2-Hydroxyphenylacetic Acid (2-HYD)	11970	C8H8O3	152.15	0.85	0.7971	-1.298	117.47	57.53	0.334	-1.721	0.614	0.636	0.552	0.65162	0.84615
8	Bensulfuron-methyl (BEN)	54960	C16H18N4O7S	410.4	1.6	1.7953	-4.966	298.08	154.19	0.435	-4.523	0.209	0.536	0.498	0.78115	0.68374
GROUP 2: Esterase/Lipase Substrates																
9	4-Nitrophenyl Acetate (4-NPA)	13243	C8H7NO4	181.15	1.5	0.7247	-2.376	136.94	72.12	0.390	-7.124	0.515	0.692	0.407	0.59725	0.80547
10	4-Nitrophenyl Butyrate (4-NPBu)	75834	C10H11NO4	209.2	2.3	1.6335	-2.916	164.46	72.12	0.325	-9.988	0.377	0.733	0.496	0.56718	0.77446
11	4-Nitrophenyl Benzoate (4-NPBe)	70396	C13H9NO4	243.21	3.4	2.1685	-3.546	184.44	72.12	0.290	-6.721	0.316	0.667	0.411	0.62054	0.75582
12	4-Nitrophenyl Octanoate (4-NPO)	97416	C14H19NO4	265.3	4.5	3.4511	-3.996	219.5	72.12	0.244	-31.690	0.290	0.789	0.527	0.58727	0.71354
13	4-Nitrophenyl Palmitate (4-NPP)	73891	C22H35NO4	377.5	8.8	7.0863	-6.156	329.58	72.12	0.162	-31.592	0.210	0.852	0.518	0.60487	0.63213
14	4-Methylumbelliferyl Butyrate (4-MUBu)	87247	C14H14O4	246.26	2.8	2.4711	-2.939	192.01	52.6	0.240	-10.497	0.309	0.611	0.358	0.76987	0.75045

Table B3. Catalytic triad and oxyanion hole residue numbers and atom numbers used for distance measurements.

PDB	Name	Ser Nucleophile Residue No.	Nucleophile O Atom No.	His Donor Residue No.	Asp/Glu Acid Residue No.	Oxyanion Residue No.	Oxyanion N/O Atom No.	Source
4KRX	Acetyl esterase (Aes)	165	1283	292	Asp262	Gly93; Gly94	715, 719	Schiefner et al. (2014)
4CCY	Carboxylesterase	130	931	274	Glu245	Gly64; Leu131	932, 412	Rozeboom et al. (2014)
1QJV	Pectin methylesterase	Asp199	1289	Ala154	-	Gln153	943,	Jenkins et al. (2001)
4ZWN	Monoglyceride Lipase	123	998	281	Asp251	Met124; Phe49	329, 999	Aschauer et al. (2016)
3RLI	Monoacylglycerol lipase	97	759	226	Asp196	Met98; Phe29	760, 209	Rengachari et al. (2012)
1HQD	Lipase (LipA)	87	660	286	Asp264	Leu17; Gln88	126, 661	Luic et al. (2001)
3D2B	Lipase (LipA)	77	578	156	Asp133	Met78; Ile12 (putative; this study)	579, 69	Ahmad et al. (2008)
5MAL	Extracellular Lipase	10	70	216	Asn213	Gly54; Asn82	580, 382	Asler et al. (2017)
1CUG	Cutinase	120	916	188	Asp175	Ser42; Gln121	232, 237, 919	Longhi et al. (1996)
1ODS	Cephalosporin C deacetylase	181	1436	298	Asp269	Tyr91; Gln182	725, 1437	Vincent et al. (2003)
1QOZ	Acetyl xylan esterase	90	631	187	Asp175	Thr13	92, 97	Hakulinen et al. (2000)
1UZA	Feruloyl esterase	133	1024	247	Asp194	Thr68; Leu134	517, 1032	McAuley et al. (2004)
3GBS	Cutinase	126	720	194	Asp187	Ser48; Gln127	721, 172	Liu et al. (2009)
1Q0R	Alacinomycin methylesterase	102	765	276	Asp248	Gly32; Met103	225, 766	Jansson et al. (2003)

Table B4. Regression coefficients and F statistics from Group 2 activity assays.

Treatment	y_intercept	slope	F_value
MUBu_1CUG	-8.0E-06	0.0313	23965.8
MUBu_1ODS	-1.9E-05	0.0846	4238.1
MUBu_1Q0R	1.0E-05	0.0232	24154.6
MUBu_1QJV	3.1E-06	0.0270	158.5
MUBu_1QOZ	-5.3E-06	0.0215	1396.7
MUBu_1UZA	7.7E-07	0.0256	7915.4
MUBu_3D2B	5.7E-07	0.0976	3827.7
MUBu_4CCY	-1.2E-04	0.0528	3012.5
MUBu_4ZWN	-3.5E-05	0.0702	2132.5
MUBu_5MAL	-2.5E-05	0.0560	430.3
NPA_1CUG	1.3E-05	0.0245	688.5
NPA_1ODS	3.8E-05	0.0515	1185.6
NPA_1Q0R	-2.4E-05	0.0379	207.5
NPA_1QJV	1.7E-04	0.0411	61.3
NPA_1QOZ	6.0E-05	0.0432	83.3
NPA_1UZA	3.4E-05	0.0576	1649.3
NPA_3D2B	-5.8E-05	0.0532	588.6
NPA_4KRX	-3.0E-05	0.0412	259.1
NPA_5MAL	-1.0E-04	0.0426	1129.6
NPBe_1CUG	-2.5E-05	0.0395	922.6
NPBe_1ODS	1.9E-04	0.0213	29.7
NPBe_1Q0R	6.8E-05	0.0320	191.4
NPBe_1QJV	1.9E-04	0.0074	13.5
NPBe_1QOZ	-1.1E-05	0.0098	257.5
NPBe_1UZA	2.2E-04	-0.0005	0.0
NPBe_3D2B	5.1E-05	0.0465	138.7
NPBe_4KRX	-2.2E-05	0.0408	214.6
NPBe_5MAL	-4.0E-05	0.0228	234.0
NPBu_1CUG	2.2E-05	0.0233	169.5
NPBu_1ODS	1.8E-04	0.0506	66.9
NPBu_1Q0R	3.0E-05	0.0357	4597.9
NPBu_1QJV	2.7E-04	0.0136	6.9
NPBu_1QOZ	-6.8E-06	0.0289	7201.2
NPBu_1UZA	1.5E-04	0.0202	2744.4
NPBu_3D2B	-2.8E-06	0.0509	2200.2
NPBu_4KRX	-1.6E-05	0.0317	53.6
NPBu_5MAL	-1.7E-04	0.0595	1267.6
NPO_1CUG	-4.4E-05	0.0362	175.8
NPO_1ODS	2.2E-04	0.0448	419.1
NPO_1Q0R	2.2E-04	0.0448	43.9
NPO_1QJV	2.1E-04	0.0123	7.9
NPO_1QOZ	1.3E-05	0.0307	120.0
NPO_1UZA	1.2E-04	0.0280	198.0
NPO_3D2B	1.4E-04	0.0354	89.9
NPO_4KRX	-3.9E-05	0.0373	661.4
NPO_5MAL	-7.5E-05	0.0304	404.9
NPP_1CUG	9.9E-05	0.0231	10.4
NPP_1ODS	1.6E-04	0.0340	18.7
NPP_1Q0R	6.5E-05	0.0439	172.7
NPP_1QJV	1.3E-04	0.0037	0.5
NPP_1QOZ	3.3E-05	0.0057	75.5
NPP_1UZA	1.5E-04	0.0105	5.9
NPP_3D2B	1.9E-04	0.0325	2.2
NPP_4KRX	5.2E-05	0.0020	3.2
NPP_5MAL	-3.0E-05	0.0466	1328.6

Table B5. Final activity designations of substrate/enzyme combinations. Activities shown with (Ac) are instances where parent compound losses were borderline (not clear dose dependency), or measured in only one sample dilution replicate.

	Enzyme PDB ID													
GROUP 1: Pesticides & Alternative Esters	**1CUG**	**1HQD**	**1ODS**	**1Q0R**	**1QJV**	**1QOZ**	**1UZA**	**3D2B**	**3GBS**	**3RLI**	**4CCY**	**4KRX**	**4ZWN**	**5MAL**
1. Bifenthrin (BIF)	In	In	In	In	In	In	In	In	In	Ac	In	In	In	In
2. Cypermethrin (CYP)	In	In	In	In	In	In	In	In	In	Ac	(Ac)	(Ac)	In	In
3. Deltamethrin (DEL)	Ac	In	In	Ac	In	In	(Ac)	(Ac)	In	(Ac)	(Ac)	In	In	In
4. Esfenvalerate (ESF)	In	In	In	Ac	In	In	In	(Ac)	In	Ac	In	In	In	In
5. Azoxystrobin (AZO)	In	In	In	In	In	In	In	In	In	In	In	In	In	In
6. Phenyl Salicylate (PS)	Ac	In	In	In	In	Ac	In	Ac	In	In	Ac	In	In	In
7. 2-Hydroxyphenylacetic acid (2-HYD)	In	In	In	In	In	In	In	In	In	In	In	In	In	In
8. Bensulfuron-methyl (BEN)	In	In	In	In	In	In	In	In	In	In	In	In	In	In
GROUP 2: Esterase/Lipase Substrates														
9. 4-Nitrophenyl Acetate (4-NPA)	Ac	NA	Ac	Ac	(Ac)	(Ac)	Ac	Ac	NA	NA	P	Ac	P	Ac
10. 4-Nitrophenyl Butyrate (4-NPBu)	Ac	NA	(Ac)	Ac	In	Ac	Ac	Ac	NA	NA	P	(Ac)	P	Ac
11. 4-Nitrophenyl Benzoate (4-NPBe)	Ac	NA	(Ac)	Ac	In	Ac	In	Ac	NA	NA	P	Ac	P	Ac
12. 4-Nitrophenyl Octanoate (4-NPO)	Ac	NA	Ac	(Ac)	In	Ac	Ac	(Ac)	NA	NA	P	Ac	P	Ac
13. 4-Nitrophenyl Palmitate (4-NPP)	In	NA	In	Ac	In	(Ac)	In	In	NA	NA	P	In	P	Ac
14. 4-Methylumbelliferyl Butyrate (4-MUBu)	Ac	NA	Ac	Ac	Ac	Ac	Ac	Ac	NA	NA	Ac	NA	Ac	Ac

APPENDIX C: SUPPLEMENTARY INFORMATION FOR CHAPTER 4

C.1 Figures

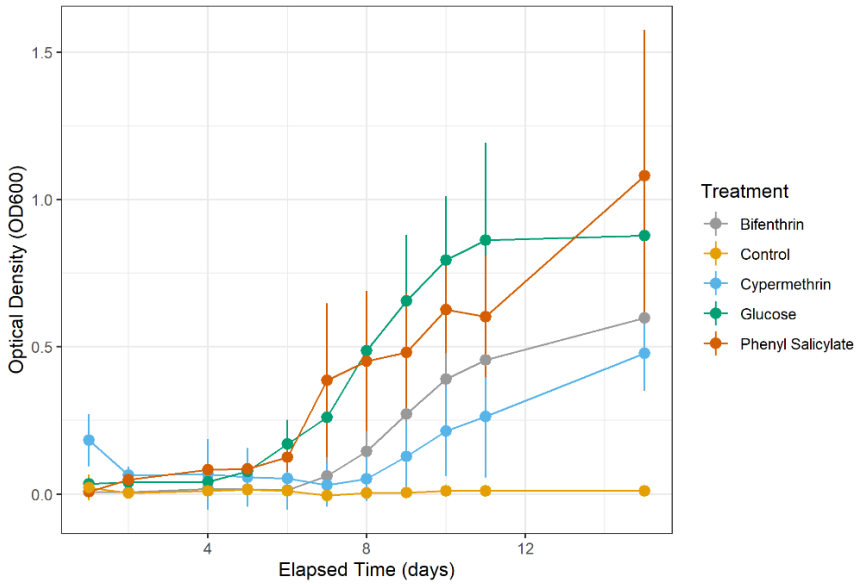

Figure C1. Growth curves of the four treatment and control flasks (n = 6)

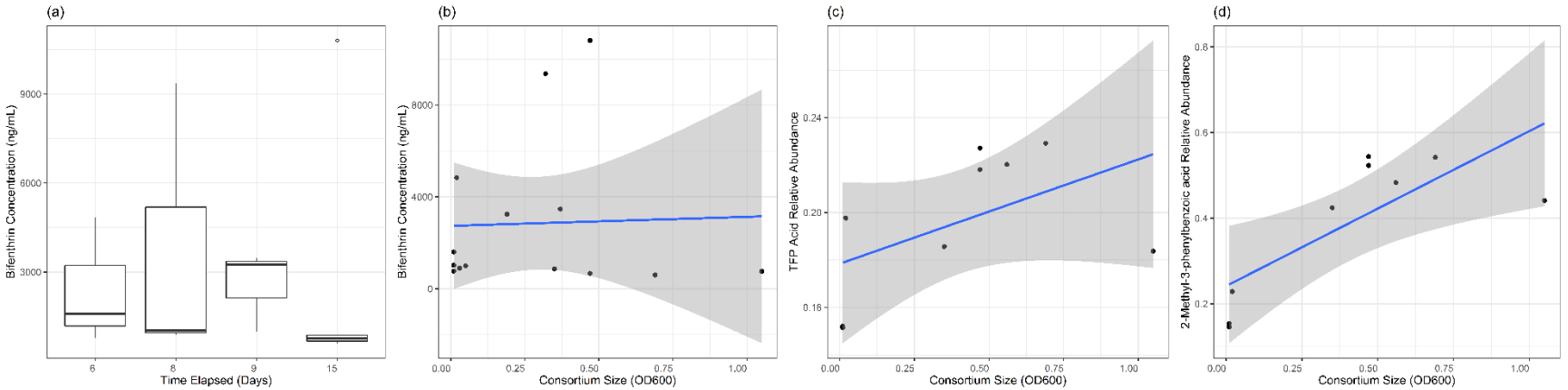

Figure C2. Bifenthrin concentration with respect to elapsed time (a), consortium growth (b), and transformation product TFP acid (c) and 2-methyl-3-phenylbenzoic acid (d) relative abundance with respect to consortium growth.

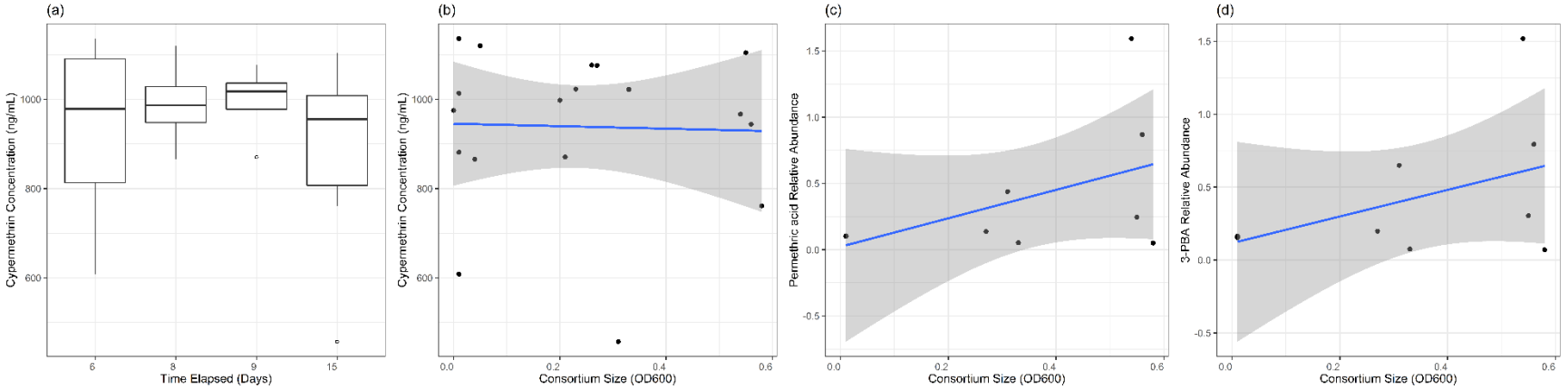

Figure C3. Cypermethrin concentration with respect to elapsed time (a), consortium growth (b), and transformation products permethric acid (c) and 3-PBA (d) relative abundance with respect to consortium growth.

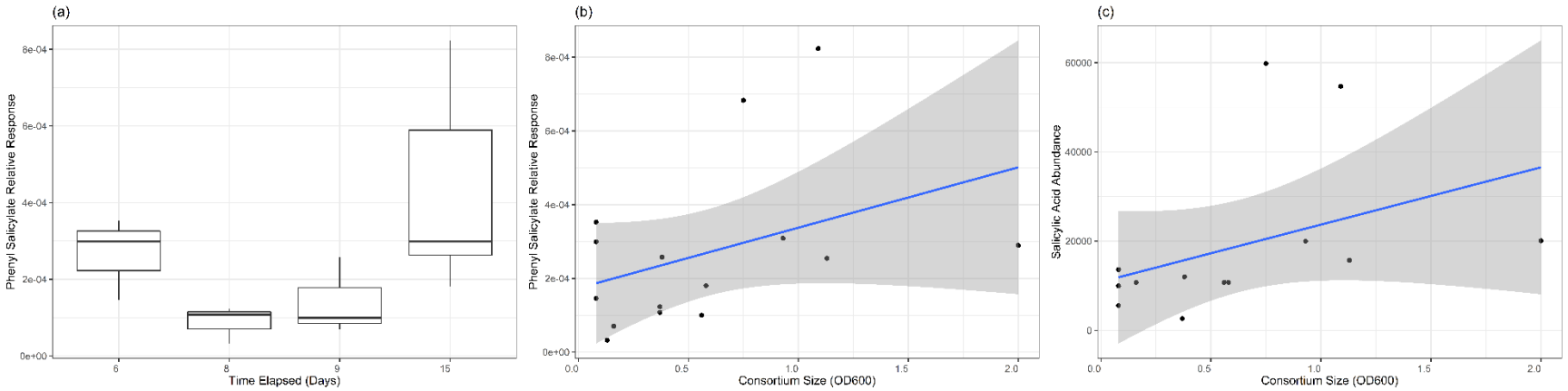

Figure C4. Phenyl salicylate concentration with respect to elapsed time (a), consortium growth (b), and transformation product salicylic acid relative abundance with respect to consortium growth (c

C.2 Tables

Table C1. PCDL compounds used for metabolite/transformation product analysis.

Compound Name	Formula	Mass	CAS
Cyclopropane carboxylic acid	C4H6O2	86.03678	1759-53-1
phenol	C6 h6O	94.04186	108-95-2
catechol	C6 h6O2	110.0368	120-80-9
Benzeneacetic acid (phenylacetic acid)	C8H8O2	136.0524	103-82-2
4-hydroxybenzoate (4-hydroxybenzoic acid)	C7H6O3	138.0317	99-96-7
muconic acid	C6 h6O4	142.0266	3588-17-8
4-propylbenzaldehyde	C10 h12O	148.0888	28785-06-0
protocatechuic acid (3,4-dihydroxybenzoic acid)	C7H6O4	154.0266	99-50-3
2,3-Dihydroxybenzoic acid	C7H6O4	154.0266	303-38-8
4-trifluoromethoxy phenol	C7H5F3O2	178.0242	828-27-3
2-phenoxyphenol	C12 h10O2	186.0681	
3-phenoxybenzaldehyde	C13H10O2	198.0681	39515-51-0
2-methyl-3-biphenylyl methanol (the alcohol)	C14H14O	198.1045	76350-90-8
(1RS)-cis,trans-3-(2,2-Dicholorovinyl)-2,2-dimethylcyclopropanecarboxylic acid	C8H10Cl2O2	208.0058	
3-(2,2-dichlorovinyl)-2,2-dimethylcyclopropane carboxylic acid	C8H10Cl2O2	209.07	55701-05-8
2-(4-Chlorophenyl)-3-methylbutanoic acid	C11H13ClO2	212.0604	
2-methyl-3-phenylbenzoic acid	C14H12O2	212.0837	
3-phenoxybenzoic acid	C13H10O3	214.063	3739-38-6
4-Hydroxy-3-phenoxybenzoic acid	C13H10O4	230.0579	
diruon d6	C9H4D6Cl2N2O	238.0547	
3-(2-Chloro-3,3,3-trifluoroprop-1-enyl)-2,2-dimethylcyclopropane-1-carboxylic acid	C9H10ClF3O2	242.0321	74609-46-4
imidacloprid d4	C9H6D4ClN5O2	259.0774	
2,2-Dimethyl-3-(2,2-dibromovinyl)-cyclopropane-carboxylic acid	C8H10Br2O2	295.9048	
Salicylic acid	C7H6O3	138.032	